

**The Development of d^8 Transition Metal Catalysts for the
Single-Step Production of Vinyl Arenes**

Benjamin Austin Vaughan
Dover, NH

B.S. Chemistry, University of Vermont, 2012

A Dissertation presented to the Graduate Faculty
of the University of Virginia in Candidacy for the Degree of
Doctor of Philosophy

Department of Chemistry

University of Virginia
May 2017

ABSTRACT

VAUGHAN, BENJAMIN A. The Development of d^8 Transition Metal Catalysts for the Single-Step Production of Vinyl Arenes. (Under the direction of Professor T. Brent Gunnoe)

Vinyl arenes are produced on a multi-million ton scale annually and are valuable industrial precursors to plastics, elastomers, surfactants, and detergents. Current industrial methods for vinyl arene production involve acid-mediated arene alkylation via Friedel-Crafts or zeolite catalysis, *trans*-alkylation to optimize yield of mono-alkyl arene, and subsequent dehydrogenation to afford the desired vinyl arene product. While this type of process has been operative in industry for decades, there are a number of deficiencies that suggest that an alternative method for vinyl arene production could be beneficial. Transition metal-mediated oxidative arene vinylation, in which a transition metal catalyst and oxidant mediate the direct and single-step conversion of arenes and olefins to vinyl arenes, offers a potential alternative to traditional acid-mediated mechanisms. Examples of this type of process have been reported previously for catalyst systems based on Pd, Ru, and Ir; however, all of these processes suffer from low selectivity, low yield, or both.

$\text{Pd}(\text{OAc})_2$ has been reported to catalyze the conversion of arenes and olefins to vinyl arenes, although with low selectivity. It was hypothesized that the addition of ligands to $\text{Pd}(\text{OAc})_2$ could offer the opportunity to tune the selectivity of oxidative arene vinylation reactions. A variety of bidentate and tridentate nitrogen and phosphine ligands were screened for activity and selectivity in oxidative benzene vinylation experiments to determine which could bias the selectivity towards styrene. The Pd(II) complex $(^{\text{dipp}}\text{DAB})\text{Pd}(\text{OAc})_2$ [$^{\text{dipp}}\text{DAB} = N,N'$ -bis(2,6-di-isopropylphenyl)-2,3-dimethyl-1,4-diaza-

1,3-butadiene] was the most selective for the formation of styrene over stilbene or biphenyl, two common byproducts in these reactions. Catalytic reactions with $(^{\text{dipp}}\text{DAB})\text{Pd}(\text{OAc})_2$ using a $\text{Cu}(\text{OAc})_2$ oxidant afforded reasonable yields of styrene with high selectivity for stilbene or biphenyl.

Performing catalysis under aerobic conditions, which allows for aerobic regeneration of the Cu oxidant in a manner akin to the Wacker process, afforded styrene in excess of 3000 turnovers. Unfortunately, under aerobic conditions, significant production of vinyl acetate (~ 700 turnovers) was also observed. This prompted us to re-examine control reactions with $\text{Pd}(\text{OAc})_2$ alone under optimized aerobic conditions, which showed that while reported reactions with $\text{Pd}(\text{OAc})_2$ alone afforded $\sim 34\%$ selectivity for styrene, selectivity under our optimized conditions was $\sim 84\%$ for both $\text{Pd}(\text{OAc})_2$ and $(^{\text{dipp}}\text{DAB})\text{Pd}(\text{OAc})_2$.

The lack of selectivity observed for catalysis with Pd(II) complexes prompted us to shift our focus to isoelectronic Rh(I) complexes. The rhodium catalyst $(^{\text{Fl}}\text{DAB})\text{Rh}(\text{TFA})(\eta^2\text{-C}_2\text{H}_4)$ [$^{\text{Fl}}\text{DAB} = N,N'$ -bis(pentafluorophenyl)-2,3-dimethyl-1,4-diaza-1,3-butadiene; TFA = trifluoroacetate] converts benzene, ethylene and air-recyclable Cu(II) oxidants to styrene with yields $\geq 95\%$ (based on Cu(II) as the limiting reagent) and with quantitative selectivity. Turnover numbers > 800 have been demonstrated with catalyst stability up to 96 hours.

Examining catalysis with the complex $(^{\text{Fl}}\text{DAB})\text{Rh}(\text{OAc})(\eta^2\text{-C}_2\text{H}_4)$ shows that the reaction rate has a dependence on catalyst concentration between first- and half-order that varies with both temperature and ethylene concentration, a first-order dependence on ethylene concentration with saturation at higher concentrations of ethylene, and a zero-

order dependence on the concentration of Cu(II) oxidant. The kinetic isotope effect was found to vary linearly with the order in (^{F1}DAB)Rh(OAc)(η^2 -C₂H₄), exhibiting no KIE when [Rh] was in the half-order regime, and a k_H/k_D value of 6.7(6) when [Rh] was in the first-order regime. From these combined experimental and computational studies, competing pathways, which involve all monomeric Rh intermediates and a binuclear Rh intermediate in the other case, were proposed.

Finally, a number of promising new applications for this research are discussed. In addition to summarizing other promising developments based on this research, preliminary results investigating the impact of the carboxylate moiety on the selectivity of oxidative arene vinylation reactions using α -olefins are described. Work on the development of aerobically-stable Rh(I) complexes for oxidative arene vinylation is also discussed, as well as efforts to transition to inexpensive Ni(II) catalysts for arene vinylation. Results from the projects discussed herein are then summarized to provide insight into new catalyst design.

DEDICATION

*For Majestic Cedarwood, Onyx P. Dition, and Nessarose,
my faithful companions.*

*And for Thomas Leavitt, Jr. M.D.,
my loving grandfather and scientific inspiration.*

ACKNOWLEDGEMENTS

At the end of this five year journey, I wish I could say that I had time to sit down and reflect on everything I've done during my whirlwind of a graduate career, but the truth is that I haven't stopped moving yet, and my reflection has been more like a year long retrospective that's taken approximately 0.1% of my focus at sporadic points throughout the year. Now that I've made it to the finish, there are a great many people who help me get here who need to be recognized.

I've enjoyed science and technology since I was a young child. That being said, I always considered it more to be a hobby than a job. During my years in the Montessori educational system, I enjoyed all the subjects I was learning equally. Nothing was made too serious as to not be enjoyable. For this, I have to thank the exceptional educators at Cornerstone, assembled and led by the fearless and dynamic Margaret Rice, who made my education at Cornerstone unique.

While everyone at Cornerstone made my time there special, I would be remiss if I didn't acknowledge my Lower Elementary teachers Janice Darling and Kathy Doar, who taught us time management and subjects based on practical life applications. I will never forget learning fractions through cooking and how I was always encouraged to read the biggest books I could find. Where else would you find elementary school teachers who not only trusted their students to manage their own time but also encouraged a second grader to read the Lord of the Rings?

This encouragement continued in Upper Elementary, with Rob Keys and Gunnar MacCormick for my first year, and Deanna Rieden-Carson after that. In Upper El, we took on tasks like planning and budgeting a trip to Newfoundland, built our own

darkroom and learned about the chemistry of developing film and photos, and staged theater productions that we wrote and directed ourselves. We learned mentoring and management alongside science and humanities and had fun along the way.

My time in the Junior Class with Gunnar, Chris Rainville, and Gary Davidson was some of the most valuable of my entire Cornerstone education. Learning algebra with Gunnar was just as much fun as reading Shakespeare and learning about British history with Chris. Gary taught us practical life lessons about how to start a business and how to conduct ourselves in a professional setting. We prepped for the SSATs with Chris, and practiced writing 5 paragraph essays about every topic under the sun. My go-to example of one of the ridiculous essay topics we were given is “Chickens are better than turkeys. Discuss.” The ability to write about any topic is a skill that helped me survive high school, college, graduate school, and I’m sure will prove invaluable for my future career in patent law. I cannot say enough to convey my gratitude toward everyone at Cornerstone for giving me the strongest educational foundation that anyone could ask for.

After my time at Cornerstone, I moved to St. Thomas Aquinas High School for what proved to be a trying first year. The introduction of teachers who didn’t trust my ability to manage my own time combined with actual graded assessments proved exceptionally challenging. While the overall process was overwhelming, I grew to thrive, and came out all the stronger for it. My survival at STA is entirely due to the exceptional teaching and support provided by a select number of teachers who made my high school experience bearable.

After a number of years of being told that I was stupid because I didn’t think about math problems the same way the teachers did, Diane Casselberry reminded me that my

atypical way of thinking about math problems was actually an asset and not a curse. When confronted with teachers who didn't trust me to manage my own time, English teachers like Alysson Parker and Kathleen Collins valued my writing skills and trusted that I had done the reading even when my learning disabilities meant that while I could discuss the reading assignment in depth, I would fail the multiple choice reading check quiz. Science was somewhere I always felt at home, with teachers like Susan Graham and Ron Holtz who encouraged me to excel and thrive. Laverne Burrigde helped me learn to cope with my medical issues and was there when I needed someone to talk to, or when I really didn't feel like going to AP Stats class.

Through it all, Daryl Robertson was my rock. I had been singing in choirs since I was 7, but I had never learned to harness my talent and put it to use until joining the music program at STA. D-Rob had built an impressive music program with 13 performing ensembles that was one of the best in New England, which was a superhuman feat for one person to run. I learned what it was like to compete in (and win) choir competitions up and down the eastern seaboard, how to arrange music and conduct choirs, how to organize a concert, and more than that, I learned what it was like to be part of a team. D-Rob taught us all how to excel, to thrive, and he taught us that hard work and dedication could turn two groups of kids from southern New Hampshire into the top-ranked jazz and select choirs in the northeast. D-Rob was a friend, a teacher, and a mentor, and the world is a worse place without him in it.

Starting my undergraduate career at the University of Vermont made me feel like I had finally found my place. I was surrounded by others who loved to learn and faculty and staff that were passionate about teaching. To Emily Manetta, thank you for being an

inspiration, and for showing me that an analytical mind can be just as much of an asset in linguistics as it is in chemistry. To Angie Gatesy, thank you for teaching me everything I know about blowing glass, dealing with troublesome professors, and being there when I just needed someone to talk to. I would've been hard-pressed to survive my undergraduate career without these two incredible women.

To Rory Waterman (who will always be the “boss man”), thank you for introducing me to the joys of research. You made me feel like a valued member of the lab, even as an undergraduate, and the four years I spent working for you were some of the best of my life. Our lab lunches at RiRa, working side-by-side with you in the glovebox, and trying to convince you that my half-baked ideas about what was going on in my organometallic reactions were possible (based on barely having a year of Gen Chem under my belt) are memories I will always cherish. I will never forget that, without fail, any time you sent me in the lab with instructions to use a particular reagent and I couldn't find it, you could walk in and find it within 30 seconds (it was always exactly where you said it would be). You taught me that good research was based on curiosity, not flash, and that my interest in my research was more important than anyone else's. You taught me how to give a good talk and how to write a good paper. You, Sarah, and Mae were like a second family to me, and words cannot express how grateful I am. I cannot overstate the value of everything I learned from you, and I'm looking forward to being closer to home so I can come visit more often.

As I continued my education at the University of Virginia, I found a new group of peers and mentors both inside and outside of the chemistry department. In particular, I had the opportunity to interact with an amazing group of students, faculty, staff, and

administrators through my work with the graduate student council. To Dean Ed Barnaby, thank you for everything you have taught me about academic administration and management. You have been a valued colleague and academic inspiration, and it has been a pleasure growing together at UVA. To Dean Aaron Laushway, thank you for teaching me diplomacy, the way of the world, and that a wine & cheese reception will always be popular and well attended. Without your help, support, and advice, I'm sure I would have run Grad Council into the ground during my tenure as President, and I probably would have killed one particular administrator who shall remain nameless... To Amy Clobes, thank you for helping me figure out what I wanted to do with my life, reading through countless cover letters, and ultimately helping me ace my interview for the job of my dreams. These three amazing people were instrumental in my development into a well-rounded individual with the necessary skills to succeed in the career of my choosing.

To Molly Angevine, thank you for always being there for me. Whether I was having a bad day in lab, there was a massive organizational snafu with Grad Council (probably relating to orientation), or I had something to celebrate, you were always up for grabbing coffee (if I needed to vent or just take a break) or a glass of wine (if we were celebrating!). I could not have stayed sane (well, as sane as I have) without your help. You are a true friend, and I hope you know how much I value you.

To Chuck Arrington, thank you for the support and faith you have shown in me over the years. You've always been there to help when I didn't know what to do with a problem student, or just needed to vent, and I appreciate it more than you know. To Cindy Knight, thank you for the constant help and advice you give to all of us. I don't

know how you do what you do without going crazy, but you have always been there for me when I needed a helping hand, and you've always been able to make me smile when I was ready to scream or cry. You already know this, but this department would not run without you. The three of you have been valuable colleagues and friends to me these last five years, and I could not have done it without you.

To all the members of the Gunnoe group, past and present, thank you for all your help, hard work, and friendship. It's been a wild ride, and the end is bittersweet. To Joanna Webb, thank you for putting up with my enthusiastic naïveté when I joined the lab, and for not killing me when I asked you all sorts of questions while you were writing your thesis. Now that I'm there, I understand how frustrating the constant interruptions probably were! To Jeremy Andreatta, when I started in the Gunnoe lab all those years ago, you helped me get my bearings even when I managed to piss off Evan, Joanna, and Samantha in my first week. Thank you for being a friend and mentor, and I'm glad we are still close to this day.

To George Fortman, thank you for teaching me everything I know about building reactors, fixing gloveboxes, and turning crazy ideas about chemistry into something practical. To Evan, Samantha, and Kathleen, thank you for keeping the trains on the tracks. I miss talking about chemistry and venting with you all about the stupid things people were doing in the lab!

To my minion John Gordon, thank you for being the best undergrad a senior graduate student could ask for. Your intellect and independence in the lab are truly assets, and you have become a good friend as well. Wherever you land, I know you will go on to do amazing things, and I wish you the best of luck!

To Brad McKeown, thank you for being a friend and mentor to me at the beginning and end of my career in the lab. When I started in the lab, you were an invaluable resource, helping me understand the background and implications of my results. I was thrilled when Brent hired you back to help run the group, and I was honored to be invited to yours and Katie's wedding. You are a gentleman and a scholar, and I wish you all the best in your future endeavors.

To Nichole Schwartz, I have to confess, I was skeptical when I heard that there was a 19-year-old that wanted to come to UVA to work for Brent, but since you arrived, you have run circles around your peers and proven yourself to be an asset to the group. Thank you for reading numerous drafts of job applications, papers, and thesis chapters when there was nobody else to share the burden with you. I'm also sorry to have thrust all of the group jobs and responsibilities I've accumulated over the years onto you, but I know that you will manage them admirably. I couldn't have picked a better student to replace me; consider the mantle officially passed.

To Dean Harman, Lin Pu, and Cam Mura, my committee who saw me through the endeavor that was my candidacy exam, I am eternally grateful that you all saw fit to give me a second chance, and for the advice you've given me over the years. To Bob Burnett and Linda Columbus, who helped me understand what was going on when I found out that I did not pass my candidacy exam the first time, I cannot express how grateful I am for your care and compassion, and I would not have made it through the second time without you. To Bob Davis, thank you for agreeing to be my external committee member and for your help on our collaborative paper.

To Charlie Machan, thank you for being a valuable friend and colleague and for agreeing to be on my committee even though you had just joined the department. In the short time you've been a part of the department, you've reminded me that I could still have fun in the lab, and that means more to me than you know. I truly appreciate everything you have done for me, and I know you will go on to be an amazing PI and run a thriving research program. Give me a call when you're ready to file your first patent! You and Amanda have been so caring and kind to me, and you had better keep in touch and send lots of pictures of Hattie as she grows up!

To Brent Gunnoe, thank you for seeing me through the marathon that is graduate school. Being in your group, I have learned how to be a mentor, a leader, and how to be confident in the face of doubt. I'm proud of the work that I have done while I have been in your group, and I'm honored to have authored your first *Science* paper. We've had our ups and downs, but at least we've always seen eye-to-eye when it comes to being OCD about presentations and posters. I'll still never understand how people can't tell the difference between a superscript letter O and a degree sign, and when people can't recognize the difference between Times New Roman and Arial; I've found a kindred spirit in you in this regard. And you can take pleasure in the fact that after 5 years, whenever I edit a paper, it comes out sounding like your writing style. You, Trecia, and Leah have been incredibly thoughtful and caring throughout my time here, and I greatly appreciate it.

Throughout it all, my friends have always been there to support me when I needed them the most. Christine Williams and Kati Taylor, we've been through some crazy times together! From all the craziness with Hilltop, to getting kicked out of the hot tub at Kati's

wedding, you've both always been there for me, and it means so much to me. To Meghan Roy, you're officially the only friend from high school I still keep in touch with, and it's probably because we legitimately share the same brain most of the time. I'm glad you're enjoying life in Texas, but I'm glad I'll get to see you at holidays with my other mother now! I know that no matter where we all are in the world, and how long it has been since we've talked, we can pick up the phone and talk like we saw each other yesterday. The three of these crazy ladies have been the closest thing I have to sisters, and I love them more than words can say.

To Lise Harbom, I'm quite confident I wouldn't have made it through this without you. You have always been there for me when I needed support, whether it be drinks at lunchtime when I needed to get away from lab to avoid killing one of the young grad students, or just a good old fashioned bitch session when I'd had a bad day in lab. Together we have built the First Harmonics into a force to be reckoned with, and I know that it will continue to thrive in your hands once I'm gone. Your next responsibility is to go get that postdoc in Australia so I can come and visit you! To Chet Szwejkowski, thank you for stepping in to take over the musical directing for the group when I had to leave 2 months earlier than planned. You'll do great, just remember to kick ass and take names, and don't forget that we aren't the Pentatonix! To Meaghan Szwejkowski, thank you for being an amazing member of the group, and more importantly, for introducing me to my big black pup Nessa. For anyone else reading this, never tell your friend who runs the SPCA exactly what you're looking for in a dog unless you're prepared to get one the next day.

To Scott and Lindsey Ugrin, you were some of my first and best friends in Charlottesville, and I'm better off for having you in my life. Thank you for letting me do my laundry at your house when I was too poor to afford the coin-op laundry at my first apartment complex here, and accepting a home-cooked meal as the only payment. You and your families have made me feel so loved throughout my time here, and it was so much fun to meet all your friends from home I had heard stories about when I was the "Jack of All Trades" at your wedding. You both are amazing friends, and I hope that we stay close, wherever the job market takes you both.

To Lissa Anderson, thank you for being an amazing roommate, colleague and friend. You may not know this, but talking with you about a cappella at my visitation weekend is one of the things that helped me decide to come to UVA. I miss our joint group meetings in Room 1, and singing together in beautiful harmony whenever the occasion warranted, though I'm sorry I regularly forgot that I was supposed to be singing the melody.

To Maura Belanger, thank you as well for being an amazing roommate and friend. You're the real MVP, because if you hadn't been able to take care of Nessa in the evenings as often as you have, this dissertation wouldn't have gotten written. I'll miss our lazy weekends on the couch ordering takeout and far too many donuts, and how Nessa would always sneak into your room to cuddle with you once she thought I'd left for the day. Thank you for everything, but most of all, for putting up with me.

To all of my Grad Council friends, including Amy Grady, Evan Wolfe, Alex Natoli, Nick Rich, Stephanie Miller Lehman, Tony Boese, Kristin Connor, and Leeza Constantoulakis, thank you for some amazing fun times. I wouldn't have been able to build council into the successful organization that it is today without your help.

Finally, to my family, thank you for supporting me and providing me with much needed encouragement throughout this 26-year journey. To my Mom and Dad, you have always supported me, no matter what. I have lived most of my life by hearing your opinions and recommendations, and often making decisions that directly contradicted what you thought I should do. I want you to know that I really did hear what you had to say, and I truly do value your opinions, even if I don't always show it. Thank you for believing in me, even when it seemed like I was destined to fail. And thank you for always being there for me, whether it was when I couldn't afford groceries and payday wasn't for another week, or this past year when I would get a rejection from a job I had applied for, or I just generally felt hopeless while writing this dissertation, you were always just a phone call away.

To my grandfather, Thomas Leavitt, thank you for being my inspiration for going into science. As the only other doctor in the family, you always seemed to understand my thought process better than anyone else, and I am a better person for having earned your respect. I am grateful that you shared some of your life experiences with me toward the end, and I am still humbled by the groundbreaking you performed in your day. While you got to see my first paper published all those years ago, I regret that you will not get to see me at the finish line of this journey.

If you have read this far and haven't found your name, know that you were not forgotten. As you can see, I've rambled on for a good 10 pages now, and eventually someone is going to cut me off. That being said, everyone I've known has made an impact on my life and my journey in some way, so if you manage to track me down, not being mentioned by name is a perfect excuse to convince me that I owe you a beer.

LIST OF FIGURES	XVIII
LIST OF SCHEMES.....	XXIII
LIST OF TABLES.....	XXV

1. Introduction.....	1
1.1 Catalysis with Organometallic Complexes.....	1
1.1.1 History/Background	1
1.1.2 Transition Metal Catalyzed C–C Bond Forming Reactions.....	2
1.1.2.1 C–C Coupling Reactions Based on C–X Activation	2
1.1.2.2 C–C Coupling Reactions Based on C–H Activation	3
1.1.2.3 Mechanisms for C–H Activation	4
1.1.3 Metrics for Comparing Catalysts	6
1.1.4 Elucidating the Nature of the Active Catalyst.....	9
1.2 Industrial Process Chemistry	11
1.2.1 Overview	11
1.2.2 Nature of Industrial Catalytic Systems.....	11
1.2.3 Process Chemistry and Industrial Viability.....	15
1.2.4 Alkyl and Vinyl Arenes.....	17
1.2.4.1 Friedel-Crafts Catalysis	18
1.2.4.2 Zeolites.....	20
1.3 Transition Metal-Catalyzed Olefin Hydroarylation.....	21
1.3.1 Overview	21
1.3.2 Ruthenium(II) Catalysts	22
1.3.3 Iridium(III) Catalysts.....	23
1.3.4 Platinum(II) Catalysts.....	24
1.4 Thesis Aims	26
1.5 References.....	27
2. Study of Palladium Catalysts for the Oxidative Vinylation of Benzene.....	33
2.1 Introduction	33
2.2 Results and Discussion.....	35
2.2.1 Optimization of Selectivity for Stoichiometric Reactions	35
2.2.2 Optimization of Catalytic Conditions.....	37
2.2.3 Oxidative Vinylation of Benzene Using O ₂ as the Terminal Oxidant	38
2.3 Summary and Conclusions.....	40

2.4	Experimental.....	41
2.5	References	45
3.	Development and Mechanistic Studies of a Rhodium Catalyst for the Oxidative Vinylation of Benzene	47
3.1	Introduction	47
3.2	Catalyst Development	52
3.2.1	Optimization of Reaction Conditions with 1-TFA.....	53
3.3	Mechanistic Studies of Catalysis with 1-OAc.....	60
3.3.1	Apparent Induction Period	61
3.3.2	Testing for Nanoparticle Formation	61
3.3.3	Comparison of Catalysis with 1-TFA and 1-OAc.....	65
3.3.4	Computational Studies: Overview.....	68
3.3.5	Computational Studies: Selectivity for Styrene	75
3.3.6	Kinetic and Mechanistic Studies	77
3.3.7	Proposed Mechanism for the Catalytic Cycle.....	93
3.4	Summary and Conclusions	104
3.5	Experimental.....	105
3.6	References	121
4.	Advances in Catalyst Development for the Direct Synthesis of Alkyl and Alkenyl Arenes: Mechanistic Insights and Future Outlook.....	126
4.1	Overview	126
4.2	Ruthenium(II) Catalysts	127
4.3	Platinum(II) Catalysts.....	130
4.4	Rhodium(I) Catalysts.....	133
4.5	Aerobic Arene Vinylation	135
4.6	Comparison of Mechanisms	137
4.6.1	Selectivity for Styrene or Ethylbenzene	137
4.6.2	Potential Formation of η^3 -allyl Complexes.....	141
4.7	Looking Forward: Future Outlook and Insights into Catalyst Design	142
4.7.1	Future Outlook	142
4.7.2	Impact of Metal–Carboxylate Functionality	143
4.7.3	Development of Air-Stable Rh(I) Catalysts for Styrene Production.....	145
4.8	References	146

LIST OF FIGURES

- Figure 1.1. Structure of ZSM-5 Zeolite. Babu, K.; Gadre, S.R.; *J. Comput. Chem.* 2004, 24, 484. Reproduced with permission. 21
- Figure 1.2. Correlation of Ru(III/II) Potential with TON for Ethylene Hydrophenylation using TpRu(L)(NCMe)(Ph) Complexes. 23
- Figure 3.1. Plots of TO for styrene production vs. time as a function of oxidant using (^{F1}DAB)Rh(TFA)(η^2 -C₂H₄) (1-TFA). A) Cu(OAc)₂, B) Cu(TFA)₂, C) Cu(OPiv)₂, D) Cu(OHex)₂. Reaction conditions: 0.001 mol % 1-TFA, 25 psig C₂H₄, 120 equivalents oxidant, 150 °C, theoretical maximum TON = 60. Data for two independent runs are shown for each oxidant. 54
- Figure 3.2. Effect of oxidant amount on styrene production using (^{F1}DAB)Rh(TFA)(η^2 -C₂H₄) (1-TFA). Reaction conditions: 0.001 mol % 1-TFA, 25 psig C₂H₄, 120 °C. Percent yield is reported relative to oxidant, assuming 2 equivalents are required per TO. Data for two independent runs are shown for each oxidant amount. 55
- Figure 3.3. TO vs. Time plot for catalysis with 0.0001 mol % (^{F1}DAB)Rh(TFA)(η^2 -C₂H₄) (1-TFA). Reaction conditions: 0.0001 mol % 1-TFA, 2400 equiv. Cu(OAc)₂, 75 psig C₂H₄, 150 °C, theoretical maximum TON = 1200. Data for two independent runs are shown. 56
- Figure 3.4. Effect of temperature on styrene production using (^{F1}DAB)Rh(TFA)(η^2 -C₂H₄) (1-TFA). Reaction conditions: 0.001 mol % 1-TFA, 120 equivalents Cu(OAc)₂, 25 psig C₂H₄. Data for two independent runs are shown for each temperature. 56
- Figure 3.5. Effect of ethylene pressure on catalysis with (^{F1}DAB)Rh(TFA)(η^2 -C₂H₄) (1-TFA). Reaction conditions: 0.001 mol % 1-TFA, 120 equivalents Cu(OAc)₂, 150 °C, 4 h. 58
- Figure 3.6. Mass spectra for kinetic isotope effect experiments using a 1:1 molar mixture of C₆H₆ and C₆D₆. Reaction conditions: 5 mL C₆H₆, 5 mL C₆D₆, 0.001 mol % 1-TFA, 200 equiv. Cu(OAc)₂, 50 psig C₂H₄, 150 °C. 59
- Figure 3.7. TO vs. time plot for catalysis with 1-TFA. Reaction conditions: 0.112 mM 1-TFA, 20 mL C₆H₆, 25 psig ethylene, 13.4 mM Cu(OAc)₂ (120 equiv. relative to 1-TFA), 150 °C. Each data point is the average of two independent catalytic reactions, each analyzed in duplicate by GC/FID. Error bars represent the standard deviation of all four values. 61
- Figure 3.8. TEM images of unwashed samples from catalysis with 1-TFA. Energy-dispersive X-ray spectroscopy (EDS) was performed on areas circled in red. Reaction conditions for catalysis: 0.112 mM 1-TFA, 20 mL C₆H₆, 50 psig ethylene, 13.4 mM Cu(OAc)₂, 150 °C, 12 h. 63
- Figure 3.9. TEM images of samples from catalysis with 1-TFA sonicated in 1,4-dioxane. EDS was performed on areas circled in red or the whole area of the image if no circle is shown. Reaction conditions for catalysis: 0.112 mM 1-TFA, 20 mL C₆H₆, 50 psig ethylene, 13.4 mM Cu(OAc)₂, 150 °C, 12 h. 64

- Figure 3.10. TO vs. time plot with the reaction solution filtered at 3 h. Reaction conditions: 0.112 mM 1-TFA, 20 mL C₆H₆, 50 psig ethylene, 13.4 mM Cu(OPiv)₂ (120 equiv. relative to 1-TFA), 150 °C. Each data point is the average of two independent catalytic reactions, each analyzed in duplicate by GC/FID. Error bars represent the standard deviation of all four values. 65
- Figure 3.11. A) [Styrene] vs. time plot for catalysis with 1-TFA and 1-OAc using Cu(OPiv)₂ as the oxidant. Reaction conditions: 0.112 mM 1-TFA or 1-OAc, 20 mL C₆H₆, 13.4 mM Cu(OPiv)₂ (120 equiv. relative to 1-TFA or 1-OAc), 50 psig C₂H₄, 150 °C. Data for 1-OAc are offset from t = 0.5 h to t = 1.5 h to overlap with data from 1-TFA, and non-offset times are labeled in red. B) [Styrene] vs. time plot for catalysis with 1-OAc from Figure 3.11A without time offset, which is consistent with the absence of an induction period. Each data point is the average of two independent catalytic reactions, each analyzed in duplicate by GC/FID. Error bars represent the standard deviation of all four values. 67
- Figure 3.12. TO vs. time plot for catalysis with 1-TFA using Cu(OAc)₂ or Cu(TFA)₂ as the oxidant. Reaction conditions: 0.112 mM 1-TFA, 20 mL C₆H₆, 13.4 mM CuX₂ (120 equiv. relative to 1-TFA), 25 psig C₂H₄, 150 °C. Each data point is the average of two independent catalytic reactions, each analyzed in duplicate by GC/FID. Error bars represent the standard deviation of all four values. 68
- Figure 3.13. Ball and stick model of isotropically refined core structure of 1D-OAc. CH₃ groups on one of the DAB backbones and C₆F₅ groups were not located, and the positions of hydrogens in the entirety of the structure were not calculated. 69
- Figure 3.14. Optimized calculated geometries for the transition states for benzene C–H activation by (A) (^F1DAB)Rh(η²-C₆H₆)(TFA) (2-TFA), and (B) (^F1DAB)Rh(η²-C₆H₆)(OAc) (2-OAc). Bond lengths in Å. 73
- Figure 3.15. Concentration of styrene vs. time plot for the initial rate regime of catalysis with 1-OAc at various ethylene pressures/concentrations: 35 psig (slope = 0.0031), 50 psig (slope = 0.0055), 75 psig (slope = 0.009), and 100 psig (slope = 0.011). Reaction conditions: 20 mL C₆H₆, 0.11 mM 1-OAc, 13.4 mM Cu(OPiv)₂, 150 °C. Data for two independent reactions at each concentration level are shown. Data for initial time points were used to calculate *k*_{obs}. 79
- Figure 3.16. Log-log plot of observed rate constant as a function of concentration of C₂H₄ (slope = 1.02(8), R² = 0.99). Reaction conditions: 0.11 mM 1-OAc, 20 mL C₆H₆, 13.4 mM Cu(OPiv)₂, 150 °C. Each data point represents the average of two independent catalytic reactions, each analyzed in duplicate by GC/FID. Error bars represent the standard deviation of all four values. 79
- Figure 3.17. Concentration of styrene vs. time plot for the initial rate regime of catalysis with 1-OAc at various concentrations of Cu(OPiv)₂: 13.4 mM (slope = 0.0048, R² = 0.99), 19.0 mM (slope = 0.0046, R² = 0.99), 26.9 mM (slope = 0.0044, R² = 0.99), 38.1 mM (slope = 0.0041, R² = 0.99), and 53.8 mM (slope = 0.0038, R² = 0.99). Reaction conditions: 20 mL C₆H₆, 0.11 mM 1-OAc, 50 psig C₂H₄, 150 °C. Data for two independent reactions at each concentration level are shown. 80

- Figure 3.18. Log-log plot of observed rate constant as a function of concentration of $\text{Cu}(\text{OPiv})_2$ (slope = $-0.17(2)$, $R^2 = 0.99$). Reaction conditions: 0.11 mM 1-OAc, 20 mL C_6H_6 , 50 psig C_2H_4 , 150 °C. Each data point represents the average of two independent catalytic reactions, each analyzed in duplicate by GC/FID. Error bars represent the standard deviation of all four values..... 81
- Figure 3.19. Concentration of styrene vs. time plot for the initial rate regime of catalysis with 1-OAc at 50 psig C_2H_4 with various catalyst concentrations: 0.23 mM (slope = 0.0077, $R^2 = 0.98$), 0.17 mM (slope = 0.0059, $R^2 = 0.99$), 0.112 mM (slope = 0.0048, $R^2 = 0.99$), 0.079 mM (slope = 0.0035, $R^2 = 0.97$), and 0.056 mM (slope = 0.0025, $R^2 = 0.97$). Reaction conditions: 20 mL C_6H_6 , 26.9 mM $\text{Cu}(\text{OPiv})_2$, 50 psig C_2H_4 , 150 °C. Data for two independent reactions at each concentration level are shown..... 82
- Figure 3.20. Concentration of styrene vs. time plot for the initial rate regime of catalysis with 1-OAc at 35 psig C_2H_4 with various catalyst concentrations: 0.23 mM (slope = 0.0048, $R^2 = 0.96$), 0.112 mM (slope = 0.0034, $R^2 = 0.99$), and 0.056 mM (slope = 0.0022, $R^2 = 0.99$). Reaction conditions: 20 mL C_6H_6 , 26.9 mM $\text{Cu}(\text{OPiv})_2$, 35 psig C_2H_4 , 150 °C. Data for two independent reactions at each concentration level are shown..... 82
- Figure 3.21. Concentration of styrene vs. time plot for the initial rate regime of catalysis with 1-OAc at 75 psig C_2H_4 with various catalyst concentrations: 0.23 mM (slope = 0.0176, $R^2 = 0.99$), 0.112 mM (slope = 0.0089, $R^2 = 0.99$), and 0.056 mM (slope = 0.0047, $R^2 = 0.99$). Reaction conditions: 20 mL C_6H_6 , 26.9 mM $\text{Cu}(\text{OPiv})_2$, 75 psig C_2H_4 , 150 °C. Data for two independent reactions at each concentration level are shown..... 83
- Figure 3.22. Log-log plot of observed rate constant vs. $[\text{1-OAc}]$ at 35 psig of C_2H_4 (slope = 0.58, $R^2 = 0.99$), 50 psig of C_2H_4 (slope = 0.67, $R^2 = 0.99$), and 75 psig of C_2H_4 (slope = 0.96, $R^2 = 0.99$). Reaction conditions: 20 mL C_6H_6 , 26.9 mM $\text{Cu}(\text{OPiv})_2$, 150 °C..... 83
- Figure 3.23. Concentration of styrene vs. time plot for the initial rate regime of catalysis with 1-OAc at 130 °C with various catalyst concentrations: 0.23 mM (slope = 0.003, $R^2 = 0.99$), 0.112 mM (slope = 0.0017, $R^2 = 0.96$), and 0.056 mM (slope = 0.0009, $R^2 = 0.99$). Reaction conditions: 20 mL C_6H_6 , 26.9 mM $\text{Cu}(\text{OPiv})_2$, 30 psig C_2H_4 , 130 °C. Data for two independent reactions at each concentration level are shown..... 84
- Figure 3.24. Concentration of styrene vs. time plot for the initial rate regime of catalysis with 1-OAc at 160 °C with various catalyst concentrations: 0.23 mM (slope = 0.0126, $R^2 = 0.99$), 0.112 mM (slope = 0.0084, $R^2 = 0.99$), and 0.056 mM (slope = 0.0051, $R^2 = 0.99$). Reaction conditions: 20 mL C_6H_6 , 26.9 mM $\text{Cu}(\text{OPiv})_2$, 60 psig C_2H_4 , 160 °C. Data for two independent reactions at each concentration level are shown..... 84

- Figure 3.25. Log-log plot of observed rate constant vs. [1-OAc] at 130 °C (slope = 0.83, $R^2 = 0.99$), 150 °C (slope = 0.67, $R^2 = 0.99$), and 160 °C (slope = 0.64, $R^2 = 0.99$). Reaction conditions: 20 mL C_6H_6 , 26.9 mM $Cu(OPiv)_2$ 85
- Figure 3.26. Mass spectra for kinetic isotope effect experiments using a 1:1 molar mixture of C_6H_6 and C_6D_6 . Reaction conditions: 5 mL C_6H_6 , 5 mL C_6D_6 , 0.112 mM 1-OAc, 26.9 mM $Cu(OPiv)_2$, 50 psig C_2H_4 , 150 °C. 87
- Figure 3.27. Mass spectra for H/D exchange experiments using a 1:1 molar mixture of C_6H_6 and C_6D_6 . Reaction conditions: 5 mL C_6H_6 , 5 mL C_6D_6 , 0.112 mM 1-OAc, 13.4 mM $Cu(OPiv)_2$, 150 °C. 89
- Figure 3.28. Mass spectra for H/D exchange experiments with added CD_3COOD . Reaction conditions: 10 mL C_6H_6 , 0.112 mM 1-OAc, 13.4 mM $Cu(OPiv)_2$, 56 mM CD_3COOD , 150 °C..... 90
- Figure 3.29. Mass spectra for H/D exchange experiments with added CD_3COOD and ethylene. Reaction conditions: 10 mL C_6H_6 , 0.112 mM 1-OAc, 13.4 mM $Cu(OPiv)_2$, 56 mM CD_3COOD , 50 psig C_2H_4 , 150 °C. 92
- Figure 3.30. Plot of k_H/k_D vs. order in [Rh] ($R^2 = 0.99$). Reaction conditions: 0.11 mM 1-OAc, 10 mL 1:1 C_6H_6 and C_6D_6 , 26.8 mM $Cu(OPiv)_2$, 35-150 psig C_2H_4 , 150 °C. Order in [Rh] (and the corresponding horizontal error bars) was determined using the data shown in Figure 3.25. Each data point represents the average of three independent catalytic reactions, each analyzed in triplicate by GC/MS. Vertical error bars represent the standard deviation of all nine values. 101
- Figure 3.31. Plot of k_{obs} vs. [C_2H_4]. Reaction conditions: 0.11 mM 1-OAc, 20 mL C_6H_6 , 13.4 mM $Cu(OPiv)_2$, 150 °C. Each data point represents the average of two independent catalytic reactions, each analyzed in duplicate by GC/FID. Error bars represent the standard deviation of all four values. 102
- Figure 3.32. [Styrene] vs. time plot for the initial rate regime of catalysis with 1-OAc upon the addition of 0 equiv. (slope = 0.005, $R^2 = 0.99$), 500 equiv. (slope = 0.0016, $R^2 = 0.99$), and 1000 equiv. (slope = 0.0008, $R^2 = 0.99$) AcOH relative to the concentration of 1-OAc. Reaction conditions: 20 mL C_6H_6 , 13.4 mM $Cu(OPiv)_2$, 50 psig C_2H_4 , AcOH (0, 500, or 1000 equiv. relative to 1-OAc), 150 °C. Each data point represents the average of two independent catalytic reactions, each analyzed in duplicate by GC/FID. Error bars represent the standard deviation of all four values. ...
..... 103
- Figure 3.33. [Styrene] vs. time plot for the initial rate regime of catalysis with 1-OAc upon the addition of 0 equiv. (slope = 0.012, $R^2 = 0.98$), 500 equiv. (slope = 0.0014, $R^2 = 0.99$), and 1000 equiv. (slope = 0.013, $R^2 = 0.98$) AcOH relative to the concentration of 1-OAc. Reaction conditions: 20 mL C_6H_6 , 13.4 mM $Cu(OPiv)_2$, 400 psig C_2H_4 , AcOH (0, 500, or 1000 equiv. relative to 1-OAc), 150 °C. Each data point represents the average of two independent catalytic reactions, each analyzed in duplicate by GC/FID. Error bars represent the standard deviation of all four values. ...
..... 103

- Figure 4.1. Plot of Hammett σ_p vs. Ethylbenzene:Styrene ratio for ethylene hydrophenylation using $[(^X\text{bpy})\text{Pt}(\text{Ph})(\text{THF})][\text{BAr}^{\text{F}}_4]$. Reprinted (adapted) with permission from reference¹². Copyright 2013 American Chemical Society. 131
- Figure 4.2. Hammett plot for propylene hydrophenylation using $[(^X\text{bpy})\text{Pt}(\text{Ph})(\text{THF})][\text{BAr}^{\text{F}}_4]$. Reprinted (adapted) with permission from reference¹⁶. Copyright 2014 American Chemical Society. 132
- Figure 4.3. Plot of ethylbenzene TO vs. time for catalysis with $^t\text{bpyPt}$ and dpmPt . Reprinted (adapted) with permission from reference¹⁴. Copyright 2013 American Chemical Society. 133
- Figure 4.4. Plot of KIE vs. order in Rh for oxidative arene vinylation using $^{\text{Fl}}\text{DABRhOAc}$. Reprinted (adapted) with permission from reference¹⁷. Copyright 2017 American Chemical Society. 134

LIST OF SCHEMES

Scheme 1.1. General mechanism for Stille coupling.....	2
Scheme 1.2. Mechanisms for C–H Activation.....	4
Scheme 1.3. Catalytic cycle for the Wacker-Hoechst process for ethylene oxidation.	13
Scheme 1.4. Catalytic Cycle for the Monsanto Acetic Acid Process.	14
Scheme 1.5. Catalytic Cycle for Cobalt-Catalyzed Hydroformylation.	15
Scheme 1.6. Comparison of Current Industrial Process for Styrene Production with a Transition Metal-Mediated Process. Reprinted (adapted) with permission from reference ⁵¹ . Copyright 2015 AAAS.	18
Scheme 1.7. Deficiencies of Friedel-Crafts Arene Alkylation.	19
Scheme 1.8. Regioselectivity of Friedel-Crafts Arene Alkylation with α -Olefins.	19
Scheme 1.9. General mechanism for transition metal-mediated olefin hydroarylation. ..	22
Scheme 1.10. Comparison of ethylene hydrophenylation using (acac) ₂ Ir and (trop) ₂ Ir ...	24
Scheme 1.11. Mechanism for ethylene hydrophenylation using ^t bpyPt. Reprinted (adapted) with permission from reference ⁶⁸ . Copyright 2011 American Chemical Society.	26
Scheme 2.1. Oxidative benzene vinylation using [(^t bpy)Pd(Me)(NCMe)][BAr ^F ₄].	35
Scheme 2.2. Comparison of aerobic oxidative benzene vinylation reactions catalyzed by 1 and Pd(OAc) ₂	39
Scheme 3.1. Proposed cycle for transition metal-catalyzed styrene production from benzene and ethylene using CuX ₂ as an oxidant. The cuprous (CuX) product could be recycled to the cupric state using O ₂ from air, as shown at the upper left. Potential side reactions that a selective catalyst must avoid are shown in red.	48
Scheme 3.2. Comparison of Wacker Process and styrene process reported herein.	51
Scheme 3.3. Synthesis of (^{F1} DAB)Rh(TFA)(η^2 -C ₂ H ₄) (1-TFA).	52
Scheme 3.4. Kinetic isotope effect experiment using a 1:1 molar ratio of C ₆ H ₆ to C ₆ D ₆ . Reported isotope effect represents the average of three independent runs, and the deviation is reported in parentheses.	58
Scheme 3.5. Calculated Gibbs free energies [B3LYP/LANL2DZ+6-311++G(d,p)] including solvent (SMD-benzene) and dispersion corrections for the lowest energy calculated pathway for styrene production using complexes 1-OAc (shown in black) and 1-TFA (shown in red) at 423.15 K in kcal/mol. The calculated energies for each reaction are relative to the energy of 1-X (X = OAc or TFA), which is set to zero energy for each reaction. Stationary points without TFA or OAc are degenerate.	70
Scheme 3.6. Comparison of Calculated Free Energies for β -Hydride Elimination to Form Styrene and Benzene C–H Activation to Form Ethylbenzene from (^{F1} DAB)Rh(CH ₂ CH ₂ Ph) [shown in black] and (^t bpy)Pt(CH ₂ CH ₂ Ph) [shown in red] in	

kcal/mol with the Important Energy Differences Between the Two Pathways Highlighted.....	77
Scheme 3.7. Kinetic isotope experiment with 1-OAc using a 1:1 molar mixture of C ₆ H ₆ :C ₆ D ₆ . k_H/k_D value represents the average of three independent catalytic reactions, each analyzed in triplicate by GC/MS. Reported error represents the standard deviation of all nine values.	86
Scheme 3.8. Kinetic isotope experiment with 1-OAc using independent reactions in C ₆ H ₆ and C ₆ D ₆ . k_H and k_D values were determined using the method of initial rates for two independent catalytic reactions each, with all samples analyzed in duplicate by GC/FID. The reported error represents the propagated standard deviation of all values and linear regressions.	86
Scheme 3.9. Proposed Mechanism and Rate Law for Catalysis with 1-OAc.....	95
Scheme 3.10. Rate Law Derivation- King-Altman Method.....	96
Scheme 3.11. Rate Law Derivation- Steady-State Method.....	98
Scheme 4.1. General Catalytic Cycles for A) Hydroarylation of Olefins, and B) Oxidative Arene Vinylation.	126
Scheme 4.2. Comparison of catalysis with TpRuBP, (Pz ⁵) ₃ Ru, and BzTTMRu.....	129
Scheme 4.3. Comparison of oxidative benzene vinylation using (acac) ₂ Rh(Cl)(H ₂ O) and Pd(OAc) ₂	136
Scheme 4.4. Calculated Gibbs Free Energies for β -Hydride Elimination to Form Styrene and Benzene C–H Activation to Form Ethylbenzene from (^{F1} DAB)Rh(CH ₂ CH ₂ Ph) [shown in black] and (^t bpy)Pt(CH ₂ CH ₂ Ph) [shown in red] in kcal/mol with the Important Energy Differences Between the Two Pathways Highlighted.	139
Scheme 4.5. Calculated Gibbs Free Energies for β -Hydride Elimination to Form Styrene and Benzene C–H Activation to Form Ethylbenzene from TpRu(CO)(CH ₂ CH ₂ Ph) in kcal/mol with the Important Energy Differences Between the Two Pathways Highlighted.	139
Scheme 4.6. Comparison of energetics of ethylene C–H activation and ethylene insertion for several reported catalysts with $\Delta\Delta G^\ddagger$ highlighted.	141
Scheme 4.7. Comparison of hydrophenylation of propylene using [(^t bpy)Pt(Ph)] ⁺ and (^t bpy)Pt(OAc) ₂	145

LIST OF TABLES

Table 2.1. Relative ratios of products produced in stoichiometric oxidative benzene vinylation experiments using the <i>in situ</i> generated complexes (Ligand)Pd(OAc) ₂ . ^a	36
Table 2.2. Results of oxidant screening. ^a	37
Table 3.1. Comparison of previously reported catalysts for styrene production. TON = turnover number for styrene. Selectivity is defined as turnovers styrene/total turnovers (all products), and is given as a percentage. Yield of styrene is reported relative to the limiting reagent.	51
Table 3.2. Effect of ethylene pressure on catalysis with (^{F1} DAB)Rh(TFA)(η^2 -C ₂ H ₄) (1-TFA). Reaction Conditions: 0.001 mol % 1-TFA, 120 equiv. Cu(OAc) ₂ , 150 °C, 4 h.	57
Table 4.1. Proposed complexes to examine the linear to branched selectivity for the hydrophenylation of propylene. Group 9 M = Co, Rh, Ir; Group 10 M = Ni, Pd, Pt....	144

1. Introduction

1.1 Catalysis with Organometallic Complexes

1.1.1 History/Background

Organometallic chemistry, the field of chemistry focused on metal–carbon bonds, formally began in 1827 with the discovery of Zeise’s salt, $[\text{K}][(\eta^2\text{-C}_2\text{H}_4)\text{PtCl}_3]$.¹ The discovery of various transition metal–carbonyl complexes and main group metal–alkyl complexes (e.g., Grignard reagents and organolithiums) followed closely behind in the later 1800s.² The 1950s were a prolific time for discoveries in the field, including that of ferrocene, metal-to-ligand π -backbonding, and oxidative addition reactions, which inspired the study of structure and mechanism that still constitutes the basis of modern organometallic chemistry.^{3,4}

One of the most common uses of transition metal complexes today is as catalysts that lower the activation barrier for organic chemical transformations. While catalysis may seem like a more modern application that stemmed from classical inorganic coordination chemistry, the discovery that transition metals can catalyze certain processes actually dates back to the 1800s,⁵ and by the early 1900s, catalysts were being used in industrial process chemistry.¹

A catalyst, by its most basic definition, must meet three criteria: 1) it must lower the activation barrier of the process it is catalyzing; 2) it must be regenerated upon completion of the reaction; and 3) it must be present in a sub-stoichiometric amount.⁶ Catalysts generally fall into one of two main classes: homogeneous catalysts, which exist in the same phase as the reactants, or heterogeneous catalysts, which exist in a different phase as the reactants.⁷ While heterogeneous catalysts are more common in industrial

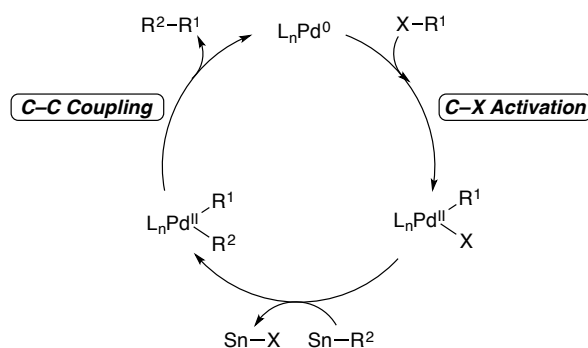
transformations, there are notable examples of homogeneous catalysts for industrial processes (see Section 1.2.2), and homogeneous catalysts are commonly used for fine-chemical transformations.⁸ Homogeneous catalysts also offer advantages in that they are generally easier to study and modify in an effort to tune product selectivity and yield.⁹ There have also been cases where reactions have been optimized using homogeneous catalysts and subsequently commercialized using heterogenized variants of the homogeneous system.⁷

1.1.2 Transition Metal Catalyzed C–C Bond Forming Reactions

1.1.2.1 C–C Coupling Reactions Based on C–X Activation

A variety of catalytic C–C coupling reactions have been developed based on Suzuki, Sonogashira, Stille, Heck, and other related reactions, which operate through C–X activation followed by C–C coupling (Scheme 1.1).¹⁰ These types of reactions have been broadly studied, and variants exhibiting high tolerance of substrates and functional groups while affording high selectivity have been developed.¹⁰

Scheme 1.1. General mechanism for Stille coupling.



While these types of C–C bond forming reactions are useful for fine chemical synthesis, there are a number of drawbacks that prevent their viability for commodity-scale processes. For example, many of these reactions require the use of pre-functionalized (often aryl halide) substrates or stoichiometric transmetallating reagents, use expensive Pd catalysts that often do not afford high turnover numbers prior to deactivation, and result in stoichiometric quantities of halogenated waste.¹¹ These drawbacks make these types of C–C bond forming reactions unsuitable for large-scale processes involving simple hydrocarbons, and as such, there is motivation for the development of new catalytic processes that can afford the C–C coupling of simple hydrocarbons.

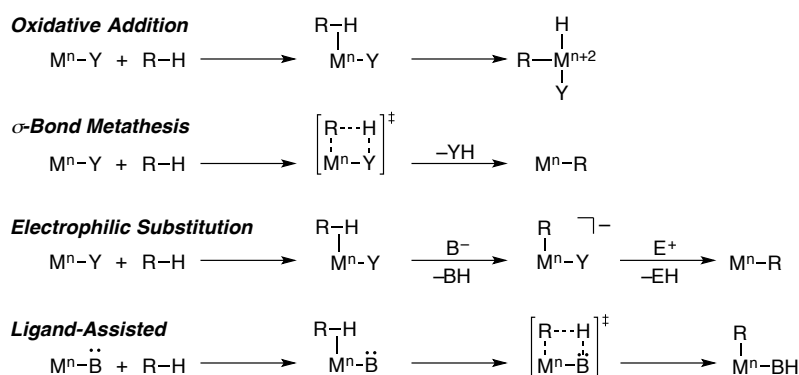
1.1.2.2 C–C Coupling Reactions Based on C–H Activation

C–H functionalization reactions, in which a C–H bond is cleaved and ultimately replaced with a functional group, have the potential to be the most useful transformations in organic chemistry. These types of transformations can allow for selective installation of functional groups in an organic molecule without the need for promoters or directing groups. However, C–H bond activation and functionalization reactions are particularly challenging due to the typically unreactive nature of C–H bonds (BDE = ~95 – 120 kcal/mol).¹² Additionally, even where conditions exist that allow for the activation of C–H bonds, selectivity is often low. For this reason, a main focus of organometallic chemistry over the last half-century has been the development of catalysts that can selectively activate C–H bonds.

1.1.2.3 Mechanisms for C–H Activation

Transition metal catalysts offer a number of advantages in C–H functionalization reactions compared to typical (often acid or radical-based) processes. It is possible to develop catalysts that can selectively activate particular C–H bonds in a given substrate based on sterics or electronics, and they can often activate stronger C–H bonds selectively over weaker ones, unlike traditional methods. There are four general classes of mechanisms by which transition metal-mediated C–H activation can occur (Scheme 1.2), including oxidative addition, σ -bond metathesis, electrophilic substitution, and ligand-assisted C–H activation (which includes concerted metallation-deprotonation, 1,2-CH-addition, etc.).

Scheme 1.2. Mechanisms for C–H Activation.



One type of C–H activation is oxidative addition, which occurs when coordinatively-unsaturated metal complex breaks a C–H bond to form new M–C and M–H bonds.¹³ This reaction results in a net increase of the metal oxidation state by 2, and thus is inaccessible for metal complexes that are already in the d^0 oxidation state. Given that this type of C–H

activation affords a complex with both the resulting carbon and hydrogen fragments bound to the metal center, if C–H functionalization is desired, this reaction must be followed by subsequent functionalization reactions.

C–H σ -bond metathesis can be formally defined as the concerted exchange of a metal–ligand σ -bond with a hydrocarbon C–H σ -bond, resulting in either a new M–C bond with liberation of ligand–H, or a new M–H bond with liberation of ligand–C. σ -Bond metathesis proceeds through a highly ordered 4-center, 4-electron [$2\sigma + 2\sigma$] transition state which is generally accepted to be kite-shaped.¹⁴ This type of C–H activation mechanism results in no net change of metal oxidation state, and therefore is accessible to metals without an available $n+2$ oxidation state.¹⁴

Electrophilic substitution proceeds through coordination of a C–H bond to a coordinatively-unsaturated metal center followed by deprotonation by a base to afford a new M–C bond. Variants of this type of mechanism have also been proposed based on the nature of the scission of the C–H bond of the substrate, whether a M–C adduct is formed as an intermediate or transition state, and whether the base is internal or external to the complex in question.¹³

Ligand-assisted C–H activation encompasses a broad class of reactions in which the ligands on a metal center participate in the C–H activation event.¹⁵ There are numerous examples of this type of mechanism (with many different names assigned to each type), including 1,2-CH-addition (also called internal electrophilic substitution or IES),^{13,16} concerted metallation-deprotonation (CMD),¹⁷ and ambiphilic metal ligand activation (AMLA).^{18,19} Most germane to the work presented herein are carboxylate-mediated C–H activation processes, in which a metal–carboxylate complex coordinates a C–H bond,

which is then deprotonated by the carboxylate ligand to liberate a carboxylic acid and a new M–C complex.

1.1.3 Metrics for Comparing Catalysts

Papers that disclose new homogeneous catalysts for a given transformation often discuss the advantages their catalyst provides over existing technologies. These improvements can be qualitative (i.e., the synthesis of new and desirable products) or quantitative (i.e., the reported catalyst is more active, more selective, or longer-lived than existing catalysts) in nature, and while these types of comparisons are necessary to demonstrate the impact of the research, quantitative measures of improvement in particular are often misused or compared improperly.

Part of the problem is that there is significant debate in the field about the different quantitative metrics used, how they should be defined, and whether it is appropriate to compare catalysts under identical conditions or under the optimal conditions for each.²⁰⁻²³ Commonly used metrics for evaluating catalytic processes are turnover number (TON) and turnover frequency (TOF), which emphasize the role of the catalyst itself, along with an observed rate constant (k_{obs}), conversion, and yield, which provide information about the overall reaction.

To understand the turnover number, the term turnover (TO) must first be defined. A catalytic turnover formally represents 100% yield relative to catalyst, and therefore represents one passage through the catalytic cycle. For example, a process that produces 500% yield relative to catalyst is said to have produced 5 TO of product. The TON is defined as the number of TO completed before catalyst deactivation, that is, the number

of turnovers once the reaction is complete (no additional turnovers are possible). It is important to note that TON is often misused to report TO at a given time (when the reaction is not complete). The TON of a catalytic system gives insight into the longevity of the catalyst under a certain set of conditions. This necessarily requires that TON be reported in tandem with the time after which no additional turnovers were observed (e.g., the catalyst achieved a TON of 20 after 24 h), as there is no way to determine the longevity of the catalyst without this second piece of data.²⁰⁻²³

The TOF is an approximation of the rate of catalysis and therefore the activity of a catalyst, although its use and formal definition are contested.²⁰⁻²³ Generally, the TOF is defined as the number of TOs completed per unit time, and has the units of s^{-1} . It is important to distinguish between TOF, which is invariant over the course of the reaction for a catalytic process without any sort of induction period or deactivation, and *apparent* TOF, which is a raw measure of the turnovers completed at a given time. The apparent TOF is often reported given the experimental ease with which it can be obtained, requiring measurement of TOs at only one time point. However, given that the apparent TOF obscures any potential deactivation and/or induction periods, it should be evaluated with caution. When reporting the apparent TOF, it is necessary to report the time at which it was determined alongside the apparent TOF itself (e.g., the apparent TOF at 4 h was determined to be 5 s^{-1}).

The use of apparent TOF is disputed mainly due to the fact that while it approximates the rate of the reaction, it neglects many factors that could impact the rate including induction periods, non-linear rates, catalyst deactivation, and changes in substrate concentration. This approximation can very easily lead to an over- or

underestimation of the true TOF. For this reason (among others), many in the field are in favor of assessing catalytic activity through more rigorous kinetic analyses that allow the determination of rate constants or the actual TOF.

Despite the controversy surrounding its determination and usage, TOF has the potential to be the most useful metric when evaluating catalysts. In an empirical sense, the number of turnovers that can occur in a given unit of time is a more direct measure of catalyst activity, compared to k_{obs} , which contains a collection of rate constants and concentrations that can involve off-cycle processes not relevant to catalytic activity and can often be difficult to deconvolute. Overall, TOF can be a very useful metric, though it should always be evaluated critically before comparisons are made.

The observed rate constant, k_{obs} , is arguably the most accurate and rigorously determined metric when evaluating the rate and activity of a catalyst; however, it is often one of the most difficult to determine. The unambiguous determination of k_{obs} requires detailed kinetic studies, and its interpretation requires experimental studies of elementary reaction steps and/or computational modeling of the catalytic cycle. For simple reactions, this type of kinetic and mechanistic study can be trivial to complete, but for many others it becomes much more complex.

One commonly used method to determine k_{obs} is the method of initial rates.²⁴ This involves plotting concentration of product vs. time (or alternatively, loss of starting material vs. time) for the initial rate regime of catalysis (where no catalyst deactivation is occurring) and performing linear regression analysis. The slope of the linear fit for the initial rate plot gives information about k_{obs} .

Conversion and yield are also important metrics to consider when evaluating both commercial viability and potential for fine chemical applications. In the context of catalysis, the yield of the reaction refers to the amount of product (usually one particular product, but can refer to a sum of all products) relative to the limiting reagent. For this reason, it is important to define what yield is reported relative to. This is also important to remember when comparing catalysts in the literature, as yields may be reported relative to different components of the reaction and need to be corrected for an accurate comparison.

The conversion of a given reaction refers to the percentage of starting material that is converted to any product, but does not necessarily give any information about the selectivity of the conversion (e.g., a reaction could give 100% conversion of starting materials, but only give 5% yield of the desired product, with 95% yield of a byproduct). While the formation of byproducts in industrial reactions is not necessarily undesirable if the byproducts have inherent value, there is typically an additional cost associated with separation. For fine chemical processes, the formation of byproducts is almost exclusively undesirable, which is why both conversion and yield are almost always included for fine chemical reactions discussed in the literature.

1.1.4 Elucidating the Nature of the Active Catalyst

For homogeneous catalysts, often one of the most challenging aspects of characterization involves determining the nature and structure of the active catalyst. It is often assumed that the homogeneous transition metal complex that is added at the start of the reaction is the active catalyst, but often this species is merely the precatalyst, which

converts to the active catalyst under the reaction conditions. For many catalytic systems, this conversion can be trivial, such as the loss of a labile ligand, but for other systems it can be significantly more drastic.

Previous work from our lab and others has demonstrated that reactions that were originally reported as metal-mediated processes were actually catalyzed by acid that had either been added to the reaction or generated *in situ*.²⁵ Additionally, the *in situ* decomposition of homogeneous transition metal complexes to form catalytically active nanoparticles has been observed in many cases that were previously thought to be catalyzed by homogeneous complexes.²⁶⁻²⁸

To say with certainty that the active catalyst is in fact a homogeneous transition metal complex, it is imperative to either monitor catalytic reactions *in situ* (to demonstrate that the homogeneous complex remains present in the same concentration over the course of the reaction), or to perform rigorous kinetic studies including all pertinent control reactions. For example, reactions in which a homogeneous metal complex decomposes to catalytically active nanoparticles often show an induction period, which is only observed upon kinetic analysis. While an induction period can also signify any number of other processes that may not be related to decomposition, if one is observed, it merits further scrutiny. To determine the role of acid in reactions (especially in reactions where acid is or could be generated *in situ*), not only should the reaction profile be carefully scrutinized in an effort to identify multiple kinetic regimes, but reactions with added acid and control reactions with acid alone should also be carried out to determine its impact. These reactions with acid can also prove useful when testing rate laws for proposed mechanisms.

1.2 Industrial Process Chemistry

1.2.1 Overview

The transition from laboratory-scale catalysis to process plant scale reactions faces a number of obstacles including scalability of the process, safety concerns, air-stability and nature of the catalyst (see section 1.1.4), and reactor design. The scale-up of laboratory-scale processes is also hindered by fundamental differences between the nomenclature and metrics used to determine industrial viability and the metrics used to assess catalyst performance on the laboratory scale. This lack of consistency in metrics and terminology between chemists and chemical engineers make it very difficult to determine whether a process has the potential to be industrially viable. This section is designed to discuss the types of industrial catalysts and reactors (section 1.2.2) and the different metrics used to determine the efficiency and viability of a process (section 1.2.3).

1.2.2 Nature of Industrial Catalytic Systems

The two distinct types of industrial catalytic processes are defined by the nature of the catalyst. In homogeneous reactions, the substrates and catalyst exist in the same phase, where in heterogeneous catalysis they are in different phases. In general, most industrial processes are heterogeneous due to the ease in separation of the catalyst from the reaction mixture, but examples of commercialized homogeneous processes exist.⁷ In addition to the rigorously homo- and heterogeneous systems, biphasic systems, mainly based on aqueous, fluoruous, or ionic liquid solvents, have been commercialized, including a variant of hydroformylation (*vide infra*).²⁹⁻³⁶ In these systems, the catalyst and

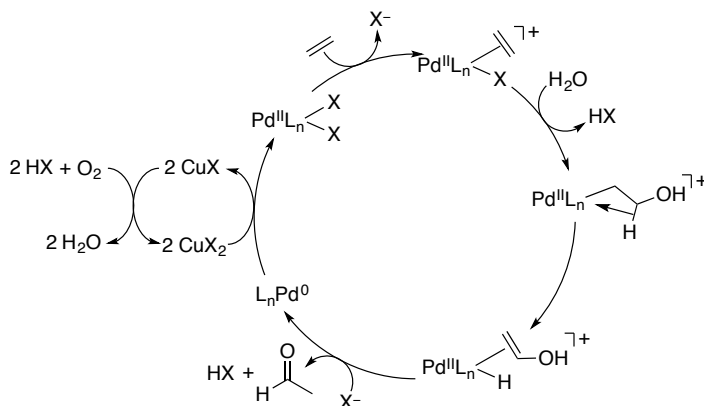
substrate are generally soluble in one phase of the reaction mixture, while the product is soluble in the other layer, which leads to partitioning and aids in separation. Additional hybrid variants exist that are based on homogeneous catalysts that have been heterogenized either through grafting to surfaces, or through “ship in a bottle” encapsulation in heterogeneous frameworks.⁷

As mentioned above, heterogeneous catalysts offer advantages in product separation, and also in the type of reactor setups that can be used. Where homogeneous catalysts are generally limited to batch or continuously stirred tank reactors, heterogeneous systems can operate in flow (fixed- or fluidized-bed) reactors.⁷ These types of reactors allow gas-phase reactants to pass over solid (or fluidized) catalyst beds with more precise temperature and pressure control compared to typical batch or tank reactors. Reactions that can operate in the gas phase also offer additional advantages in product separation and purification, as well as separation of the catalyst from the reaction medium. Mass transfer is also hindered by liquid-phase reactions, as intensive stirring and therefore mechanically stable catalysts are required.

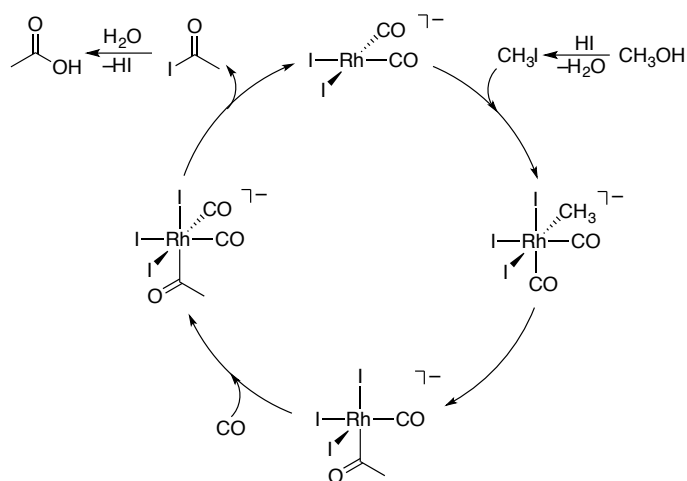
While heterogeneous catalysts offer a number of technical advantages for industrial processes, a few commercialized processes are based on homogeneous catalysts. This is, in part, due to the higher activity and selectivity generally provided by homogeneous catalysts.^{29,37,38} One of the first examples of a commercialized homogeneous catalytic process is the Wacker-Hoechst process for ethylene oxidation (Scheme 1.3). This process was developed by Wacker Chemie in 1956, and was the main industrial source of acetaldehyde until the 1980s.^{39,40} Using a homogeneous Pd(II) catalyst and an aerobically recycled Cu(II) oxidant, this process was considered to be particularly elegant and

efficient until the technology was rendered effectively obsolete by new methods for the production of acetic acid and *n*-butanol.⁴⁰

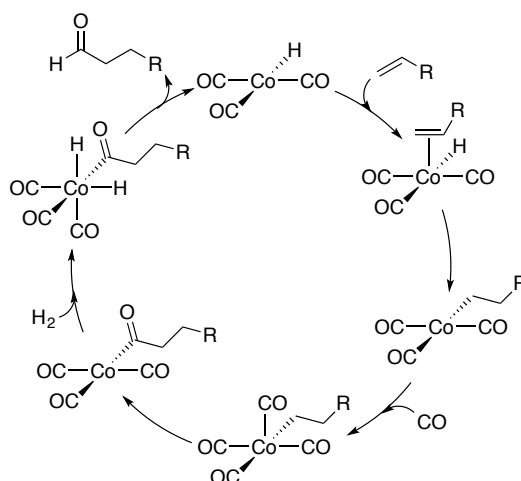
Scheme 1.3. Catalytic cycle for the Wacker-Hoechst process for ethylene oxidation.



Another homogeneous-catalyzed industrial process is the Monsanto acetic acid process, which converts methanol to acetic acid using a homogeneous Rh(I) catalyst (Scheme 1.4). This process was developed in 1966 by the Monsanto Company, improving on an existing process developed by BASF.^{40,41} This process was the dominant method for the production of acetic acid until the development of the Cativa Process by BP in 1996, which also uses a homogeneous catalyst, though it is Ir-based. While these two processes are nearly identical and can even operate in the same plants without retrofitting, the Ir-based process offers advantages in post-catalytic separation in that less water is required, and catalytic quantities of Ru can be added to prevent the formation of undesired byproducts such as propionic acid.⁴⁰

Scheme 1.4. Catalytic Cycle for the Monsanto Acetic Acid Process.

One of the largest homogeneous-catalyzed industrial processes is hydroformylation, which converts a mixture of syngas ($\text{CO} + \text{H}_2$) and olefins to aldehydes on the million ton/annum (t/a) scale using homogeneous Rh or Co catalysts (Scheme 1.5). This process has been commercialized by BASF, Shell, Exxon, and others, and has been operational on plant-scale since 1942.⁴² Early variants of these processes used inexpensive Co catalysts, but most have moved to Rh, with the exception of the Shell and BASF-oxo processes which still use Co.⁴³

Scheme 1.5. Catalytic Cycle for Cobalt-Catalyzed Hydroformylation.

Other examples of homogeneous industrial processes exist, though many operate on smaller scales. Hydrocyanation (DuPont) also uses a Ni catalyst and operates on a ~1000 t/a scale. Ethylene oligomerization (SHOP process, Shell) uses a Ni catalyst and operates on a 870 t/a scale. The acetic anhydride process (Eastman) uses a Rh catalyst and operates on a 230 t/a scale. There are also various other small-scale fine chemical processes that operate in industry to this day.⁷

1.2.3 Process Chemistry and Industrial Viability

For laboratory chemists, one of the most difficult aspects of determining the industrial viability of a catalytic process lies in lack of a set metrics for industrial viability, as these will inherently depend on the type of process, catalyst, etc. While it is difficult to provide hard numbers that define an industrially viable process as these differ greatly between chemical reactions and also whether there is an existing process to displace, the metrics used to assess commercial viability are catalyst activity, selectivity,

and stability (the so-called Catalytic Trinity).⁴⁴ Activity is based on the contact time required between the substrates and the catalysts (for a batch reactor, the contact time is the total time of the reaction, but this becomes much more relevant for flow reactors, in which the flow rate can greatly influence catalysis), and influences reactor design. Activity is also based on the rate of the reaction, which is determined by the TOF as defined above for homogeneous catalysts, and for heterogeneous catalysts as the amount of reacted substrate per active site per unit time. Typical TOFs for industrially viable catalysts range from $10^{-2} - 10^2 \text{ s}^{-1}$.⁴⁴

Selectivity is based on the proportion of desired product to undesired byproducts, and is arguably one of the most important characteristics of a given catalyst. However, a catalyst that makes multiple products is not necessarily undesirable if the products are easily separable and of value. Stability is a measure of the catalyst lifetime and tolerance of reaction conditions. Another important factor to consider is the recyclability of the catalyst, since a short-lived catalyst that can be easily and inexpensively recycled can be just as viable as a long-lived catalyst for which recycling is not facile.⁴⁴

One of the most common misconceptions about industrial processes is that it is most desirable to design a process that works at room temperature. For exothermic processes, it is actually ideal to design a process where the heat generated in the reaction is proportional to the amount of heat required for the process to operate. This indirectly reduces CO₂ emissions by using heat produced by the reaction for a productive purpose. If any step of a reaction requires cooling in excess of what can be provided by cooling water alone, scale-up is often more capital-intensive than for a process that requires external heating.⁴⁵

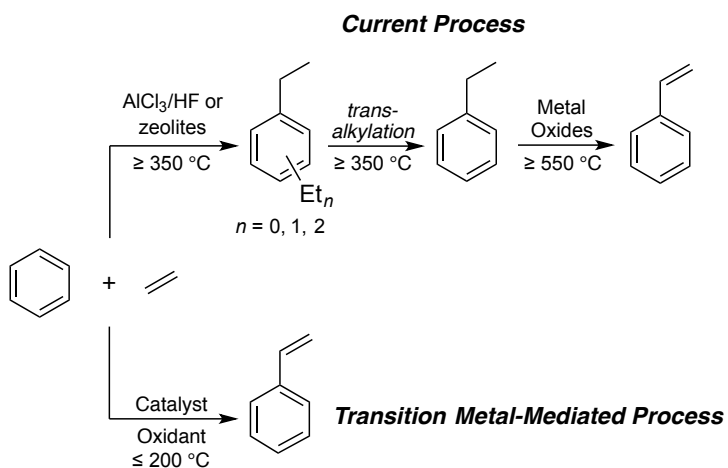
Another common misconception about industrial processes is that a catalyst that can only operate under anaerobic conditions cannot be industrially viable. While an air-stable catalyst makes handling easier, some processes are run under an inert atmosphere mostly due to safety considerations.⁴⁵ For example, in the Wacker process for ethylene oxidation, which requires both ethylene as a substrate and O₂ to regenerate the Cu(II) oxidant, two commercialized variants exist: one in which ethylene and O₂ are flowed through the reactor concurrently, and one in which the reaction is run to completion and the Cu oxidant is removed and regenerated with air in a separate reactor. While the first variant may seem to be more economical, the safety concerns that result from using mixtures of hydrocarbons and oxygen as well as the relative prices of air vs. purified O₂ generally make the two processes approximately equal in cost, though this depends on the expense of purified O₂ versus the cost of separation.³⁹

1.2.4 Alkyl and Vinyl Arenes⁴⁶

Alkyl and vinyl arenes are important precursors for fine chemical synthesis as well as for the preparation of plastics, elastomers, and surfactants.^{8,40,47-49} For example, styrene is produced globally on a scale of ~18.5 million t/a.⁴⁷ Current methods for the large-scale production of vinyl arenes involve multiple steps, typically beginning with arene alkylation using a Friedel-Crafts (e.g., AlCl₃ with HF) or zeolite catalyst followed by energy-intensive dehydrogenation of the alkyl group, but there have been recent developments in transition metal catalyzed arene vinylation (Scheme 1.6, see Chapter 3).^{8,40,47-50} Generally, acid-based (i.e., Friedel-Crafts or zeolite catalysts) catalysis occurs

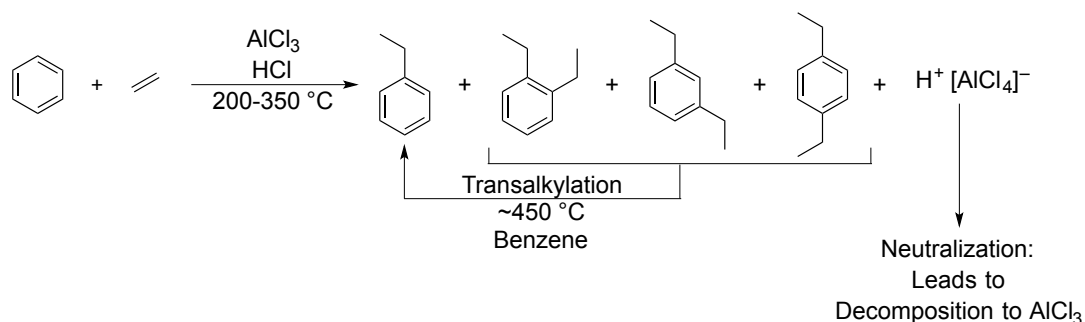
by electrophilic aromatic substitution and does not offer a viable pathway to directly generate vinyl arenes.

Scheme 1.6. Comparison of Current Industrial Process for Styrene Production with a Transition Metal-Mediated Process. Reprinted (adapted) with permission from reference⁵¹. Copyright 2015 AAAS.

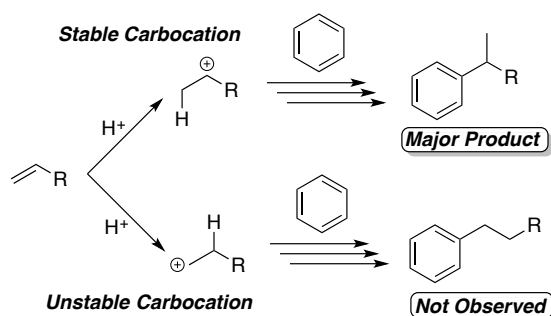


1.2.4.1 Friedel-Crafts Catalysis

While Friedel-Crafts alkylation (FC) catalysis can effectively produce ethylbenzene, it suffers from a number of deficiencies that make it less desirable (Scheme 1.7). FC catalysis requires the use of both Lewis and mineral acids, including HF, making these reactions highly corrosive and the reagents hazardous to transport. Additionally, product separation requires neutralization of the reaction mixture, which in turn decomposes the catalyst and produces stoichiometric quantities of halogenated waste. This lack of recyclability and the halogenated waste generated from neutralization increases the capital expense associated with these processes.

Scheme 1.7. Deficiencies of Friedel-Crafts Arene Alkylation.

Also, the acid-based mechanism relies on the formation of a carbocation, and therefore, arene alkylation using α -olefins always results in the formation of the branched (Markovnikov) product (Scheme 1.8). Finally, acid-based catalysis will always result in the functionalization of the most reactive C–H bond, which results in over-alkylation of alkyl benzene products since the C–H bonds of the alkyl benzene product are more reactive than those of benzene.

Scheme 1.8. Regioselectivity of Friedel-Crafts Arene Alkylation with α -Olefins.

1.2.4.2 Zeolites

To combat some of the deficiencies of traditional FC catalysis, solid-acid catalysts have been developed. The most common types of solid-acid catalysts used for arene alkylation in industry are zeolites.^{8,47} Zeolites are porous aluminosilicates that function as Lewis acids (Figure 1.1).^{47,52} The porous nature of these catalysts allows for the tuning of pore size, which can be used to bias product ratios through shape-selectivity.^{47,53,54} For arene alkylation reactions, zeolites can be doped with other elements, and their pore size can be tuned to reduce the production of poly-alkyl benzene products and to bias regioselectivity for dialkyl benzene production.^{47,55} For example, the ZSM-5 zeolite has traditionally been used for the conversion of benzene and ethylene to styrene, but has suffered from significant dialkyl benzene production. Mobil-Badger developed a new process using MCM-22 zeolite, which features reduced pore sizes compared to ZSM-5 which are also doped with boron, and their ethylbenzene process results in > 95% selectivity.⁵⁵ Zeolites are also much more readily recycled given their heterogeneous nature.^{8,47} While zeolites represent a fundamental advancement over traditional FC catalysis, they still require high temperatures and do not allow for the direct formation of vinyl arenes.

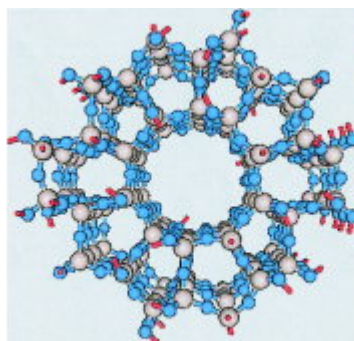


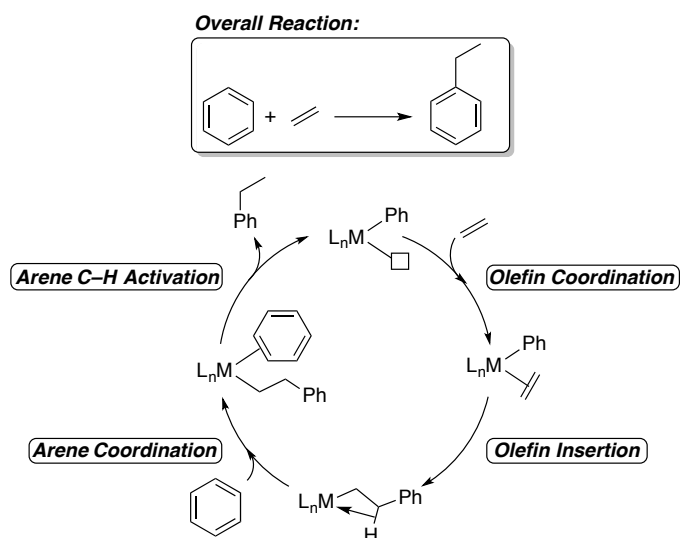
Figure 1.1. Structure of ZSM-5 Zeolite. Babu, K.; Gadre, S.R.; *J. Comput. Chem.* **2004**, *24*, 484. Reproduced with permission.

1.3 Transition Metal-Catalyzed Olefin Hydroarylation

1.3.1 Overview

An alternative to traditional acid-based arene alkylation is a transition metal-mediated process that operates through aromatic C–H activation and olefin insertion into a metal–aryl bond. This reaction is a type of olefin hydroarylation, which is defined as the net addition of an arene C–H bond across an olefin C=C bond (Scheme 1.9). Our group has studied transition metal catalysts for the production of alkyl arenes for the past 18 years.^{51,56-73} A summary of our work, and that of others in the field, based on our review from 2011 is presented here.⁶¹ For a summary of our work since 2011, along with mechanistic comparisons and insights into future catalyst design, see Chapter 4.

Scheme 1.9. General mechanism for transition metal-mediated olefin hydroarylation.



1.3.2 Ruthenium(II) Catalysts

Our group has previously studied overall charge-neutral ruthenium(II) complexes of the type TpRu(L)(NCMe)(R) [Tp = hydridotris(pyrazolyl)borate; L = CO , $\text{P}(N\text{-pyrrolyl})_3$, $\text{P}(\text{OCH}_2)_3\text{CEt}$, $\text{P}(\text{OCH}_2)_2(\text{O})\text{CCH}_3$, PMe_3 ; R = Me or Ph] for the hydroarylation of olefins. This family of Ru complexes, in particular the CO variant, is effective for the catalytic hydrophenylation of ethylene under mild conditions. At 90°C , the reaction of benzene and ethylene (25 psi) is catalyzed by $\text{TpRu}(\text{CO})(\text{NCMe})(\text{Ph})$ [0.1 mol % relative to benzene, **TpRuCO**] to afford 77 TO of ethylbenzene after 24 h.⁶⁵

To gain insight into the effect of electronic modulation of the metal center within the TpRu framework, the apical CO ligand was exchanged for a variety of phosphines and phosphites with varying steric and electronic profiles (L = $\text{P}(N\text{-pyrrolyl})_3$, **TpRuPPyr**; $\text{P}(\text{OCH}_2)_3\text{CEt}$, **TpRuBP**; $\text{P}(\text{OCH}_2)_2(\text{O})\text{CCH}_3$, **TpRuSP**; PMe_3 , **TpRuPMe₃**). The electron density of these metal center for these catalysts was compared by measuring the

Ru(III/II) potential using cyclic voltammetry (Figure 1.2). Examining the rate of stoichiometric C–D activation of benzene- d_6 for the TpRu(L)(NCMe)(Ph) series showed that the rate of C–D activation increased with increasing electron density at the metal center (based on the donor ability of the ligands, and therefore the Ru(III/II) potentials of the resulting complexes) by the following trend: **TpRuPMe₃** > **TpRuBP** > **TpRuSP** > **TpRuPPyr** ~ **TpRuCO**.^{61,62}

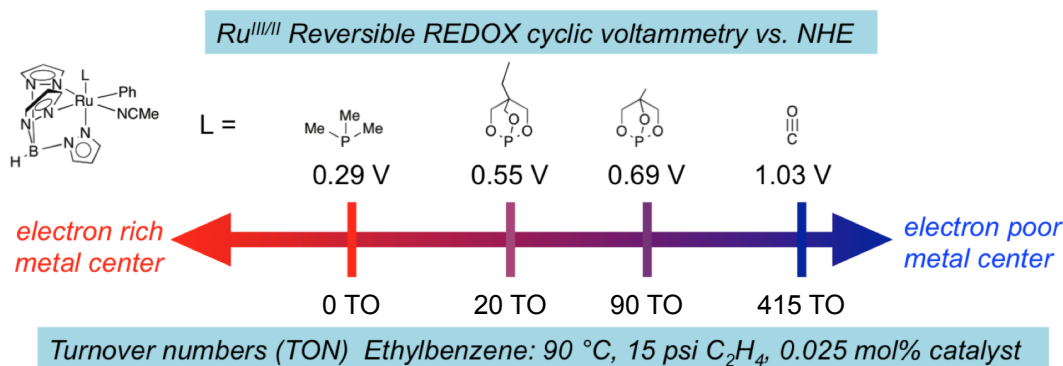


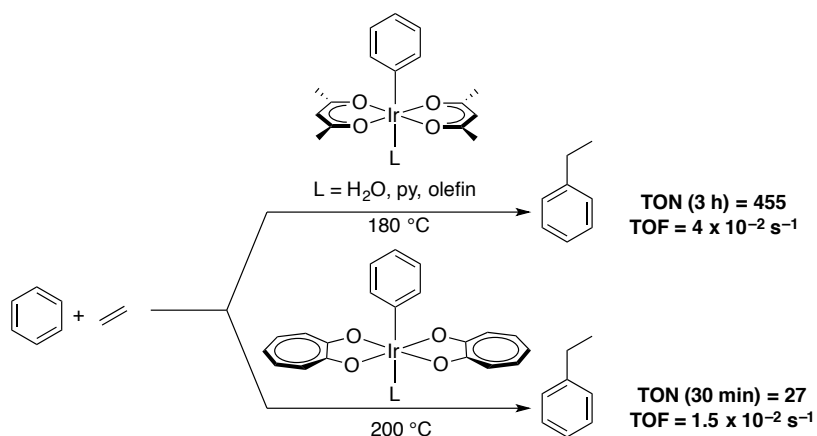
Figure 1.2. Correlation of Ru(III/II) Potential with TON for Ethylene Hydrophenylation using TpRu(L)(NCMe)(Ph) Complexes.

1.3.3 Iridium(III) Catalysts

Ir(III)-catalyzed hydroarylation of olefins has been reported by Periana, Goddard, and coworkers.^{74,75} The complex *trans*-(κ^2 -*O,O*-acac)₂Ir(Ph)(L) [acac = acetylacetonate; L = H₂O, py, olefin; (**acac**)₂Ir] catalyzes the hydrophenylation of ethylene to form ethylbenzene at 180 °C. The TOF for catalysis with (**acac**)₂Ir is in the industrially relevant region at $4 \times 10^{-2} \text{ s}^{-1}$ and the TON is high (455 TO of EtPh produced in 3 h).^{74,75} To examine the effect of electronics on catalysis with (**acac**)₂Ir, tropolonate, which should be less electron donating, was substituted for acac to form the complex (trop-

$O,O)_2\text{Ir}(\text{Ph})(\text{py})$ [trop = tropolonato, py = pyridine, **(trop)₂Ir**]. Catalysis with **(trop)₂Ir** only proceeded at 200 °C and was less active and lower yielding than its acac counterpart (TOF = $1.5 \times 10^{-2} \text{ s}^{-1}$ TON = 27 after 30 min).⁷⁶

Scheme 1.10. Comparison of ethylene hydrophenylation using **(acac)₂Ir** and **(trop)₂Ir**.

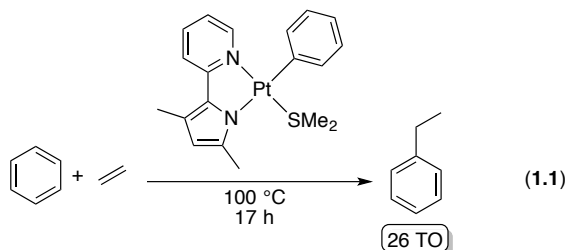


The hydrophenylation of α -olefins using **(acac)₂Ir** and **(trop)₂Ir** has also been reported.^{74,77} These reactions are generally slower and lower-yielding than reactions with ethylene. For the hydrophenylation of propylene, both Ir complexes produce *n*-propyl benzene (linear) and cumene (branched) in a 1.6:1 ratio, which is comparable to results using **TpRuCO**.⁶¹

1.3.4 Platinum(II) Catalysts

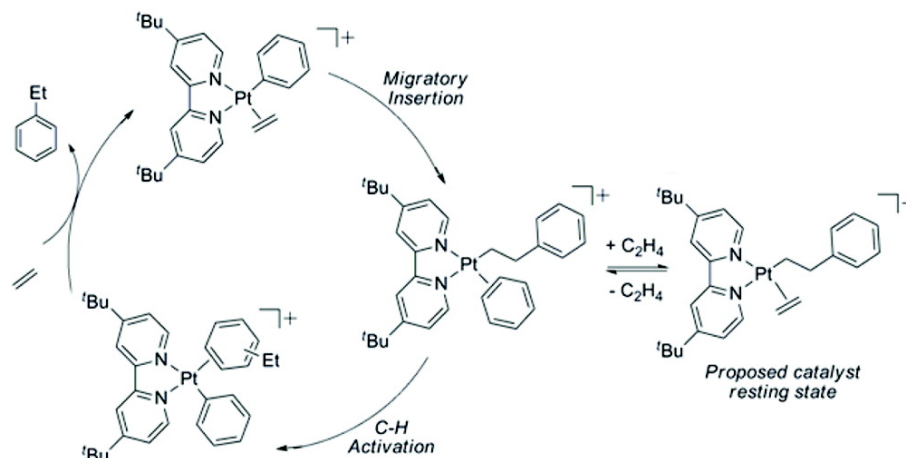
Hydroarylation of olefins using Pt(II) catalysts has been reported by Goldberg and coworkers and by our group.^{66-71,78} In 2008, Goldberg and coworkers reported platinum(II)-catalyzed hydrophenylation of ethylene using a neutral **(dmpp)Pt(Ph)(SMe₂)**

complex (dmpp = 3,5-dimethyl-2-(2-pyridyl)pyrrolide).⁷⁸ Heating a benzene solution of this complex with 0.26 mmol of ethylene to 100 °C for 17 h produced 26 TO of ethylbenzene (Eq. 1.1).⁷⁸



Our group has reported that the cationic complex $[(^t\text{bpy})\text{Pt}(\text{Ph})(\text{THF})][\text{BAr}^{\text{F}}_4]$ (^tbpy = 4,4'-di-tert-butyl-2,2'-bipyridyl, Ar^{F} = 3,5-bis(trifluoromethyl)phenyl, $^t\text{bpyPt}$) catalyzes the hydrophenylation of ethylene.⁶⁶ As with our TpRu(II) complexes, an inverse dependence on ethylene pressure was observed, indicating that $[(^t\text{bpy})\text{Pt}(\text{CH}_2\text{CH}_2\text{Ph})(\eta^2\text{-C}_2\text{H}_4)]^+$ is the likely catalyst resting state. This was confirmed by ^1H NMR spectroscopy, and detailed mechanistic studies allowed for the determination that this intermediate was off-cycle.⁶⁸ Compared to related Ru(II) complexes, the $^t\text{bpyPt}$ catalysts showed lower selectivity for mono-alkyl product ($\sim 25\%$ of total alkyl arene products were dialkyl benzenes).⁶⁶

Scheme 1.11. Mechanism for ethylene hydrophenylation using **^tBpyPt**. Reprinted (adapted) with permission from reference⁶⁸. Copyright 2011 American Chemical Society.



1.4 Thesis Aims

The aim of this dissertation is to discuss the development and optimization of d^8 transition metal catalysts for oxidative arene vinylation. The ultimate goal of this research is to design a catalyst for oxidative arene vinylation that is sufficiently active, stable, and long-lived as to be industrially viable. The added challenge is that an industrially viable catalyst for styrene production must not only represent a fundamental cost-savings to operate, and must be so much less expensive as to offset the cost required to take a revenue-producing plant offline for retrofitting and to cover the cost of the retrofit itself. While this may seem like an insurmountable obstacle, the age of styrene-producing infrastructure in the US (and therefore the need for complete overhaul and retrofitting of many styrene plants) provides a potential opportunity to introduce a new technology without overcoming the cost of retrofit and lost revenue. To take advantage of this, we need to develop a transition metal catalyst for styrene production that is suitable for

industrial application before this window of opportunity closes. This requires a thorough mechanistic understanding of single-step styrene production, as well as the characteristics of catalyst architecture and electronics that afford tunability. This work provides detailed mechanistic insight into the pathway for transition metal-catalyzed arene vinylation that can aid in this pursuit. Discussed herein will be: 1) a study of Pd(II) catalysts for styrene production under aerobic conditions, 2) the development and detailed mechanistic studies of a Rh(I) catalyst that can produce styrene in a single step with 100% selectivity and quantitative yields based on Cu(II) oxidant, and 3) mechanistic comparisons, insights into catalyst design, preliminary new projects, and the outlook of the field.

1.5 References

- (1) Crabtree, R. H. *The Organometallic Chemistry of the Transition Metals*; 5th ed.; Wiley: Hoboken, NJ, 2009.
- (2) Hartwig, J. F. *Organotransition Metal Chemistry*; University Science Books: Mill Valley, CA, 2010.
- (3) Wilkinson, G.; Rosenblum, M.; Whiting, M. C.; Woodward, R. B. *J. Am. Chem. Soc.* **1952**, *74*, 2125.
- (4) Chatt, J.; Shaw, B. L. *J. Chem. Soc.* **1959**, 4020.
- (5) Döbereiner, J. W. *J. für Chem.* **1823**, *38*, 321.
- (6) Miessler, G. L.; Tarr, D. A. *Inorganic Chemistry*; 3rd ed.; Pearson Prentice Hall: Upper Saddle River, NJ, 2004.
- (7) Hagen, J. *Industrial Catalysis*; 2nd ed.; Wiley-VCH Verlag: Weinheim, Germany, 2006.
- (8) Olah, G. A.; Molnár, Á. *Hydrocarbon Chemistry*; 2 ed.; Wiley: Hoboken, NJ, 2003.
- (9) Herrmann, W. A.; Cornils, B. *Angew. Chem. Int. Ed. Engl.* **1997**, *36*, 1048.

- (10) Miyaura, N. *Cross-Coupling Reactions: A Practical Guide*; Springer: New York, 2002.
- (11) Farina, V. *Adv. Synth. Catal.* **2004**, *346*, 1553.
- (12) In *CRC Handbook of Chemistry and Physics* Weast, R. C., Ed.; CRC Press/Taylor & Francis: Boca Raton, FL, 1977.
- (13) Webb, J. R.; Burgess, S. A.; Cundari, T. R.; Gunnoe, T. B. *Dalton Trans.* **2013**, *42*, 16646.
- (14) Waterman, R. *Organometallics* **2013**, *32*, 7249.
- (15) Ackermann, L. *Chem. Rev.* **2011**, *111*, 1315.
- (16) Oxgaard, J.; Tenn, W. J.; Nielsen, R. J.; Periana, R. A.; Goddard, W. A. *Organometallics* **2007**, *26*, 1565.
- (17) Lapointe, D.; Fagnou, K. *Chem. Lett.* **2010**, *39*, 1118.
- (18) Boutadla, Y.; Davies, D. L.; Macgregor, S. A.; Poblador-Bahamonde, A. I. *Dalton Trans.* **2009**, 5820.
- (19) Boutadla, Y.; Davies, D. L.; Macgregor, S. A.; Poblador-Bahamonde, A. I. *Dalton Trans.* **2009**, 5887.
- (20) Bligaard, T.; Bullock, R. M.; Campbell, C. T.; Chen, J. G.; Gates, B. C.; Gorte, R. J.; Jones, C. W.; Jones, W. D.; Kitchin, J. R.; Scott, S. L. *ACS Catal.* **2016**, *6*, 2590.
- (21) Kozuch, S.; Martin, J. M. L. *ACS Catal.* **2012**, *2*, 2787.
- (22) Lente, G. *ACS Catal.* **2013**, *3*, 381.
- (23) Kozuch, S. *ACS Catal.* **2013**, *3*, 380.
- (24) Blackmond, D. G. *Angew. Chem., Int. Ed.* **2005**, *44*, 4302.
- (25) Munz, D.; Webster-Gardiner, M.; Fu, R.; Strassner, T.; Goddard, W. A.; Gunnoe, T. B. *ACS Catal.* **2015**, *5*, 769.
- (26) Webb, J. R.; Pierpont, A. W.; Munro-Leighton, C.; Gunnoe, T. B.; Cundari, T. R.; Boyle, P. D. *J. Am. Chem. Soc.* **2010**, *132*, 4520.
- (27) Widegren, J. A.; Finke, R. G. *J. Mol. Catal. A* **2003**, *198*, 317.

- (28) de Vries, J. G. When Does Catalysis with Transition Metal Complexes Turn into Catalysis by Nanoparticles? In *Selective Nanocatalysts and Nanoscience*; Wiley-VCH Verlag GmbH & Co. KGaA: 2011, pp 73.
- (29) Cole-Hamilton, D. J. *Science* **2003**, *299*, 1702.
- (30) Cornils, B.; Kuntz, E. G. *J. Organomet. Chem.* **1995**, *502*, 177.
- (31) Cornils, B. *Angew. Chem. Int. Ed. Engl.* **1997**, *36*, 2057.
- (32) Sellin, M. F.; Bach, I.; Webster, J. M.; Montilla, F.; Rosa, V.; Aviles, T.; Poliakov, M.; Cole-Hamilton, D. J. *J. Chem. Soc., Dalton Trans.* **2002**, 4569.
- (33) Bronger, R. P. J.; Silva, S. M.; Kamer, P. C. J.; Leeuwen, P. W. N. M. v. *Chem. Commun.* **2002**, 3044.
- (34) Keim, W.; Vogt, D.; Waffenschmidt, H.; Wasserscheid, P. *J. Catal.* **1999**, *186*, 481.
- (35) Brasse, C. C.; Englert, U.; Salzer, A.; Waffenschmidt, H.; Wasserscheid, P. *Organometallics* **2000**, *19*, 3818.
- (36) Horváth, I. T. *Acc. Chem. Res.* **1998**, *31*, 641.
- (37) Dijkstra, H. P.; van Klink, G. P. M.; van Koten, G. *Acc. Chem. Res.* **2002**, *35*, 798.
- (38) Eckert, M.; Fleischmann, G.; Jira, R.; Bolt, H. M.; Golka, K. Acetaldehyde. In *Ullmann's Encyclopedia of Industrial Chemistry*; Wiley-VCH Verlag GmbH & Co. KGaA: 2000.
- (39) *Chemical & Engineering News Archive* **1961**, *39*, 52.
- (40) Wittcoff, H. A.; Reuben, B. G.; Plotkin, J. S. Chemicals and Polymers from Ethylene. In *Industrial Organic Chemicals*; Wiley: Hoboken, NJ, 2004, pp 100.
- (41) Chenier, P. J. *Survey of Industrial Chemistry*; 2nd ed.; Wiley VCH: New York, 1992.
- (42) Franke, R.; Selent, D.; Börner, A. *Chem. Rev.* **2012**, *112*, 5675.
- (43) In *Catalysis from A to Z*; Cornils, B.; Herrmann, W. A.; Muhler, M.; Wong, C.-H., Eds.; Wiley: New York, 2007.
- (44) Murzin, D. Y. *Engineering Catalysis*; Walter de Gruyter GmbH: Berlin/Boston, 2013.

- (45) Gladysz, J. A. *Pure Appl. Chem.* **2001**, 73, 1319.
- (46) Reprinted (adapted) with permission from (Vaughan, B. A.; Webster-Gardiner, M. S.; Cundari, T. R.; Gunnoe, T. B. *Science*, **2015**, 348, 421.) Copyright 2015 AAAS.
- (47) Perego, C.; Pollesel, P. Advances in Aromatics Processing Using Zeolite Catalysts. In *Advances in Nanoporous Materials*; Stefan, E., Ed.; Elsevier: Oxford, 2010; Vol. 1, pp 97.
- (48) Chen, S.-S. Styrene. In *Kirk-Othmer Encyclopedia of Chemical Technology*; Wiley: Hoboken, NJ, 2000.
- (49) Chem Systems, I. Styrene/Ethylbenzene; Process Evaluation/Research Planning (PERP) Program Report 91-9; Chem Systems, Inc.: New York, 1992.
- (50) Lucchini, M.; Galeotti, A. WO2007073918A1, 2007. (International Patent WO2007073918A1)
- (51) Vaughan, B. A.; Webster-Gardiner, M. S.; Cundari, T. R.; Gunnoe, T. B. *Science* **2015**, 348, 421.
- (52) Degnan Jr, T. F.; Smith, C. M.; Venkat, C. R. *Applied Catalysis A: General* **2001**, 221, 283.
- (53) Čejka, J.; Wichterlová, B. *Cat. Rev.* **2002**, 44, 375.
- (54) Gerzeliev, I. M.; Khadzhiev, S. N.; Sakharova, I. E. *Pet. Chem.* **2011**, 51, 39.
- (55) Marcilly, C. Main Acids, Superacids and Bases of Interest in Catalysis. In *Acido-Basic Catalysis*; Editions Technip: France, 2006; Vol. 2, pp 515.
- (56) Andreatta, J. R.; McKeown, B. A.; Gunnoe, T. B. *J. Organomet. Chem.* **2011**, 696, 305.
- (57) Burgess, S. A.; Joslin, E. E.; Gunnoe, T. B.; Cundari, T. R.; Sabat, M.; Myers, W. H. *Chem. Sci.* **2014**, 5, 4355.
- (58) Foley, N. A.; Ke, Z.; Gunnoe, T. B.; Cundari, T. R.; Petersen, J. L. *Organometallics* **2008**, 27, 3007.
- (59) Foley, N. A.; Lail, M.; Gunnoe, T. B.; Cundari, T. R.; Boyle, P. D.; Petersen, J. L. *Organometallics* **2007**, 26, 5507.
- (60) Foley, N. A.; Lail, M.; Lee, J. P.; Gunnoe, T. B.; Cundari, T. R.; Petersen, J. L. *J. Am. Chem. Soc.* **2007**, 129, 6765.

- (61) Foley, N. A.; Lee, J. P.; Ke, Z.; Gunnoe, T. B.; Cundari, T. R. *Acc. Chem. Res.* **2009**, *42*, 585.
- (62) Joslin, E. E.; McMullin, C. L.; Gunnoe, T. B.; Cundari, T. R.; Sabat, M.; Myers, W. H. *Organometallics* **2012**, *31*, 6851.
- (63) Joslin, E. E.; Quillian, B.; Gunnoe, T. B.; Cundari, T. R.; Sabat, M.; Myers, W. H. *Inorg. Chem.* **2014**, *53*, 6270.
- (64) Lail, M.; Arrowood, B. N.; Gunnoe, T. B. *J. Am. Chem. Soc.* **2003**, *125*, 7506.
- (65) Lail, M.; Bell, C. M.; Conner, D.; Cundari, T. R.; Gunnoe, T. B.; Petersen, J. L. *Organometallics* **2004**, *23*, 5007.
- (66) McKeown, B. A.; Foley, N. A.; Lee, J. P.; Gunnoe, T. B. *Organometallics* **2008**, *27*, 4031.
- (67) McKeown, B. A.; Gonzalez, H. E.; Friedfeld, M. R.; Brosnahan, A. M.; Gunnoe, T. B.; Cundari, T. R.; Sabat, M. *Organometallics* **2013**, *32*, 2857.
- (68) McKeown, B. A.; Gonzalez, H. E.; Friedfeld, M. R.; Gunnoe, T. B.; Cundari, T. R.; Sabat, M. *J. Am. Chem. Soc.* **2011**, *133*, 19131.
- (69) McKeown, B. A.; Gonzalez, H. E.; Gunnoe, T. B.; Cundari, T. R.; Sabat, M. *ACS Catal.* **2013**, *3*, 1165.
- (70) McKeown, B. A.; Gonzalez, H. E.; Michaelos, T.; Gunnoe, T. B.; Cundari, T. R.; Crabtree, R. H.; Sabat, M. *Organometallics* **2013**, *32*, 3903.
- (71) McKeown, B. A.; Prince, B. M.; Ramiro, Z.; Gunnoe, T. B.; Cundari, T. R. *ACS Catal.* **2014**, *4*, 1607.
- (72) Vaughan, B. A.; Khani, S. K.; Gary, J. B.; Kammert, J. D.; Webster-Gardiner, M. S.; McKeown, B. A.; Davis, R. J.; Cundari, T. R.; Gunnoe, T. B. *J. Am. Chem. Soc.* **2017**, *139*, 1485.
- (73) Webster-Gardiner, M. S.; Chen, J.; Vaughan, B. A.; McKeown, B. A.; Shinski, W.; Gunnoe, T. B. *J. Am. Chem. Soc.* **2017**, In Press.
- (74) Matsumoto, T.; Taube, D. J.; Periana, R. A.; Taube, H.; Yoshida, H. *J. Am. Chem. Soc.* **2000**, *122*, 7414.
- (75) Matsumoto, T.; Periana, R. A.; Taube, D. J.; Yoshida, H. *J. Mol. Catal. A* **2002**, *180*, 1.

- (76) Bhalla, G.; Bischof, S. M.; Ganesh, S. K.; Liu, X. Y.; Jones, C. J.; Borzenko, A.; Tenn, I. I. I. W. J.; Ess, D. H.; Hashiguchi, B. G.; Lokare, K. S.; Leung, C. H.; Oxgaard, J.; Goddard, I. I. I. W. A.; Periana, R. A. *Green Chem.* **2011**, *13*, 69.
- (77) Oxgaard, J.; Muller, R. P.; Goddard, W. A.; Periana, R. A. *J. Am. Chem. Soc.* **2004**, *126*, 352.
- (78) Luedtke, A. T.; Goldberg, K. I. *Angew. Chem., Int. Ed.* **2008**, *47*, 7694.

2. Study of Palladium Catalysts for the Oxidative Vinylation of Benzene

2.1 Introduction

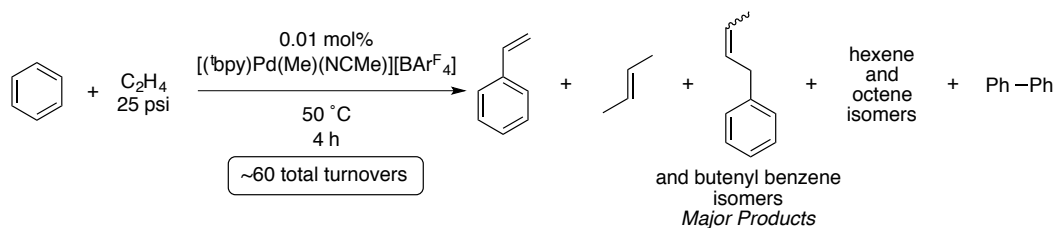
Palladium salts, in particular Pd(OAc)₂, have been reported as catalysts for the oxidative vinylation of benzene to form styrene, though they often suffer from low selectivity and/or low yield. For example, Fujiwara and coworkers reported styrene production using Pd(OAc)₂ and an AgOAc oxidant, but yields (relative to oxidant) were low (~12%), and they also observed the undesired production of stilbene and biphenyl.¹ Periana and coworkers reported styrene production using Pd(OAc)₂ with Cu(OAc)₂/O₂ as the oxidant, but they observed significant vinyl acetate production (~2.5 times the amount of styrene produced) as a byproduct.^{2,3} Ishii and coworkers reported that (DBM)Pd(OAc)₂ (DBM = dibenzoylmethane) affords 58% selectivity for styrene production (stilbene and vinyl propionate, a product of reaction with solvent, are also produced) using a polyoxometalate oxidant, but their yields were low (2%).⁴ Sanford and coworkers reported that (3,5-dichloropyridyl)Pd(OAc)₂ affords styrene with 100% selectivity; however, their process suffers from low yields (~33%) and uses an expensive, oxidant (PhCO₃^tBu) that cannot be aerobically regenerated.⁵ Based on these results, we hypothesized that the proper combination of Pd(OAc)₂ and an ancillary ligand could bias the selectivity of oxidative benzene vinylation reactions such that styrene was produced selectively.

Previously, our group has studied the use of Pt(II) complexes for ethylbenzene production.⁶⁻¹¹ These complexes have generally followed the [(^Xbpy)Pt(R)(L)][BAr^F₄] motif (^Xbpy = 4,4'-substituted 2,2'-bipyridyl, R = alkyl or aryl, L = labile ligand, Ar^F₄ = 3,5-(CF₃)₂-C₆H₃). We have shown that the selectivity can be shifted to favor styrene with

increasingly electron-withdrawing X substituents; however, while these Pt complexes are effective catalysts for ethylbenzene production, when the selectivity is shifted to favor styrene, catalyst deactivation is rapid, often affording approximately one turnover (TO) of styrene.¹⁰ For example, catalysis with $[(^{\text{NO}_2}\text{bpy})\text{Pt}(\text{Ph})(\text{THF})][\text{BAr}^{\text{F}}_4]$ ($^{\text{NO}_2}\text{bpy}$ = 4,4'-dinitro-2,2'-bipyridyl) affords > 90% selectivity for styrene, but only 1 TO is produced after 16 h. The deactivation of the Pt catalysts is likely a result of the instability of the putative Pt–H intermediates that are formed following styrene production, which may decompose to Pt^0 . For Pt, this reduction is irreversible given the energetics of reoxidation to Pt(II), but for Pd, this reoxidation is much more favorable.¹²

Initial unpublished synthetic efforts by Dr. Bradley McKeown involved the preparation and isolation of $[(^t\text{bpy})\text{Pd}(\text{Me})(\text{NCMe})][\text{BAr}^{\text{F}}_4]$ (^tbpy = 4,4'-di-*t*-butyl-2,2'-bipyridyl).¹³ Heating this complex at 50 °C in benzene with 25 psig of ethylene produced various vinyl arene products with poor selectivity (Scheme 2.1). Using GC/MS, it was estimated that ~60 TO of total products were formed (all vinyl products, no alkyl products were detected), making $[(^t\text{bpy})\text{Pd}(\text{Me})(\text{NCMe})][\text{BAr}^{\text{F}}_4]$ significantly longer-lived for the production of vinyl arenes than related platinum catalysts, which typically give 1-2 TO of vinyl arene before catalyst deactivation occurs.¹⁰ While this system is not particularly selective for a single product, it serves as proof of concept that tuning the palladium catalyst can increase selectivity for vinyl arene products over alkyl arenes and enhance catalyst longevity.

Scheme 2.1. Oxidative benzene vinylation using $[(\text{bpy})\text{Pd}(\text{Me})(\text{NCMe})][\text{BARF}_4]$.

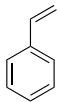
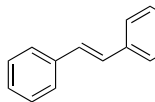
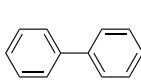
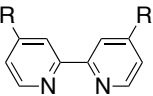
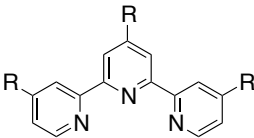
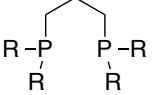
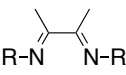


2.2 Results and Discussion

2.2.1 Optimization of Selectivity for Stoichiometric Reactions

Based on our hypothesis that ancillary ligands on $\text{Pd}(\text{OAc})_2$ could bias the selectivity of oxidative benzene vinylation reactions to favor styrene, a variety of ancillary ligands were screened in stoichiometric reactions to determine which afforded the highest selectivity for styrene over stilbene and biphenyl. For these screening reactions, a variety of monodentate, bidentate, and tridentate ligands were examined, and the putative (ligand) $\text{Pd}(\text{OAc})_2$ complexes were synthesized *in situ* upon combination of $\text{Pd}(\text{OAc})_2$ and ligand. Table 2.1 shows ratios of relative peak area (determined by GC/MS) of the three products for each ancillary ligand.

Table 2.1. Relative ratios of products produced in stoichiometric oxidative benzene vinylation experiments using the *in situ* generated complexes (Ligand)Pd(OAc)₂.^a

Ligand	Entry	R			
	1	^t Bu	1	0	13
	2	^t Bu	1	0	1
	3	Ph	3	0	1
	4	Cy ^b	0.6	1	1
	5	^t Bu	1	0	2
	6	Ph	13	1	2
	7	Mes ^c	72	1	5
	8	Dipp ^d	83	1	4
	9	C ₆ F ₅	30	1	0
	10	Cy ^b	15	1	0.7

^aReaction Conditions: 1 mol % Pd(OAc)₂ (relative to benzene), 1 mol % ligand (relative to benzene), 25 psig C₂H₄, 50 °C, 18 h. Ratios determined by GC/MS relative ratios of peak areas.

^bCy = cyclohexyl. ^cMes = 2,4,6-trimethylphenyl. ^dDipp = 2,6-diisopropylphenyl.

Subjecting a mixture of ^tbpy with Pd(OAc)₂ to catalytic conditions (entry 1) favored the formation of biphenyl over styrene in a 13:1 ratio, though no stilbene was observed. The mixture of ^tterpy with Pd(OAc)₂ (entry 2) produced biphenyl and styrene in equal ratio, with no stilbene observed. Reaction with dppp (entry 3) afforded selectivity for styrene over biphenyl in a 3:1 ratio, again with no stilbene produced. Neither mixtures of Pd(OAc)₂ with *tert*-butyl nor cyclohexyl DavePhos (entries 4 and 5) were selective for styrene production. The diazabutadiene (DAB) family of ligands (entries 6-10) all offered significant selectivity for styrene over both stilbene and biphenyl, with the 2,6-

diisopropylphenyl derivative affording the highest selectivity (83:1:4 styrene:stilbene:biphenyl).

2.2.2 Optimization of Catalytic Conditions

Given that (^{Dipp}DAB)Pd(OAc)₂ [complex **1**] afforded high selectivity for styrene production, we next conducted a temperature screening. Catalysis with **1** using 20 equiv. of Cu(OAc)₂ as the oxidant revealed over a temperature range from 50 – 120 °C showed that 120 °C was the optimum temperature for catalysis.

Table 2.2. Results of oxidant screening.^a

Catalyst	Cat. Loading ^b	Oxidant	Equiv ^c	Styrene ^d	Stilbene ^d	Biphenyl ^d
(^{Dipp} DAB ^{Me})Pd(OAc) ₂	0.1 mol %	AgOAc	20	<1	0	0
(^{Dipp} DAB ^{Me})Pd(OAc) ₂	0.1 mol %	1,4-benzoquinone	20	<1	0	0
(^{Dipp} DAB ^{Me})Pd(OAc) ₂	0.1 mol %	Cu(OAc)(OH)	20	4	<1	0
	0.05 mol %		120	12	12	0
(^{Dipp} DAB ^{Me})Pd(OAc) ₂	0.1 mol %	Cu(OAc) ₂ •H ₂ O	20	4	<1	0
	0.05 mol %		120	19	1	0
(^{Dipp} DAB ^{Me})Pd(OAc) ₂	0.025 mol %	Cu(OAc) ₂	120	24	4	0
(^{Dipp} DAB ^{Me})Pd(OAc) ₂	0.1 mol %	–	–	<1	0	0
–	–	Cu(OAc) ₂	60 ^e	0	0	0
Pd(OAc) ₂	0.1 mol %	–	–	<1	<1	0

^aReaction Conditions: 25 psig C₂H₄, 120 °C, 72 h. ^bRelative to benzene. ^cEquivalents of oxidant relative to catalyst. ^dYield of product relative to catalyst, reported as TO. ^e0.112 mM Cu(OAc)₂

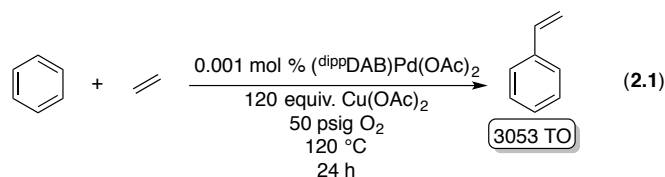
A variety of oxidants were also screened to determine which was most effective. Table 2.2 shows the results for a variety of soluble (benzoquinone) and insoluble (Cu and Ag salts) oxidants. These results indicate that Cu(OAc)₂ is the most effective oxidant for this transformation, affording 24 turnovers (TO) of styrene after 72 h. Given that two equivalents of oxidant are required per TO (the conversion of benzene and ethylene to

styrene is a two-electron process), this represents a 40% yield relative to Cu(II) [*n.b.*, yield calculated assuming that two equivalents of Cu(II) are required per TO]. It is also important to note that control reactions with **1** or Pd(OAc)₂ in the absence of Cu afforded <1 TO of styrene after 72 h, and reactions with Cu(OAc)₂ in the absence of Pd afforded no styrene production, indicating that both Pd and Cu(OAc)₂ are necessary for catalysis.

2.2.3 Oxidative Vinylation of Benzene Using O₂ as the Terminal Oxidant

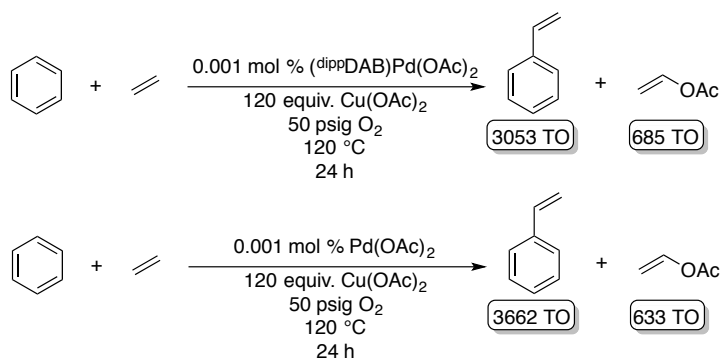
In order to increase the yield of this reaction, we hypothesized that the addition of O₂ would allow for *in situ* regeneration of Cu in a manner akin to the Wacker process. The use of O₂ as the terminal oxidant was also appealing as it made the overall process more attractive for commercialization. This approach has also been employed by Periana and coworkers with their Pd(II) and Rh(III) catalysts.^{2,3}

The addition of O₂ (and lowering the catalyst loading to 0.001 mol %) to catalysis afforded 3053(78) TO of styrene after only 24 h, which represents a ~20-fold increase (eq. 4.1). This indicates that the Cu(II) is getting recycled ~51 times over the course of the reaction, as the observed TON is 51 times higher than the theoretical maximum yield based on Cu(II). Additionally, comparison to comparable reactions at 0.001 mol % affords the observation that TO increases with decreasing catalyst loading is consistent with a bimolecular deactivation pathway, which is also observed for our Pt catalysts and some of our Ru catalysts for ethylbenzene production.^{7,14}



Unfortunately, under aerobic conditions, we also observed significant production of vinyl acetate [685(15) TO]. Production of vinyl acetate has also been reported by Periana and coworkers for catalysis with both Pd(II) and Rh(III) complexes under aerobic, although in higher proportion.^{2,3} These results prompted us to re-examine control reactions with Pd(OAc)₂ without ligands under our optimized conditions. Catalytic reactions using Pd(OAc)₂ under our optimized conditions with Cu(OAc)₂ and O₂ afforded 3662(37) TO styrene and 633(13) TO vinyl acetate, for a selectivity of 85% (Scheme 2.2). Given the deviations in the TO measurements, this result gave statistically identical selectivity to catalysis with **1**.

Scheme 2.2. Comparison of aerobic oxidative benzene vinylation reactions catalyzed by **1** and Pd(OAc)₂.



2.3 Summary and Conclusions

The use of ancillary ligands to influence the selectivity of oxidative benzene vinylation reactions using Pd(OAc)₂ was probed. Diazabutadiene ligands were found to suppress the formation of biphenyl and stilbene, but when O₂ is used as the terminal oxidant, vinyl acetate production is significant. Under optimized catalytic conditions, the ratio of styrene to vinyl acetate using **1** is statistically identical to that using Pd(OAc)₂ alone.

While this system is unsuitable for styrene production, there are other possible applications in which **1** might excel. Initial investigations into oxidative benzene vinylation using styrene as the olefin (to form stilbene) have shown that this reaction is favorable, while slower than when using ethylene. This type of chemistry is promising due to the value of functionalized styrenes in polymerization chemistry.¹⁵ Also, preliminary experiments using propylene have resulted in a 3:1 preference for the formation of linear over branched product. This is notable since the linear product is more valuable industrially, and current acid-catalyzed methods only allow for the synthesis of the branched product.¹⁵

Given the high activity of Pd catalysts for numerous C–C bond forming reactions, the lack of selectivity of this chemistry is, perhaps, not surprising. In particular, the production of vinyl acetate under aerobic conditions (in larger quantities than the amount of acetate present in the reaction) could potentially signal ethylene is being oxidized to acetate in a manner similar to that observed in the Wacker process. Since the catalyst system used herein was intentionally designed to mimic many desirable aspects of the

Wacker process, it is possible that Pd-based catalysts for aerobic styrene production will always necessarily oxidize ethylene.

Further studies are necessary to elucidate the impact of ancillary ligands on selectivity for styrene vs. vinyl acetate under aerobic conditions. While results with complex **1** appear to indicate that the addition of ancillary ligands to Pd(OAc)₂ does not bias the selectivity for styrene over vinyl acetate, no other complexes were investigated for vinyl acetate production, and therefore no broad claims can be made in this regard. To investigate this, additional ligand screening should be performed to specifically examine the ratio of styrene and vinyl acetate produced.

2.4 Experimental

General Considerations. Unless otherwise noted, all manipulations were performed under an atmosphere of dry nitrogen using standard Schlenk or high vacuum techniques and/or in a Vacuum Atmospheres Dri-Lab glovebox equipped with a Dri-Train MO40-1 purifier. Dry, oxygen-free solvents were employed throughout. Benzene, tetrahydrofuran, and acetonitrile were purified by passage through a column of activated alumina. Tetrahydrofuran was further dried by distillation from sodium/benzophenone. Acetonitrile was further dried by distillation from CaH₂. NMR spectra were recorded on a Bruker Avance II 600 MHz spectrometer (¹H, 600.13 MHz operating frequency) or a Varian Mercury 300 MHz spectrometer (¹H, 299.69 MHz operating frequency) and are reported with reference to residual solvent resonances. GC/MS was performed using a Shimadzu GCMS-QP2010 Plus system with a 30 m x 0.25 mm SHRXI-5MS column with 0.25 μm film thickness using electron impact (EI) ionization. GC/FID was

performed using a Shimadzu GC-2014 system with a 30 m x 90.25 mm HP5 column with 0.25 μm film thickness. Ethylene, oxygen, and propylene were purchased in gas cylinders from GTS-Welco and used as received. All other reagents were purchased from commercial sources and used as received. $[\text{H}(\text{Et}_2\text{O})_2][\text{BAr}^{\text{F}}_4]$ ($\text{Ar}^{\text{F}} = 3,5\text{-}(\text{CF}_3)_2\text{C}_6\text{H}_3$),¹⁶ $(\text{tmeda})\text{Pd}(\text{Me})_2$ ($\text{tmeda} = N,N,N',N'$ -tetramethylethanediamine),¹⁷ 1,4-bis(phenyl)-2,3-dimethyl-1,4-diaza-1,3-butadiene ($^{\text{Ph}}\text{DAB}^{\text{Me}}$),¹⁸ 1,4-bis(2,4,6-trimethylphenyl)-2,3-dimethyl-1,4-diaza-1,3-butadiene ($^{\text{Mes}}\text{DAB}^{\text{Me}}$),¹⁹ 1,4-bis(2,6-diisopropylphenyl)-2,3-dimethyl-1,4-diaza-1,3-butadiene ($^{\text{dipp}}\text{DAB}^{\text{Me}}$),²⁰ 1,4-bis(pentafluorophenyl)-2,3-dimethyl-1,4-diaza-1,3-butadiene ($^{\text{F1}}\text{DAB}^{\text{Me}}$),²¹ and 1,4-bis(cyclohexyl)-2,3-dimethyl-1,4-diaza-1,3-butadiene ($^{\text{Cy}}\text{DAB}^{\text{Me}}$)²² were prepared according to literature protocols. Concentrations of reagents in mol % are reported relative to benzene.

(^tbpy)Pd(Me)₂. To a stirring solution of $(\text{tmeda})\text{Pd}(\text{Me})_2$ (0.126 g, 0.395 mmol) in benzene (7 mL), ^tbpy (0.065 g, 0.40 mmol) was added and the mixture was stirred for 1 hour. The solvent volume was reduced to c.a. 2 mL *in vacuo*, and pentane (2 mL) was added to facilitate precipitation. Upon cooling to $-30\text{ }^\circ\text{C}$ overnight, the solution was filtered, and the solid was washed with cold pentane, yielding $(^t\text{bpy})\text{Pd}(\text{Me})_2$ as a yellow powder (0.106 g, 0.262 mmol, 66%). ^1H NMR (300 MHz, C_6D_6): d 8.75 (d, ^tbpy , 2H, $J_{\text{HH}} = 5.7$ Hz), 7.57 (d, ^tbpy , 2H, $J_{\text{HH}} = 1.5$ Hz), 6.64 (dd, ^tbpy , 2H, $J_{\text{HH}} = 5.7, 1.5$ Hz), 1.37 (s, CH_3 , 6H), 0.98 (s, ^tBu , 18H).

[(^tbpy)Pd(Me)(NCMe)][BAr^F₄]. A solution of $(^t\text{bpy})\text{Pd}(\text{Me})_2$ (0.015 g, 0.041 mmol) in THF (5 mL) was cooled to $-78\text{ }^\circ\text{C}$. To this was added a solution of $[\text{H}(\text{Et}_2\text{O})_2][\text{BAr}^{\text{F}}_4]$ (0.039 g, 0.032 mmol) in cold THF (5 mL) dropwise. Upon addition, the solvent volume was reduced to c.a. 2 mL *in vacuo*, and NCMe (2 mL) was added dropwise. The solution

was stirred for c.a. 5 mins, and the solvent was removed *in vacuo*. The solid was washed with pentane (2 mL) and dried *in vacuo* to afford [(^tbpy)Pd(Me)(NCMe)][BAr^F₄] as a pale yellow solid (0.039 g, 0.031 mmol, 80%). ¹H NMR (300 MHz, CDCl₃): d 8.39 (d, ^tbpy, 1H, *J*_{HH} = 6.1 Hz), 8.27 (d, ^tbpy, 1H, *J*_{HH} = 6.1 Hz), 8.03 (dd, ^tbpy, 2H, *J*_{HH} = 6.1, 2.1 Hz), 7.69 (br s, BAr^F₄, 8H), 7.56 (dd, ^tbpy, 2H, *J*_{HH} = 6.1, 2.1 Hz), 7.51 (br s, BAr^F₄, 4H), 2.34 (s, NCCCH₃, 3H), 1.40 (s, ^tBu, 9H), 1.36 (s, ^tBu, 9H), 0.99 (s, CH₃, 3H).

Reaction of [(^tbpy)Pd(Me)(NCMe)][BAr^F₄] with benzene and ethylene. [(^tbpy)Pd(Me)(NCMe)][BAr^F₄] (0.01 mol %) was dissolved in 10 mL of a stock solution of decane (0.01 mol %) in benzene. The reaction mixture was transferred to a Fisher-Porter reactor, pressurized with ethylene (25 psig), and heated to 50 °C for 4 h. The product mixture was analyzed by GC/MS.

General Procedure for Ligand Screening Reactions. A representative screening reaction is described. A PTFE-valved reaction tube was charged with Pd(OAc)₂ (0.027 g, 0.89 mmol), ^tbpy (0.241 g, 0.895 mmol), and benzene (10 mL). The vessel was sealed, pressurized with ethylene (25 psig), and the pale orange solution was stirred and heated to 50 °C for 72 h. Timepoints were taken every 24 h, at which point aliquots of the reaction mixture were removed and analyzed by GC/MS, and the vessel was recharged with ethylene.

General Procedure for Oxidant Screening Reactions. A representative screening reaction is described. A Fisher-Porter reactor was charged with ^{dipp}DAB^{Me} (0.36 g, 0.89 mmol), Pd(OAc)₂ (0.025 g, 0.89 mmol), Cu(OAc)₂ (2.16 g, 11.9 mmol), and benzene (32 mL). The vessel was sealed, pressurized with ethylene (25 psig), and the pale orange solution was stirred and heated to 50 °C for 72 h. Timepoints were taken every 24 h, at

which point aliquots of the reaction mixture were removed and analyzed by GC/MS, and the vessel was recharged with ethylene.

Catalytic Oxidative Hydrophenylation of Ethylene using (^{dipp}DAB^{Me})Pd(OAc)₂.

A representative catalytic reaction is described. A stock solution containing ^{dipp}DAB^{Me} (0.009 g, 0.02 mmol), Pd(OAc)₂ (0.005 g, 0.02 mmol), decane (40 μL, 0.20 mmol), and benzene (200 mL) was prepared. A Fisher-Porter reactor was charged with stock solution (20 mL) and Cu(OAc)₂ (0.05 g, 0.3 mmol). The vessel was sealed, pressurized with ethylene (50 psig) and oxygen (50 psig), and the pale yellow solution was stirred and heated to 120 °C for 24 h. Timepoints were taken every 4 h, at which point aliquots of the reaction mixture were removed and analyzed by GC/MS (and/or GC/FID), and the vessel was recharged with ethylene.

Catalytic Oxidative Hydrophenylation of Propylene using (^{dipp}DAB^{Me})Pd(OAc)₂.

A representative catalytic reaction is described. A stock solution containing ^{dipp}DAB^{Me} (0.009 g, 0.02 mmol), Pd(OAc)₂ (0.005 g, 0.02 mmol), decane (40 μL, 0.20 mmol), and benzene (200 mL) was prepared. A Fisher-Porter reactor was charged with stock solution (20 mL) and Cu(OAc)₂ (0.05 g, 0.3 mmol). The vessel was sealed, pressurized with propylene (50 psig) and oxygen (50 psig), and the pale yellow solution was stirred and heated to 120 °C for 24 h. Timepoints were taken every 4 h, at which point aliquots of the reaction mixture were removed and analyzed by GC/MS, and the vessel was recharged with propylene.

Catalytic Oxidative Hydrophenylation of Styrene using (^{dipp}DAB^{Me})Pd(OAc)₂.

A representative catalytic reaction is described. A stock solution containing ^{dipp}DAB^{Me} (0.009 g, 0.02 mmol), Pd(OAc)₂ (0.005 g, 0.02 mmol), decane (40 μL, 0.20 mmol), and

benzene (200 mL) was prepared. A Fisher-Porter reactor was charged with stock solution (20 mL), styrene (0.4 mL, 3.5 mmol), and Cu(OAc)₂ (0.05 g, 0.28 mmol). The vessel was sealed, pressurized with oxygen (50 psig), and the pale yellow solution was stirred and heated to 120 °C for 24 h. Timepoints were taken every 4 h, at which point aliquots of the reaction mixture were removed and analyzed by GC/MS, and the vessel was recharged with ethylene.

2.5 References

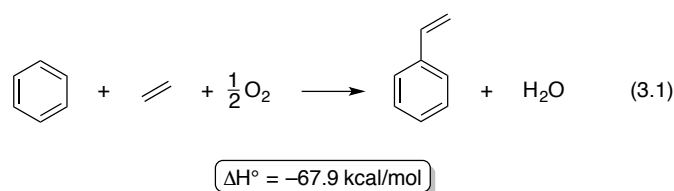
- (1) Fujiwara, Y.; Noritani, I.; Danno, S.; Asano, R.; Teranishi, S. *J. Am. Chem. Soc.* **1969**, *91*, 7166.
- (2) Taube, D.; Periana, R.; Matsumoto, T. 6127590A, 2000. (US Patent 6127590A)
- (3) Matsumoto, T.; Periana, R. A.; Taube, D. J.; Yoshida, H. *J. Catal.* **2002**, *206*, 272.
- (4) Yamada, T.; Sakakura, A.; Sakaguchi, S.; Obora, Y.; Ishii, Y. *New J. Chem.* **2008**, *32*, 738.
- (5) Kubota, A.; Emmert, M. H.; Sanford, M. S. *Org. Lett.* **2012**, *14*, 1760.
- (6) McKeown, B. A.; Foley, N. A.; Lee, J. P.; Gunnoe, T. B. *Organometallics* **2008**, *27*, 4031.
- (7) McKeown, B. A.; Gonzalez, H. E.; Friedfeld, M. R.; Gunnoe, T. B.; Cundari, T. R.; Sabat, M. *J. Am. Chem. Soc.* **2011**, *133*, 19131.
- (8) McKeown, B. A.; Gonzalez, H. E.; Michaelos, T.; Gunnoe, T. B.; Cundari, T. R.; Crabtree, R. H.; Sabat, M. *Organometallics* **2013**, *32*, 3903.
- (9) McKeown, B. A.; Gonzalez, H. E.; Gunnoe, T. B.; Cundari, T. R.; Sabat, M. *ACS Catal.* **2013**, *3*, 1165.
- (10) McKeown, B. A.; Gonzalez, H. E.; Friedfeld, M. R.; Brosnahan, A. M.; Gunnoe, T. B.; Cundari, T. R.; Sabat, M. *Organometallics* **2013**, *32*, 2857.
- (11) McKeown, B. A.; Prince, B. M.; Ramiro, Z.; Gunnoe, T. B.; Cundari, T. R. *ACS Catal.* **2014**, *4*, 1607.

- (12) In *CRC Handbook of Chemistry and Physics* Weast, R. C., Ed.; CRC Press/Taylor & Francis: Boca Raton, FL, 1977.
- (13) McKeown, B. A., Unpublished Work.
- (14) Foley, N. A.; Lee, J. P.; Ke, Z.; Gunnoe, T. B.; Cundari, T. R. *Acc. Chem. Res.* **2009**, *42*, 585.
- (15) Wittcoff, H. A.; Reuben, B. G.; Plotkin, J. S. Chemicals and Polymers from Ethylene. In *Industrial Organic Chemicals*; Wiley: Hoboken, NJ, 2004, pp 100.
- (16) Brookhart, M.; Grant, B.; Volpe, A. F. *Organometallics* **1992**, *11*, 3920.
- (17) De Graaf, W.; Boersma, J.; Smeets, W. J. J.; Spek, A. L.; Van Koten, G. *Organometallics* **1989**, *8*, 2907.
- (18) Kurokawa, H.; Miura, K.; Yamamoto, K.; Sakuragi, T.; Sugiyama, T.; Ohshima, M.-a.; Miura, H. *Catalysts* **2013**, *3*, 125.
- (19) Zhong, H. A.; Labinger, J. A.; Bercaw, J. E. *J. Am. Chem. Soc.* **2002**, *124*, 1378.
- (20) Pourtaghi-Zahed, H.; Zohuri, G. *Polym. Bull.* **2013**, *70*, 1769.
- (21) Khusniyarov, M. M.; Harms, K.; Burghaus, O.; Sundermeyer, J. *Eur. J. Inorg. Chem.* **2006**, *2006*, 2985.
- (22) De Kimpe, N.; D'Hondt, L.; Stanoeva, E. *Tetrahedron Lett.* **1991**, *32*, 3879.

3. Development and Mechanistic Studies of a Rhodium Catalyst for the Oxidative Vinylation of Benzene

3.1 Introduction

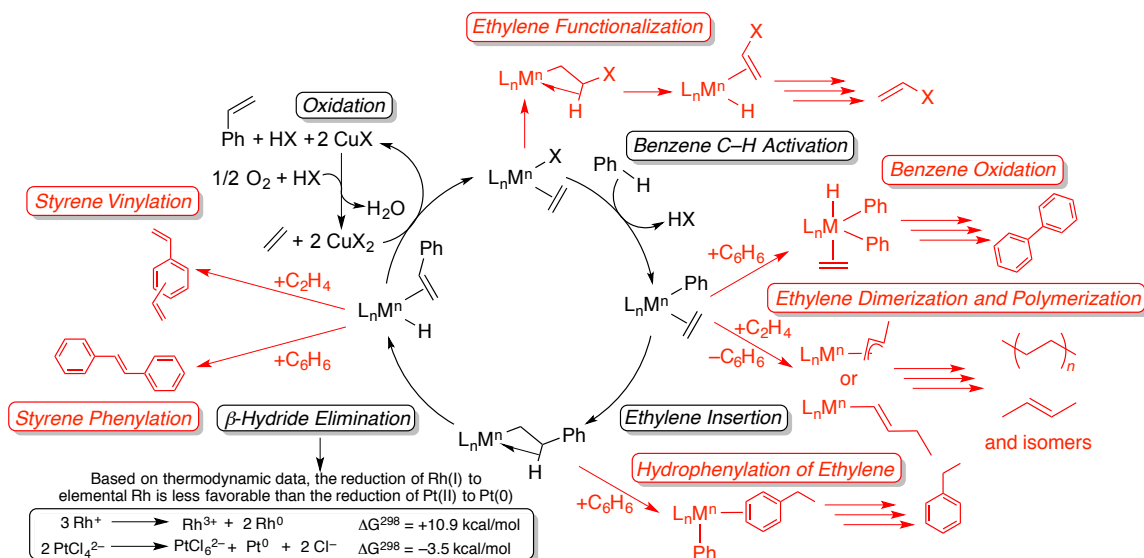
Given the scale of annual production of styrene and the disadvantages of current industrial synthesis (acid-based catalysis), the development of a novel synthetic method for the conversion of benzene and ethylene to styrene would be beneficial. One possible route involves the metal-mediated activation of a C–H bond of benzene to yield a M–Ph bond, ethylene insertion into the resulting M–Ph bond to produce a M–CH₂CH₂Ph intermediate, and β -hydride elimination from the resulting M–CH₂CH₂Ph complex to give coordinated styrene and a M–H bond (Scheme 3.1). Subsequent styrene dissociation (regardless of mechanism) and reaction with oxidant can regenerate the active catalyst, and if the oxidant is oxygen (either used *in situ* or used to recycle an *in situ* oxidant), the net reaction is the thermodynamically favorable conversion of benzene, ethylene, and oxygen to styrene and water (eq 3.1).¹



For the platinum(II) catalysts previously studied in our group, this is not a viable pathway for styrene production, as the catalysts generally decompose upon the production of styrene.² We proposed that the catalyst decomposition is the result of unstable Pt(II)–hydride complexes, formed from β -hydride elimination, that react to release H₂ and produce metallic Pt. The thermodynamic driving force for the formation of

inactive Pt^0 presents a substantial challenge to achieving long-lived vinyl arene production with these catalysts (Scheme 3.1 inset).¹

Scheme 3.1. Proposed cycle for transition metal-catalyzed styrene production from benzene and ethylene using CuX_2 as an oxidant. The cuprous (CuX) product could be recycled to the cupric state using O_2 from air, as shown at the upper left. Potential side reactions that a selective catalyst must avoid are shown in red.



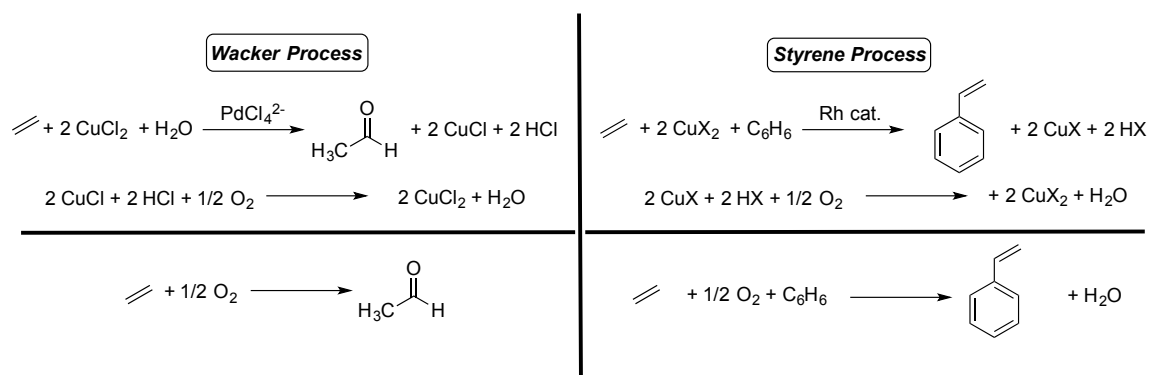
For our Pt catalysts, the formation of elemental Pt is irreversible, but for Pd, this reoxidation is more facile. Thus, we designed Pd(II) complexes and tested their activity for oxidative arene vinylation and found that, while they were highly active and stable catalysts, they were not selective, forming mixtures of products in all cases studied (see Chapter 2). Given that the formation and decomposition of Pt(II)–H species is problematic, and Pd(II) catalysts are unselective for vinyl arene product, we sought to design catalysts using Rh(I) in anticipation that Rh(I)–H intermediates would exhibit greater stability compared to related Pt species (Scheme 3.1 inset).¹

Scheme 3.1 shows a targeted catalytic cycle for the direct oxidative vinylation of benzene to produce styrene. Despite precedent for the key steps in this catalytic cycle, designing a selective catalyst represents a substantial challenge as many competing side reactions (shown in red) are likely to have activation barriers that are similar to or lower than those of the reactions along the desired catalytic cycle. In addition to these possible side reactions, designing a molecular catalyst that achieves high turnover numbers (TON) is difficult because the oxidizing conditions and the presence of potentially reactive metal–hydride intermediates could be anticipated to result in catalyst decomposition.

Table 3.1 compares previously reported homogeneous catalysts for direct oxidative styrene synthesis from ethylene and benzene.^{3–8} Generally, all suffer from one or more of the following drawbacks: low selectivity, low yield, low TON, and/or use of oxidants that cannot be regenerated using oxygen. Hong and co-workers reported a $\text{Rh}_4(\text{CO})_{12}$ catalyst (Entry 1) that gave, to our knowledge, the highest TON of styrene (472). In tandem with this process, liberated dihydrogen is consumed by 2 equivalents of ethylene and one equivalent of CO to produce 809 TO of 3-pentanone for an overall 37% selectivity for styrene.³ Periana and coworkers have disclosed a Rh(III) catalyst (Entry 2) gives 36% yield relative to a Cu(II) oxidant with high selectivity for styrene (89%).⁴ Tanaka and co-workers have reported a Rh(I) catalyst (Entry 3) that produces 3 TO of styrene (38% yield) under photolytic conditions with a selectivity of only 18%.⁸ Milstein and co-workers have disclosed a Ru(II) catalyst (Entry 4) that affords 7.5 TO of styrene (3% yield) using O_2 directly as the oxidant.⁹ Fujiwara and co-workers reported the first use of $\text{Pd}(\text{OAc})_2$ as a catalyst for the oxidative vinylation of benzene using an AgOAc oxidant,

although it only resulted in sub-stoichiometric styrene production and significant formation of stilbene (Entry 5).⁵ Periana and co-workers also reported the use of Pd(OAc)₂ for styrene production (Entry 6), although they used a Cu(II) oxidant under aerobic conditions to afford 19 TO styrene (5% yield) and 47 TO vinyl acetate (29% selectivity).⁴ Ishii and co-workers reported a Pd(II) catalyst (Entry 7) that affords 100 TO of styrene (58% yield) with 2% selectivity using a heteropoly acid oxidant.⁶ Sanford and co-workers reported that (3,5-dichloropyridyl)Pd(OAc)₂ catalyzes styrene production with 100% selectivity and a TON of 6.6 TON for styrene (33% overall yield) using PhCO₃^tBu, an oxidant which cannot be recycled with oxygen (Entry 8).⁷

Herein, we report a rhodium catalyst for the selective one-step production of styrene from benzene, ethylene and Cu(II) salts (Table 3.1, Entries 9 and 10). We chose a Cu(II) salt as the *in situ* oxidant because of industrial precedent for recycling reduced Cu(I) using oxygen. In the commercial Wacker-Hoechst process for ethylene oxidation,^{10,11} use of oxygen to reoxidize Cu(I) to Cu(II) has proven viable both *in situ* as well as in a second step, which would be required for our Rh(I)-based process (Scheme 3.2).¹² Portions of this work have been published previously.^{13,14}

Scheme 3.2. Comparison of Wacker Process and styrene process reported herein.**Table 3.1.** Comparison of previously reported catalysts for styrene production. TON = turnover number for styrene. Selectivity is defined as turnovers styrene/total turnovers (all products), and is given as a percentage. Yield of styrene is reported relative to the limiting reagent.

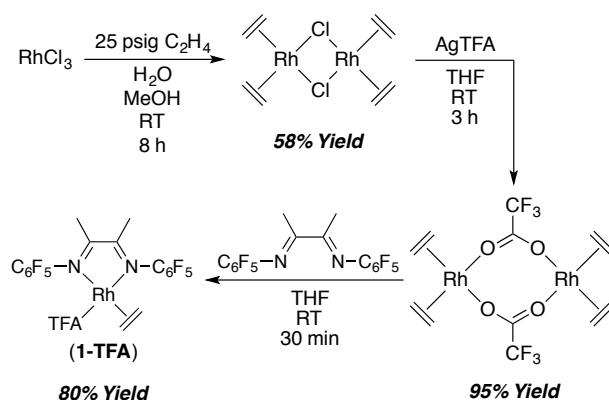
Entry	Catalyst	Oxidant	TON	Selectivity	Yield
1 ^[†]	Rh ₄ (CO) ₁₂	C ₂ H ₄ /CO	472	37%	19%
2 ^[††]	(acac) ₂ Rh(Cl)(H ₂ O)	Cu(OAc) ₂	24	89%	36%
3 ^[††]	Rh(PMe ₃) ₂ (CO)(Cl)	hν	3	38%	18%
4 ^[§]	RuCl ₃ · 3H ₂ O	O ₂	7.5	N.R.	3%
5 ^[¶]	Pd(OAc) ₂	AgOAc	0.59	44%	12%
6 ^[‡‡]	Pd(OAc) ₂	Cu(OAc) ₂ /O ₂	19	29%	5%
7 ^[¶¶]	(DBM)Pd(OAc) ₂	HPA	100	58%	2%
8 ^[**]	(3,5-DCP)Pd(OAc) ₂	PhCO ₃ ^t Bu	6.6	100%	33%
9 ^[†††]	(^{F1} DAB)Rh(TFA)(C ₂ H ₄)	Cu(OAc) ₂	115	100%	96%
10 ^[§§]	(^{F1} DAB)Rh(TFA)(C ₂ H ₄)	Cu(OAc) ₂	835	100%	70%

[*] Reference³. [†] Reference⁴, acac = acetylacetonate. [†] Reference⁸. [§] Reference⁹, N.R. = not reported. [¶] Reference⁵. [‡] Reference⁴. [†] Reference⁶, DBM = dibenzoylmethane, HPA = H₃PtMo₁₂O₄₀ · 30H₂O. [**] Reference⁷, DCP = 3,5-dichloropyridine. [††] ^{F1}DAB = *N,N'*-bis(pentafluorophenyl)-2,3-dimethyl-1,4-diaza-1,3-butadiene; TFA = trifluoroacetate; 0.001 mol % catalyst loading; described herein. [§§] ^{F1}DAB = *N,N'*-bis(pentafluorophenyl)-2,3-dimethyl-1,4-diaza-1,3-butadiene; TFA = trifluoroacetate; 0.0001 mol % catalyst loading; described herein.

3.2 Catalyst Development¹⁵

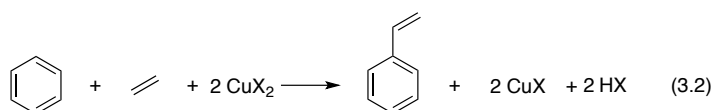
We recently reported the synthesis of an electron-deficient Rh(I) complex (^{F1}DAB)Rh(TFA)(η^2 -COE) [^{F1}DAB = *N,N'*-bis(pentafluorophenyl)-2,3-dimethyl-1,4-diaza-1,3-butadiene; TFA = trifluoroacetate; COE = cyclooctene] and demonstrated that this complex is a pre-catalyst for arene H/D exchange in trifluoroacetic acid.¹⁶ Given that arene C–H activation is a key step in transition metal-catalyzed oxidative arene vinylation, we hypothesized that this Rh(I) complex might be an effective catalyst precursor for styrene production from benzene and ethylene. Because the labile COE ligand would likely exchange for ethylene under catalytic conditions, the ethylene analog (^{F1}DAB)Rh(TFA)(η^2 -C₂H₄) (**1-TFA**) was independently synthesized and used as our catalyst precursor (Scheme 3.3).

Scheme 3.3. Synthesis of (^{F1}DAB)Rh(TFA)(η^2 -C₂H₄) (**1-TFA**).



Heating a 20 mL benzene solution of **1-TFA** (0.001 mol % relative to benzene) with ethylene (25 psig) and $\text{Cu}(\text{OAc})_2$ (120 equivalents relative to **1-TFA**) to 150 °C affords 60(2) turnovers (TO) of styrene after 24 h (for all TOs reported, standard deviations are given in parentheses). Aliquots of the reaction mixture were analyzed by GC/FID using relative peak areas versus an internal standard (decane). This corresponds to quantitative

yield based on the Cu(II) limiting reagent. The calculated yield assumes that two equivalents of Cu(II) are consumed to produce each equivalent of styrene (eq 3.2). No other products were observed upon analysis of the reaction mixture by GC/MS or GC/FID, indicating high selectivity for styrene production. Detection limits for both instruments were equivalent to ~1 TO of product. Specifically, we looked for evidence of stilbene, biphenyl, and vinyl acetate production, as these are the most commonly observed byproducts in previously reported catalysis (Table 3.1 and references therein). Control reactions with $[\text{Rh}(\mu\text{-TFA})(\eta^2\text{-C}_2\text{H}_4)_2]_2$, a precursor to complex **1-TFA**, afforded < 5 TO of styrene after 24 h with or without $\text{Cu}(\text{OAc})_2$, potentially highlighting the importance of the $^{\text{Fl}}$ DAB ligand. It is important to note that further experiments using $[\text{Rh}(\mu\text{-TFA})(\eta^2\text{-C}_2\text{H}_4)_2]_2$ revealed that the lack of reactivity after 24 h represents a long induction period,¹⁷ but for the purposes of this work, it can be concluded that observed reactivity of **1-TFA** is not a result of a $[\text{Rh}(\mu\text{-TFA})(\eta^2\text{-C}_2\text{H}_4)_2]_2$ -catalyzed process. Control reactions with $\text{Cu}(\text{OAc})_2$ alone also afforded no styrene formation.



3.2.1 Optimization of Reaction Conditions with **1-TFA**

With a competent catalyst in hand, we next sought to optimize reaction conditions. The effect of oxidant properties on catalysis with **1-TFA** was the first parameter investigated. Both soluble (copper 2-ethylhexanoate $[\text{Cu}(\text{OHex})_2]$ and copper pivalate $[\text{Cu}(\text{OPiv})_2]$) and insoluble (copper acetate $[\text{Cu}(\text{OAc})_2]$ and copper trifluoroacetate hydrate $[\text{Cu}(\text{TFA})_2]$) Cu(II) salts were screened. Figure 3.1 shows plots of turnovers versus time for each of the Cu(II) oxidants. Using an apparent turnover frequency (TOF)

calculated after 4 hours of reaction, soluble $\text{Cu}(\text{OHex})_2$ gives the fastest initial rate with a TOF of $2.8 \times 10^{-3} \text{ s}^{-1}$, but the reaction does not reach 100% yield relative to oxidant until 28 h, which may indicate that catalyst deactivation occurs. $\text{Cu}(\text{OAc})_2$ affords a slower initial rate than $\text{Cu}(\text{OHex})_2$, with a TOF of $2.8 \times 10^{-4} \text{ s}^{-1}$ after 4 h, but this oxidant provides a more stable catalytic process and reaches quantitative yield after only ~ 16 h. Both $\text{Cu}(\text{TFA})_2$ and $\text{Cu}(\text{OPiv})_2$ afford slower initial rates; reactions with $\text{Cu}(\text{OPiv})_2$ reach 92% yield after 28 h, whereas reactions with $\text{Cu}(\text{TFA})_2$ produce only 19 TO styrene (32% yield) after 20 h.

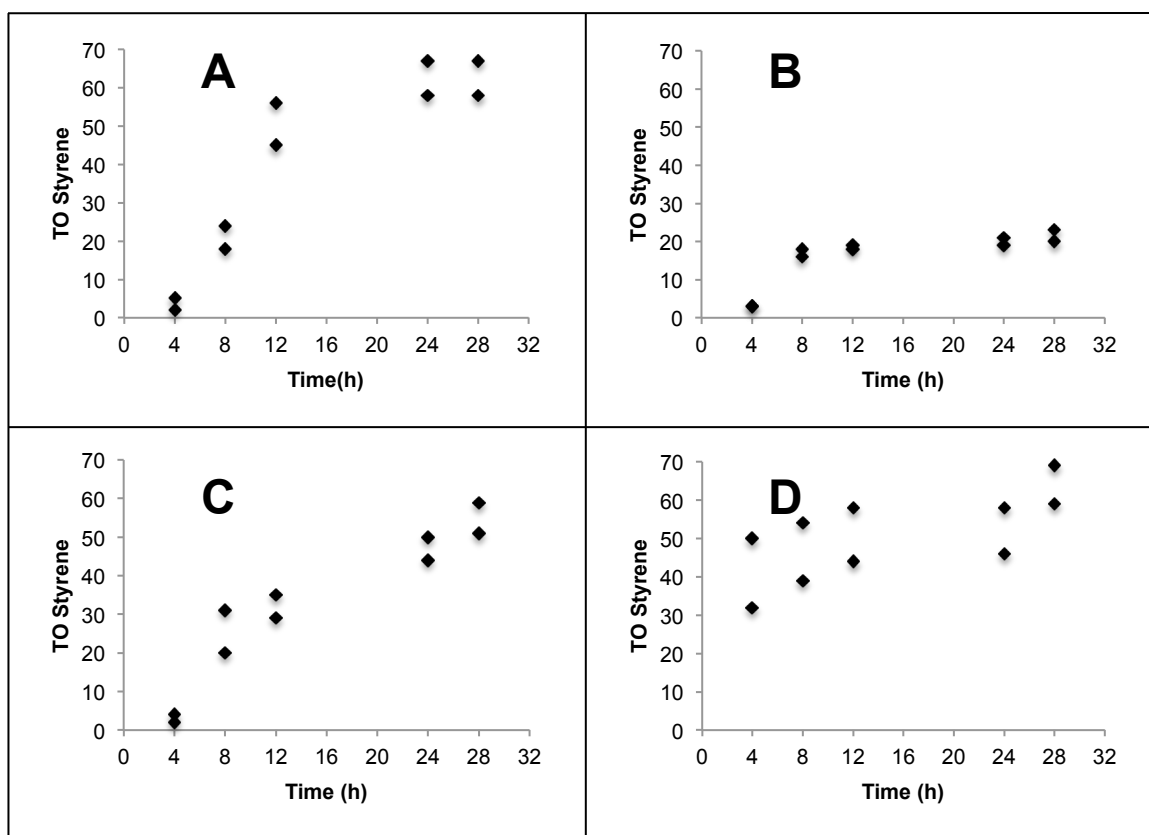


Figure 3.1. Plots of TO for styrene production vs. time as a function of oxidant using $(^{\text{Fl}}\text{DAB})\text{Rh}(\text{TFA})(\eta^2\text{-C}_2\text{H}_4)$ (**1-TFA**). A) $\text{Cu}(\text{OAc})_2$, B) $\text{Cu}(\text{TFA})_2$, C) $\text{Cu}(\text{OPiv})_2$, D) $\text{Cu}(\text{OHex})_2$. Reaction conditions: 0.001 mol % **1-TFA**, 25 psig C_2H_4 , 120 equivalents oxidant, 150 °C, theoretical maximum TON = 60. Data for two independent runs are shown for each oxidant.

In order to study catalyst longevity, we varied the amount of $\text{Cu}(\text{OAc})_2$. Within the range of 60 and 240 equivalents (relative to **1-TFA**), the yield of styrene relative to oxidant was always $> 95\%$ (Figure 3.2). These near-quantitative yields demonstrate that the catalytic process using **1-TFA** as a precursor is stable and long-lived. For a reaction using 0.0001 mol % **1-TFA** and 2400 equivalents of $\text{Cu}(\text{OAc})_2$, the catalyst remained active over a period of 96 h and afforded a TON of 835(18). A plot of TO versus time shows that the Rh catalyst is stable through at least 96 hours (Figure 3.3). The tolerance of **1-TFA** to a large excess of oxidant without any decrease in activity is promising. The effect of temperature on catalysis was also examined (Figure 3.4). Generally, the rate of reaction increased with temperature; however, at 180 °C, rapid catalyst deactivation led to a low turnover number (< 10 TO) after 12 h. Minimal activity (< 1 TO) was also observed at temperatures < 100 °C. The optimal temperature proved to be ~ 150 °C.

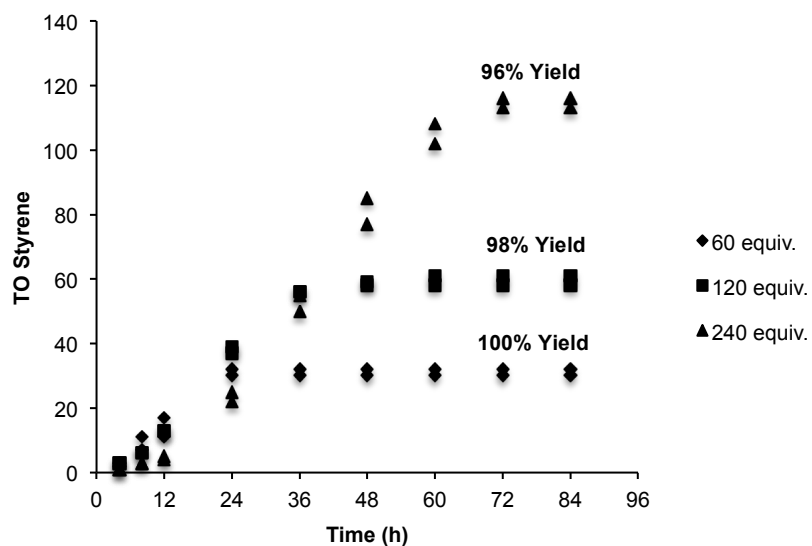


Figure 3.2. Effect of oxidant amount on styrene production using $(^{\text{Fl}}\text{DAB})\text{Rh}(\text{TFA})(\eta^2\text{-C}_2\text{H}_4)$ (**1-TFA**). Reaction conditions: 0.0001 mol % **1-TFA**, 25 psig C_2H_4 , 120 °C. Percent yield is reported relative to oxidant, assuming 2 equivalents are required per TO. Data for two independent runs are shown for each oxidant amount.

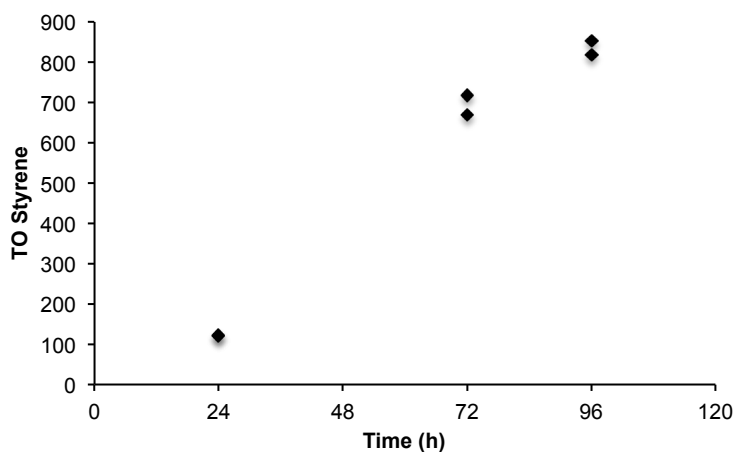


Figure 3.3. TO vs. Time plot for catalysis with 0.0001 mol % (^{F1}DAB)Rh(TFA)(η^2 -C₂H₄) (**1-TFA**). Reaction conditions: 0.0001 mol % **1-TFA**, 2400 equiv. Cu(OAc)₂, 75 psig C₂H₄, 150 °C, theoretical maximum TON = 1200. Data for two independent runs are shown.

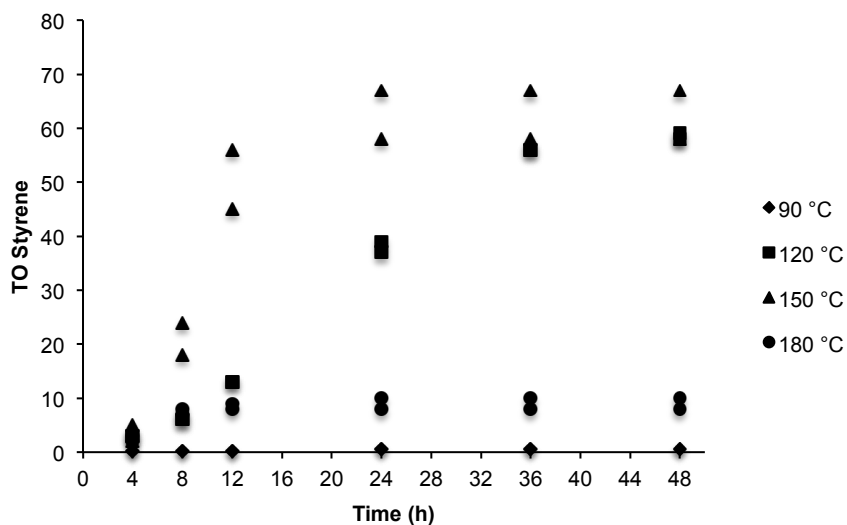


Figure 3.4. Effect of temperature on styrene production using (^{F1}DAB)Rh(TFA)(η^2 -C₂H₄) (**1-TFA**). Reaction conditions: 0.001 mol % **1-TFA**, 120 equivalents Cu(OAc)₂, 25 psig C₂H₄. Data for two independent runs are shown for each temperature.

We also observed that the reaction rate increased with increasing ethylene pressure. To determine an apparent TOF, we measured TO after 4 h of reaction (Table 3.2). Figure 3.5 shows a plot of TOF vs. ethylene pressure, where a linear correlation is observed. Thus, the reaction rate appears to have a first-order dependence on ethylene concentration. This is in contrast to previously reported Pt(II) and Ru(II) catalysts for the hydrophenylation of ethylene, which show an inverse dependence on ethylene pressure due to their off-cycle $M(\text{CH}_2\text{CH}_2\text{Ph})(\eta^2\text{-C}_2\text{H}_4)$ ($M = \text{Pt}, \text{Ru}$) resting states.^{18,19} The opposite dependence on ethylene pressure observed when using **1-TFA** as the catalyst precursor likely signals a change in the catalyst resting state and/or rate-determining step.

Table 3.2. Effect of ethylene pressure on catalysis with $(^{\text{F1}}\text{DAB})\text{Rh}(\text{TFA})(\eta^2\text{-C}_2\text{H}_4)$ (**1-TFA**). Reaction Conditions: 0.001 mol % **1-TFA**, 120 equiv. $\text{Cu}(\text{OAc})_2$, 150 °C, 4 h.

$P_{\text{C}_2\text{H}_4}$ (psig)	TON ^[^]	TOF (s^{-1}) ^[*]
15	1(0)	6.9×10^{-5}
25	4(1)	2.4×10^{-4}
50	20(2)	1.4×10^{-3}
100	45(2)	3.1×10^{-3} ^[‡]

[^] Reported TON are an average of two independent reactions, each analyzed in duplicate. The standard deviations of all four values are given in parentheses. [*] Calculated using TO styrene after 4 h of reaction. [‡] Due to catalyst deactivation, this number likely represents a lower limit.

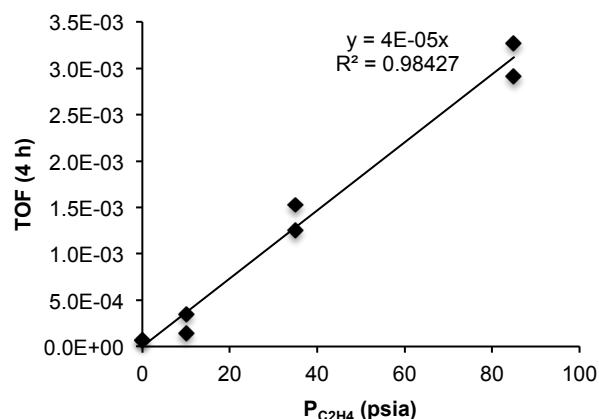
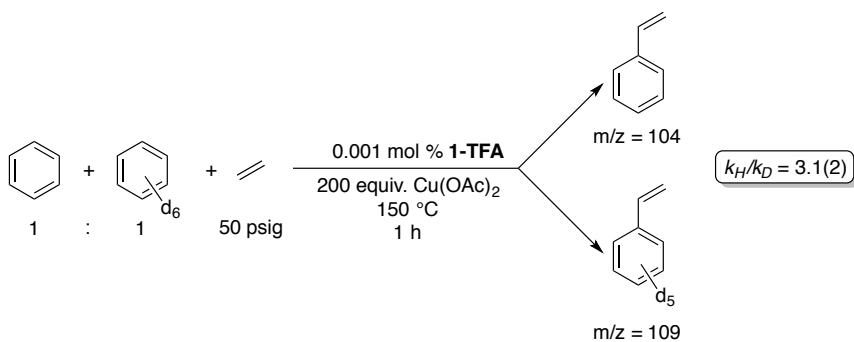


Figure 3.5. Effect of ethylene pressure on catalysis with (^{F1}DAB)Rh(TFA)(η^2 -C₂H₄) (**1-TFA**). Reaction conditions: 0.001 mol % **1-TFA**, 120 equivalents Cu(OAc)₂, 150 °C, 4 h.

To gain further insight into the reaction mechanism, we ran catalytic reactions in a 1:1 molar mixture of C₆H₆ and C₆D₆ and analyzed the resulting products by GC/MS. After 1 h, a k_H/k_D of 3.1(2) was determined by examining the ratio of undeuterated styrene ($m/z = 104$) to styrene-*d*₅ ($m/z = 109$) in the mass spectrum (Scheme 3.4). After 2 h, the observed isotope effect was 3.0(2), statistically equivalent to the data after 1 h of reaction.

Scheme 3.4. Kinetic isotope effect experiment using a 1:1 molar ratio of C₆H₆ to C₆D₆. Reported isotope effect represents the average of three independent runs, and the deviation is reported in parentheses.



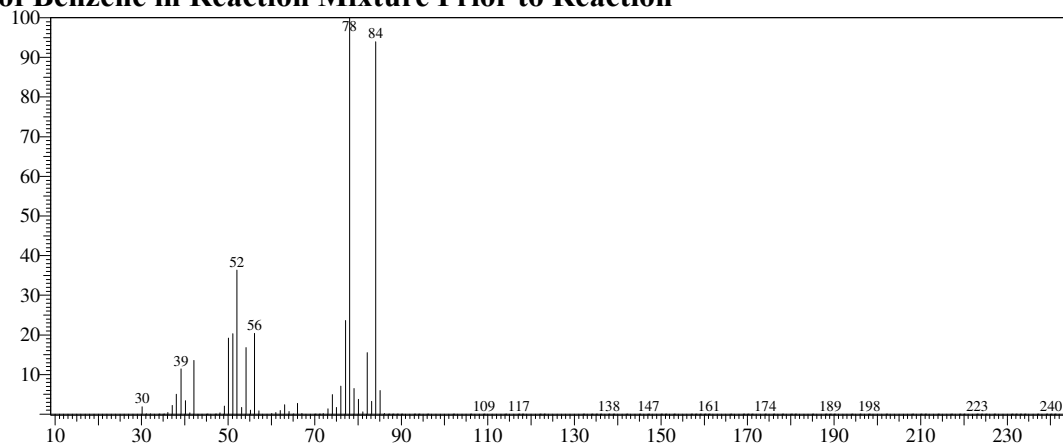
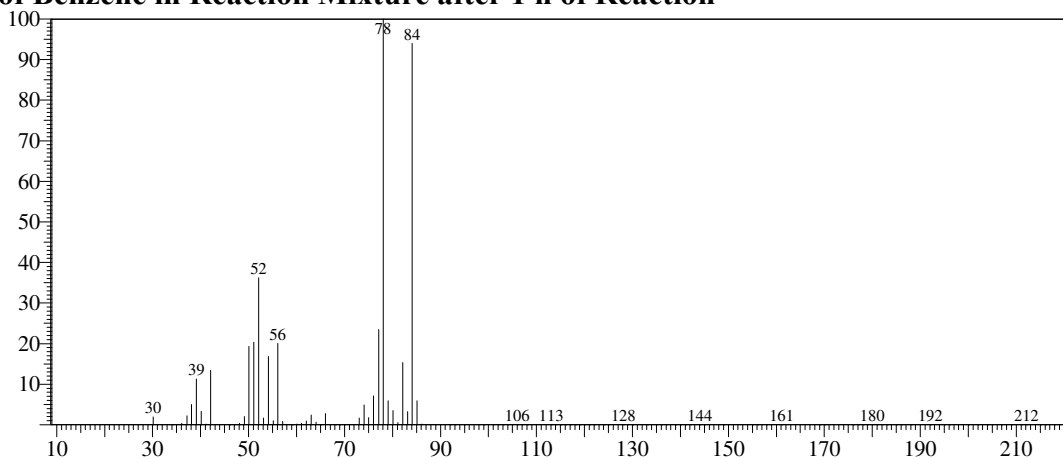
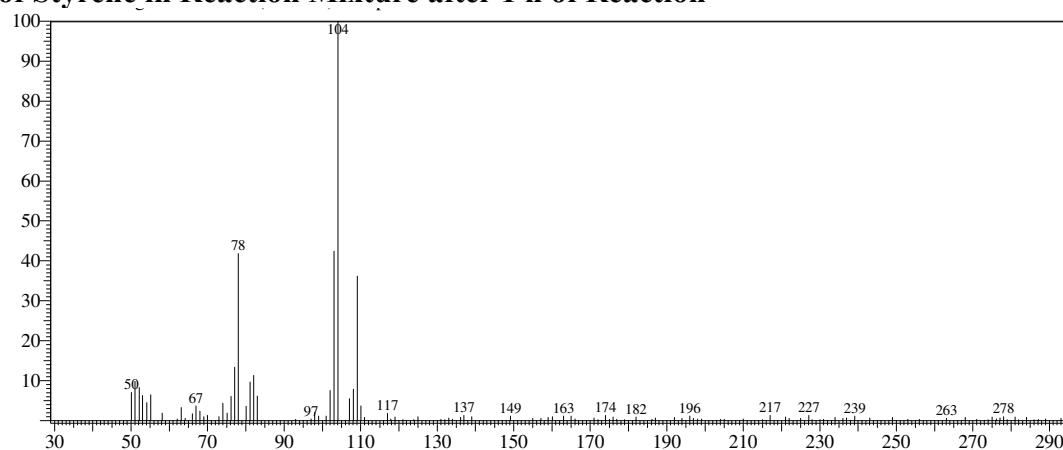
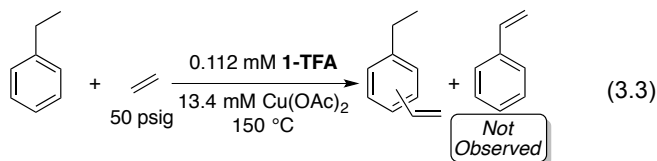
MS of Benzene in Reaction Mixture Prior to Reaction**MS of Benzene in Reaction Mixture after 1 h of Reaction****MS of Styrene in Reaction Mixture after 1 h of Reaction**

Figure 3.6. Mass spectra for kinetic isotope effect experiments using a 1:1 molar mixture of C_6H_6 and C_6D_6 . Reaction conditions: 5 mL C_6H_6 , 5 mL C_6D_6 , 0.001 mol % **1-TFA**, 200 equiv. $Cu(OAc)_2$, 50 psig C_2H_4 , 150 °C.

Thus, the observed $k_{\text{H}}/k_{\text{D}}$ of ~ 3.1 likely reflects an actual kinetic isotope effect (KIE) for the catalytic reaction. The KIE is consistent with other transition metal-mediated C–H activation reactions.^{20,21} The primary KIE supports the hypothesis that a Rh catalyst is facilitating a metal-mediated C–H activation process that occurs in the kinetically-relevant regime of the catalytic cycle. No change in the isotopic distribution for benzene was observed over the course of the reaction, and no styrene- d_{6-8} products were observed except those predicted by the natural abundance of deuterium in ethylene, indicating that H/D scrambling and reversible C–H activation were both unlikely (Figure 3.6).

3.3 Mechanistic Studies of Catalysis with 1-OAc²²

Since our general mechanistic hypothesis for styrene production (Scheme 3.1) involves the direct conversion of benzene and ethylene to styrene without the intermediacy of ethylbenzene, we first sought to confirm that ethylbenzene is not converted to styrene under catalytic conditions using **1-TFA** (eq 3.3). Heating a solution of **1-TFA** and $\text{Cu}(\text{OAc})_2$ in ethylbenzene under 50 psig of ethylene showed no formation of styrene after 8 h. Isomers of ethylvinyl benzene were detected, but not quantified, by GC/MS.



3.3.1 Apparent Induction Period

Under some conditions, monitoring the conversion of benzene, ethylene, and $\text{Cu}(\text{OAc})_2$ to styrene and CuOAc catalyzed by **1-TFA** reveals an apparent induction period (see Figure 3.7, for example). We investigated two possible rationalizations for the observed increase in rate of catalysis: 1) the active catalyst is formed by decomposition of **1-TFA** to Rh nanoparticles that catalyze the reaction,²³ and 2) during the apparent induction period, **1-TFA** converts to $(^{\text{Fl}}\text{DAB})\text{Rh}(\text{OAc})(\eta^2\text{-C}_2\text{H}_4)$ (**1-OAc**), and **1-OAc** catalyzes the reaction at a faster rate than **1-TFA**.

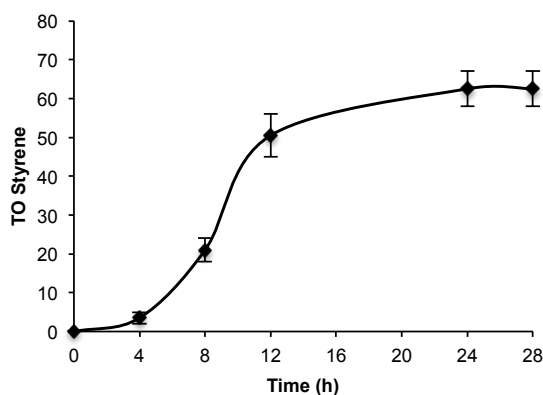


Figure 3.7. TO vs. time plot for catalysis with **1-TFA**. Reaction conditions: 0.112 mM **1-TFA**, 20 mL C_6H_6 , 25 psig ethylene, 13.4 mM $\text{Cu}(\text{OAc})_2$ (120 equiv. relative to **1-TFA**), 150 °C. Each data point is the average of two independent catalytic reactions, each analyzed in duplicate by GC/FID. Error bars represent the standard deviation of all four values.

3.3.2 Testing for Nanoparticle Formation

The decomposition of homogeneous catalysts to form nanoparticles has been well documented, and the catalytic activity of the resulting nanoparticles has been reported, particularly for hydrogenation reactions.²³⁻²⁵ As such, number of tests for the formation of nanoparticles from the decomposition of homogeneous complexes are known,²⁶ however

some of these methods are unsuitable for use with rhodium (e.g., the mercury drop test, which is unsuitable as Rh does not amalgamate well).²⁶ A method for the detection of nanoparticles that is compatible with Rh is transmission electron microscopy (TEM). While it has been argued that TEM might not provide useful information regarding the formation of nanoparticles due to its inherent inability to visualize particles smaller than 1 nm in size,²⁶ when coupled with energy-dispersive X-Ray spectroscopy (EDS), which provides information about the elemental composition of samples, this method can provide evidence for or against the formation of nanoparticles.

We performed TEM/EDS experiments on samples of reaction mixtures from catalysis with **1-TFA** in collaboration with James Kammert in the Davis Group (UVA Chemical Engineering). Catalytic reactions with **1-TFA** and $\text{Cu}(\text{OAc})_2$ were allowed to reach completion, after which samples were deposited on a grid, allowed to evaporate, and analyzed by TEM and EDS. While many of the sample regions chosen for TEM imaging appeared to contain nanoparticles (Figure 3.8), EDS results show that these regions do not contain Rh. Interestingly, some of the regions that appeared to be amorphous showed significant concentrations of Rh by EDS. We hypothesized that this was likely a result of remaining molecular Rh complex on the sample grid. To test this hypothesis, samples of neat reaction mixture were decanted to leave only solid (mostly Cu) and remove any soluble materials. The solid was subsequently sonicated in dioxane (in which **1-TFA** is soluble), decanted, and the remaining solid was deposited on the grid. Results from EDS of these washed samples showed that no Rh was present (Figure 3.9). As an additional control, the solid material isolated by filtration was subjected to catalytic conditions, and styrene production was not observed after 12 h of heating at 150 °C.

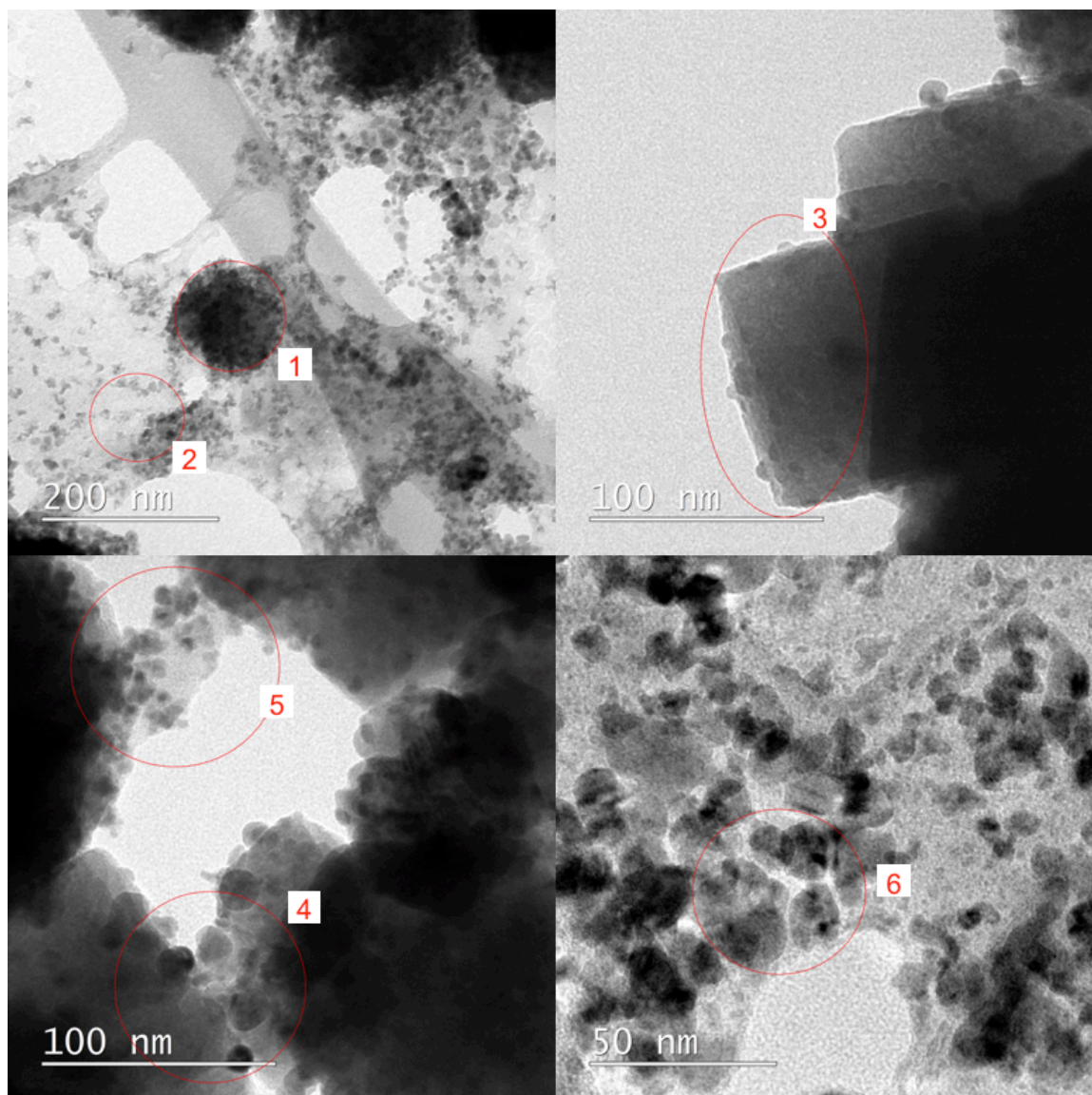


Figure 3.8. TEM images of unwashed samples from catalysis with **1-TFA**. Energy-dispersive X-ray spectroscopy (EDS) was performed on areas circled in red. Reaction conditions for catalysis: 0.112 mM **1-TFA**, 20 mL C_6H_6 , 50 psig ethylene, 13.4 mM $Cu(OAc)_2$, 150 °C, 12 h.

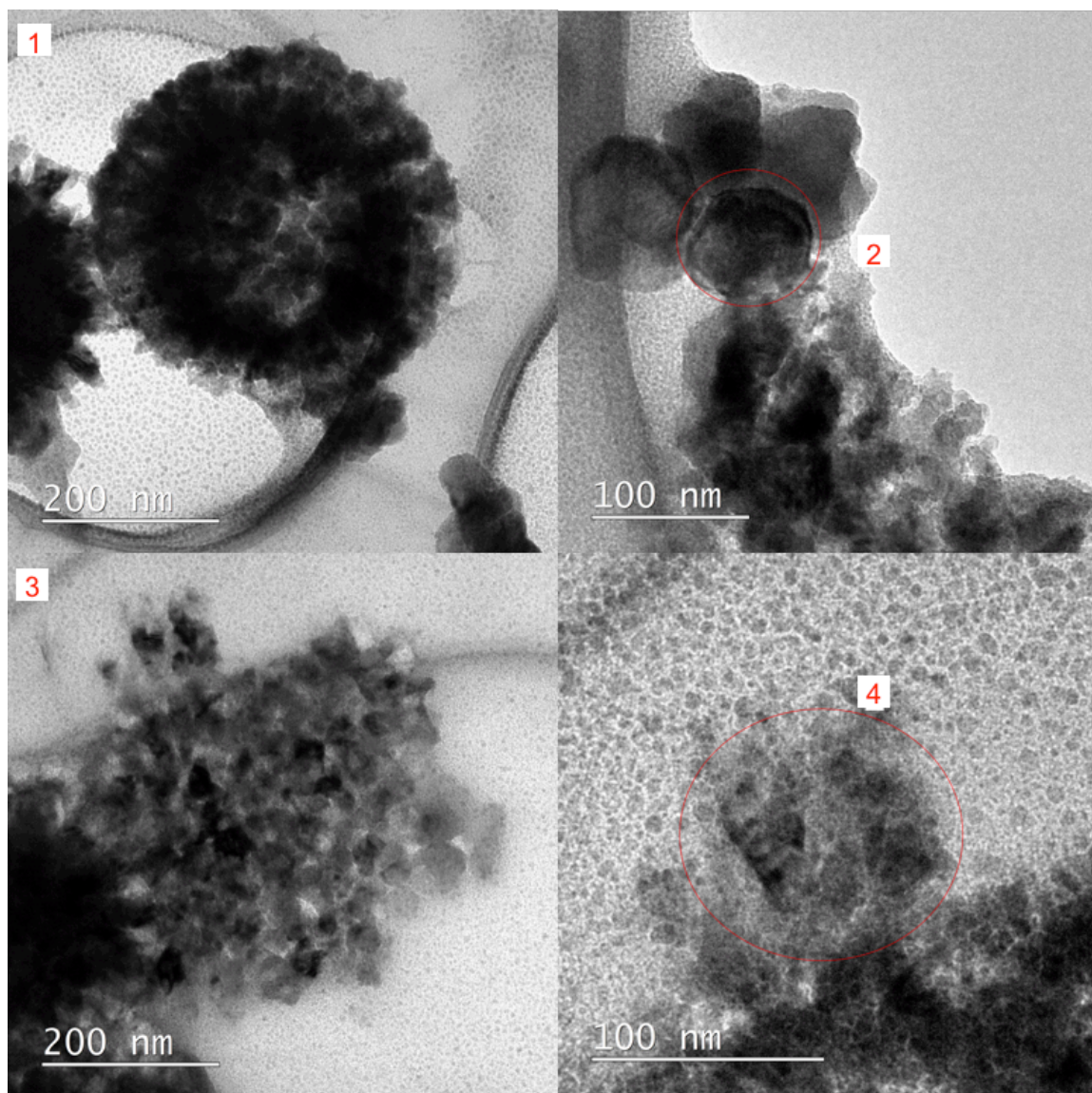


Figure 3.9. TEM images of samples from catalysis with **1-TFA** sonicated in 1,4-dioxane. EDS was performed on areas circled in red or the whole area of the image if no circle is shown. Reaction conditions for catalysis: 0.112 mM **1-TFA**, 20 mL C_6H_6 , 50 psig ethylene, 13.4 mM $Cu(OAc)_2$, 150 °C, 12 h.

In addition to the TEM/EDS analysis, we performed the Maitlis filtration test to probe for the formation of insoluble nanoparticles (Figure 3.10).²⁷ Previously, we used this technique to gain evidence for the formation of Pt(s) that catalyzes hydrogenolysis.²³

Reactions with **1-TFA** and $\text{Cu}(\text{OPiv})_2$ (*n.b.*: $\text{Cu}(\text{OPiv})_2$ was used due to its solubility in benzene) were sampled every 30 mins until 3 h (which is after the induction period), at which time the reaction mixture was filtered through Celite and the reactors were recharged with the filtrate and ethylene and heated to 150 °C. The filtration should remove insoluble Rh materials, and a second induction period would be expected if insoluble materials were serving as the active catalyst. The results from both the TEM/EDS and Maitlis test experiments suggest that insoluble materials are not serving as the catalyst, and therefore, that formation of insoluble Rh nanoparticles is likely not responsible for the apparent induction period.

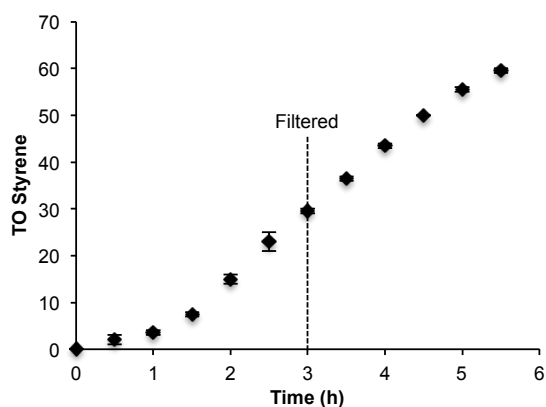


Figure 3.10. TO vs. time plot with the reaction solution filtered at 3 h. Reaction conditions: 0.112 mM **1-TFA**, 20 mL C_6H_6 , 50 psig ethylene, 13.4 mM $\text{Cu}(\text{OPiv})_2$ (120 equiv. relative to **1-TFA**), 150 °C. Each data point is the average of two independent catalytic reactions, each analyzed in duplicate by GC/FID. Error bars represent the standard deviation of all four values.

3.3.3 Comparison of Catalysis with **1-TFA** and **1-OAc**

Operating under the assumption that catalysis proceeds by a pathway similar to that shown in Scheme 3.1, we hypothesized that **1-TFA** converts to **1-OAc** *in situ* (e.g., after completing one catalytic loop and releasing HTFA). If **1-TFA** and **1-OAc** exhibit

different catalytic activities, with **1-OAc** being more active, the rate of catalysis would increase as **1-TFA** is converted to **1-OAc**. $\text{Cu}(\text{OPiv})_2$ was used in place of $\text{Cu}(\text{OAc})_2$ due to the enhanced solubility of $\text{Cu}(\text{OPiv})_2$ and the likely similar reactivity of Rh–OAc and Rh–OPiv intermediates. To test this hypothesis, **1-OAc** was independently synthesized and tested for catalytic activity. Under identical conditions as catalysis with **1-TFA**, the reaction with **1-OAc** using $\text{Cu}(\text{OPiv})_2$ as the oxidant shows no apparent induction period (Figure 3.11B). This result is consistent with **1-OAc** serving as a more active catalyst compared to **1-TFA**. We compared the rate of catalysis of **1-OAc** to **1-TFA** after the apparent induction period using a plot of [styrene] vs. time in which data for **1-OAc** are time-shifted ($t = 0.5$ h shifted to $t = 1.5$ h) and overlaid with data from reactions using **1-TFA** as the catalyst precursor (Figure 3.11). The overlap of the plots shows nearly identical [styrene] vs. time profiles for catalysis following the apparent induction period for **1-TFA**, which supports the hypothesis that **1-TFA** is converted to **1-OAc** *in situ*.

We performed catalytic experiments with **1-TFA** using both $\text{Cu}(\text{TFA})_2$ and $\text{Cu}(\text{OAc})_2$ as oxidants. Plots of TO vs. time for these reactions are shown in Figure 3.12. For catalysis using $\text{Cu}(\text{TFA})_2$, a consistently slower reaction rate is observed. For the reaction with $\text{Cu}(\text{OAc})_2$, the rate of catalysis gradually increases, which is consistent with conversion of **1-TFA** to **1-OAc**. For reactions using **1-TFA** and $\text{Cu}(\text{TFA})_2$, we do not observe induction periods.

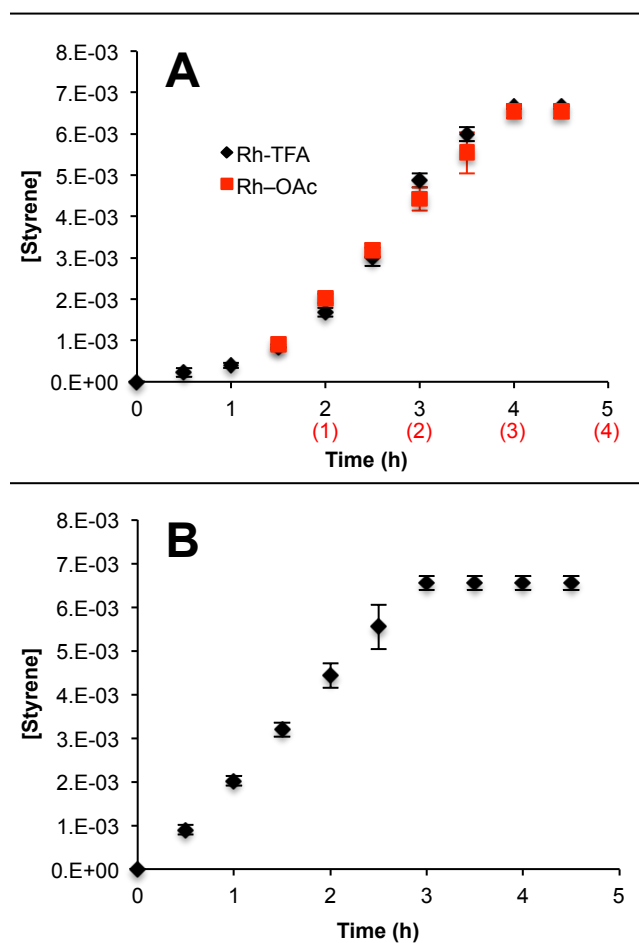


Figure 3.11. A) [Styrene] vs. time plot for catalysis with **1-TFA** and **1-OAc** using $\text{Cu}(\text{OPiv})_2$ as the oxidant. Reaction conditions: 0.112 mM **1-TFA** or **1-OAc**, 20 mL C_6H_6 , 13.4 mM $\text{Cu}(\text{OPiv})_2$ (120 equiv. relative to **1-TFA** or **1-OAc**), 50 psig C_2H_4 , 150 °C. Data for **1-OAc** are offset from $t = 0.5$ h to $t = 1.5$ h to overlap with data from **1-TFA**, and non-offset times are labeled in red. **B)** [Styrene] vs. time plot for catalysis with **1-OAc** from **Figure 3.11A** without time offset, which is consistent with the absence of an induction period. Each data point is the average of two independent catalytic reactions, each analyzed in duplicate by GC/FID. Error bars represent the standard deviation of all four values.

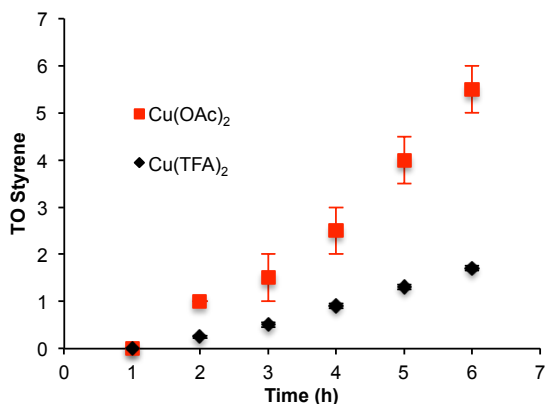


Figure 3.12. TO vs. time plot for catalysis with **1-TFA** using $\text{Cu}(\text{OAc})_2$ or $\text{Cu}(\text{TFA})_2$ as the oxidant. Reaction conditions: 0.112 mM **1-TFA**, 20 mL C_6H_6 , 13.4 mM CuX_2 (120 equiv. relative to **1-TFA**), 25 psig C_2H_4 , 150 °C. Each data point is the average of two independent catalytic reactions, each analyzed in duplicate by GC/FID. Error bars represent the standard deviation of all four values.

3.3.4 Computational Studies: Overview

To gain insight into the difference in rate of catalysis for **1-TFA** compared to **1-OAc**, Sarah K. Khani and J. Brannon Gary from the Cundari Group at the University of North Texas performed a computational study (B3LYP) of the fundamental steps involved in the proposed catalytic cycle (Scheme 3.5). The catalytic cycle we modeled involves: a) benzene coordination to $(^{\text{Fl}}\text{DAB})\text{Rh}(\eta^2\text{-C}_2\text{H}_4)(\text{X})$ by net ligand substitution with ethylene and subsequent benzene C–H activation, b) ethylene coordination and insertion into the Rh–Ph bond, c) β -hydride elimination from the Rh– $\text{CH}_2\text{CH}_2\text{Ph}$ intermediate, and d) styrene dissociation. To display and compare the results of these calculations, in Scheme 2 we set the free energy of both of the complexes **1-OAc** and **1-TFA** to zero. Our calculations also included the energetics of conversion of **1-TFA** and **1-OAc** to the dimers $[(^{\text{Fl}}\text{DAB})\text{Rh}(\mu\text{-X})]_2$ ($\text{X} = \text{OAc}$ or TFA ; **1D-OAc** or **1D-TFA**, respectively). The dimers **1D-OAc** and **1D-TFA** were investigated based on experimental

evidence that they are present during catalysis. In addition to ^1H NMR spectroscopic data (see experimental section), the dimer **1D-OAc** has been partially structurally characterized. X-Ray diffraction-quality crystals of **1D-OAc** were grown by slow evaporation of THF. While the crystals decomposed during data collection, the basic core structure of the dimer was able to be isotropically refined (Figure 3.13).

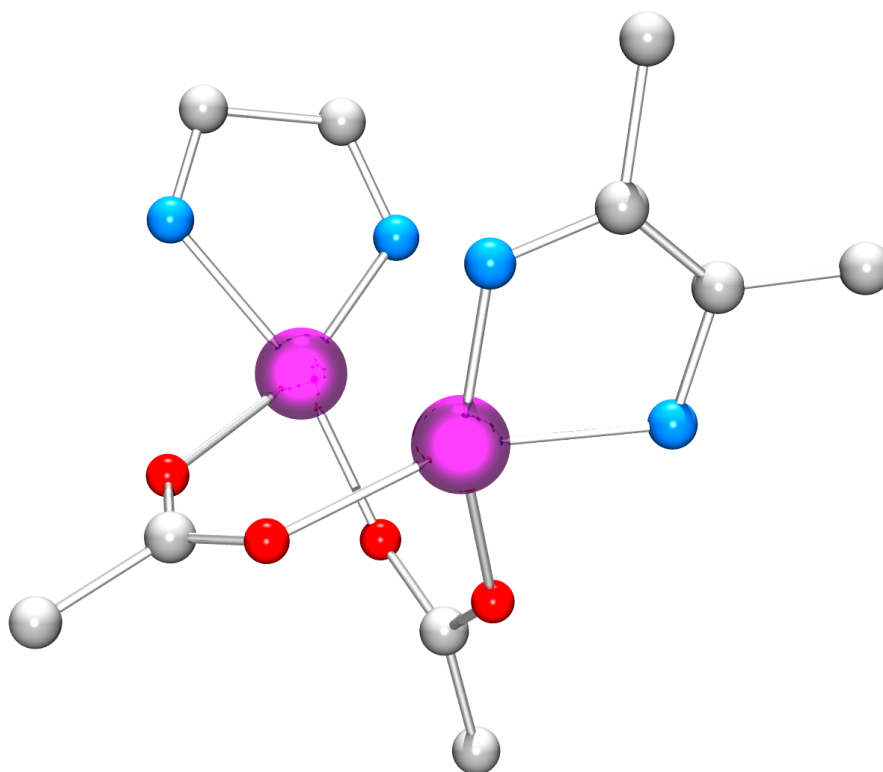
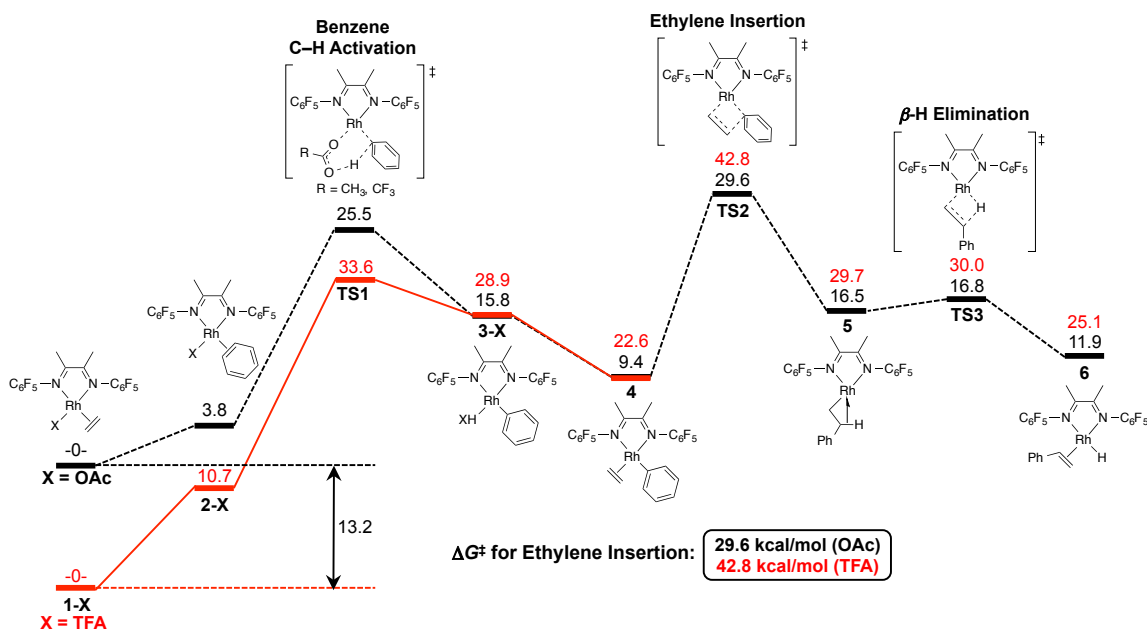


Figure 3.13. Ball and stick model of isotropically refined core structure of **1D-OAc**. CH_3 groups on one of the DAB backbones and C_6F_5 groups were not located, and the positions of hydrogens in the entirety of the structure were not calculated.

Scheme 3.5. Calculated Gibbs free energies [B3LYP/LANL2DZ+6-311++G(d,p)] including solvent (SMD-benzene) and dispersion corrections for the lowest energy calculated pathway for styrene production using complexes **1-OAc** (shown in black) and **1-TFA** (shown in red) at 423.15 K in kcal/mol. The calculated energies for each reaction are relative to the energy of **1-X** (X = OAc or TFA), which is set to zero energy for each reaction. Stationary points without TFA or OAc are degenerate.



Using the B3LYP functional, the dimers were calculated to be more stable than the monomeric species **1-TFA** and **1-OAc** by 11.2 and 6.3 kcal/mol, respectively. In contrast to these calculations, experimental results indicate that the monomeric complexes are more stable than the dimers. For example, a C_6D_6 solution of independently synthesized **1D-TFA** completely converts to **1-TFA** in the presence of ethylene at room temperature in < 1 minute. As a result of the discrepancy between experimental and computational results, the conversions of monomer to dimer were computationally modeled using the M06 functional, which gave ΔG values (dimer to monomer) of -1.8 and 1.5 kcal/mol for **1-TFA** and **1-OAc** at 423 K, respectively, which are in better agreement with experimental observations. The M06 functional is known to provide better estimates of

van der Waals interactions, which we believe gives a more accurate model of the energetics for monomer/dimer interconversion. However, to assess catalysis based on monomeric catalysts, we retained the B3LYP data. The calculations predict $\Delta G^\ddagger = 29.6$ kcal/mol using **1-OAc** and $\Delta G^\ddagger = 42.8$ kcal/mol using **1-TFA**. These barriers are consistent with experimental rates. Using the Eyring equation, rates from reactions using **1-TFA** with $\text{Cu}(\text{TFA})_2$ as the oxidant (which results in the Rh-TFA moiety being retained throughout catalysis) and **1-OAc** with $\text{Cu}(\text{OAc})_2$ as the oxidant (which results in the Rh-OAc moiety being retained throughout catalysis) give ΔG^\ddagger values which are in good agreement with ΔG^\ddagger values from computations (computational values: Rh-TFA = 42.8 kcal/mol, Rh-OAc = 29.6 kcal/mol).

From the complexes **1-OAc** and **1-TFA**, multiple possible pathways for benzene C-H activation were calculated. The lowest energy pathway for catalysis by both **1-OAc** and **1-TFA** involves the initial displacement of ethylene to afford the corresponding η^2 -benzene complexes ($^{\text{Fl}}\text{DAB}$)Rh(OAc)(η^2 -C₆H₆) [**2-OAc**] and ($^{\text{Fl}}\text{DAB}$)Rh(TFA)(η^2 -C₆H₆) [**2-TFA**] with energies of 3.8 kcal/mol and 10.7 kcal/mol relative to **1-OAc** and **1-TFA**, respectively. It is interesting to note that ethylene/benzene exchange is ~ 7 kcal/mol less favorable for **1-TFA** than for **1-OAc**, accounting for $\sim 50\%$ of the calculated overall $\Delta\Delta G^\ddagger$ of 13.2 kcal/mol for the catalytic process.

Following the formation of a benzene adduct, the lowest energy C-H activation pathway for both complexes was found to involve concerted metallation-deprotonation (CMD) of benzene using an acetate ligand,²⁸⁻³⁴ with activation barriers of 21.7 kcal/mol for the Rh-OAc complex and 22.9 kcal/mol for the Rh-TFA complex relative to **2-OAc** and **2-TFA**, respectively. After benzene C-H activation, the coordinated HX is displaced

by ethylene to generate (^{F1}DAB)Rh(Ph)(η^2 -C₂H₄) (**4**). Comparing the optimized transition state geometries for CMD of benzene from **2-OAc** and **2-TFA** (Figure 3.14), it can be observed that the Rh–C and C–O bond lengths (2.19 Å and 1.25 Å, respectively, for the Rh–TFA transition state) elongate by 0.02 Å for the Rh–OAc transition state. Conversely, the Rh–O bond length shrinks by 0.02 Å. More noticeable is the change in the benzene C–H bond distance in the Rh–TFA transition state, which is 0.06 Å longer than the corresponding bond in the Rh–OAc transition state; the O–H bond in the Rh–OAc transition state is elongated by 0.06 Å versus the same bond in the Rh–TFA transition state. Hence, the transition state for the Rh–TFA complex appears to be later than the corresponding transition state for Rh–OAc, which is consistent with the Hammond postulate as the ΔH for benzene C–H activation by **2-TFA** is calculated to be more endothermic ($\Delta H = 17.3$ kcal/mol) and endergonic ($\Delta G = 18.2$ kcal/mol) than that of **2-OAc** ($\Delta H = 12.9$ kcal/mol, $\Delta G = 12.0$ kcal/mol).

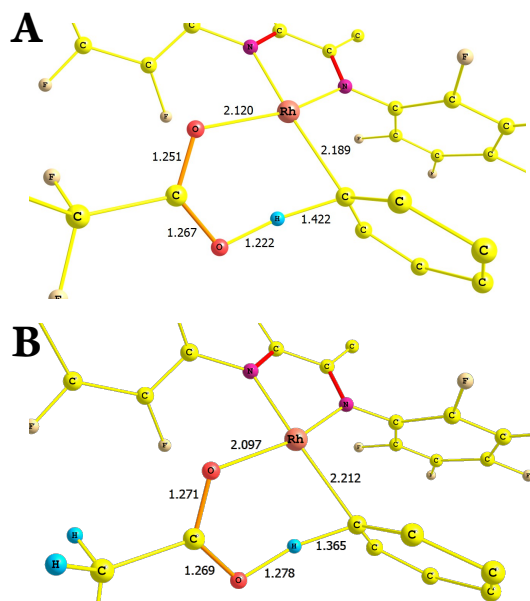


Figure 3.14. Optimized calculated geometries for the transition states for benzene C–H activation by (A) $(^{\text{F1}}\text{DAB})\text{Rh}(\eta^2\text{-C}_6\text{H}_6)(\text{TFA})$ (**2-TFA**), and (B) $(^{\text{F1}}\text{DAB})\text{Rh}(\eta^2\text{-C}_6\text{H}_6)(\text{OAc})$ (**2-OAc**). Bond lengths in Å.

Previous studies of ethylene insertion into Pt(II) hydrocarbyl and aryl bonds demonstrate the viability of such reactions for cationic complexes, but the results suggest that the activation barrier for olefin insertion might be higher for overall charge-neutral complexes than for cationic complexes.³⁵ Thus, we anticipated that activation barriers for ethylene insertion into Rh–Ph bonds of charge-neutral Rh(I) complexes might be higher than those of related Pt(II) complexes. Previously, we have shown that the conversion of $[(^{\text{t}}\text{bpy})\text{Pt}(\text{Ph})(\text{THF})]^+$ ($^{\text{t}}\text{bpy}$ = 4,4'-di-*tert*-butyl-2,2'-bipyridyl) and ethylene to $[(^{\text{t}}\text{bpy})\text{Pt}(\text{CH}_2\text{CH}_2\text{Ph})(\eta^2\text{-C}_2\text{H}_4)]^+$ at 23 °C occurs with an experimentally determined ΔG^\ddagger of 21.0(1) kcal/mol.¹⁹ This activation energy is similar to the reported ΔG^\ddagger of 19.2 kcal/mol for ethylene insertion into a Pt(II)–hydride bond.³⁶ Through the use of a diimine ligand with electron-withdrawing perfluorophenyl groups (i.e., $^{\text{F1}}\text{DAB}$) we sought to

generate a Rh center with similar properties to cationic Pt(II) such as $[(^X\text{bpy})\text{Pt}(\text{Ph})(\text{THF})]^+$ ($^X\text{bpy} = 4,4'$ -X-2,2'-bipyridyl).^{2,19,35,37-39} Insertion of ethylene into the Rh–Ph bond of $(^{\text{Fl}}\text{DAB})\text{Rh}(\text{Ph})(\eta^2\text{-C}_2\text{H}_4)$ (**4**) is calculated to have a free energy of activation of 20.2 kcal/mol from complex **4**, which is commensurate with the cationic Pt(II) complex $(^t\text{bpy})\text{Pt}(\text{Ph})(\eta^2\text{-C}_2\text{H}_4)$, for which the free energy of activation for ethylene insertion into the Pt–Ph bond was calculated to be 21.5 kcal/mol. (*n.b.*: to provide an accurate comparison, the energy values for Pt complexes¹⁹ have been recalculated using the same computational parameters as have been used for the Rh complexes presented herein).

For catalysis with **1-OAc**, the $\Delta\Delta G^\ddagger$ between C–H activation and olefin insertion is 4.1 kcal/mol, suggesting that ethylene insertion is the rate-determining step. For catalysis with **1-TFA**, the $\Delta\Delta G^\ddagger$ for the same two steps is 9.2 kcal/mol, and also predicts that ethylene insertion is the rate-determining step. This is in contrast to Pt(II)- and Ru(II)-based catalysts for ethylbenzene formation for which C–H activation is calculated to be rate-determining.^{19,40} We note that some calculations for the Ru(II) catalyst indicated ethylene insertion as the rate-determining step.⁴¹ The calculations are consistent with a kinetic advantage for **1-OAc** over **1-TFA**. The calculated $\Delta\Delta G^\ddagger$ for catalysis using **1-OAc** vs. **1-TFA** is 13.2 kcal/mol, and computational modeling suggests that the difference in ground state energies of **1-OAc** and **1-TFA** greatly influences the difference in rate of catalysis. The penultimate step in the pathway for styrene production is β -hydride elimination, which was calculated to have an activation barrier of only 0.3 kcal/mol relative to $(^{\text{Fl}}\text{DAB})\text{Rh}(\text{CH}_2\text{CH}_2\text{Ph})$ (**5**).

The calculations predict different rate-determining steps for ethylene hydrophenylation by $[(^t\text{bpy})\text{Pt}(\text{Ph})(\text{THF})]^+$ and oxidative hydrophenylation of ethylene by **1-TFA/1-OAc**. For the Pt catalyst, the transition state for benzene C–H activation is calculated to be the highest energy species, while the transition state for ethylene insertion is the calculated highest energy species for the Rh catalysis. Notably, for the Pt catalysis an *inverse* dependence on ethylene concentration was experimentally demonstrated, while for the Rh catalysis a first-order dependence is observed (*vide infra*).¹⁹

3.3.5 Computational Studies: Selectivity for Styrene

A challenge for the development of catalysts for oxidative arene vinylation has been achieving selectivity for the vinyl arene product. In fact, $[(^t\text{bpy})\text{Pt}(\text{THF})(\text{Ph})]^+$ has been reported to selectively yield ethylbenzene, even in the presence of oxidants including various Cu(II) salts (unpublished results).^{2,19} Modification of the donor ability of the 2,2'-bipyridyl ligand coordinated to Pt(II) can result in the production of styrene, and in one case a few turnovers are observed with ethylene as the oxidant.² From a $\text{M}-\text{CH}_2\text{CH}_2\text{Ph}$ intermediate, ethylbenzene is formed from benzene C–H activation, whereas styrene is formed from β -hydride elimination and net styrene dissociation. In order to understand why the $[(^t\text{bpy})\text{Pt}(\text{Ph})]^+$ catalyst intermediate is selective for ethylbenzene production while $(^{\text{F1}}\text{DAB})\text{Rh}(\text{Ph})$ intermediate is selective for styrene production, we modeled the likely reaction steps for each product, which are shown in Scheme 3.6. The two pathways to form either styrene or ethylbenzene diverge from the $\text{M}-\text{CH}_2\text{CH}_2\text{Ph}$ intermediate. In the pathway to form styrene, β -hydride elimination occurs to give a $\text{M}(\text{H})(\eta^2\text{-styrene})$

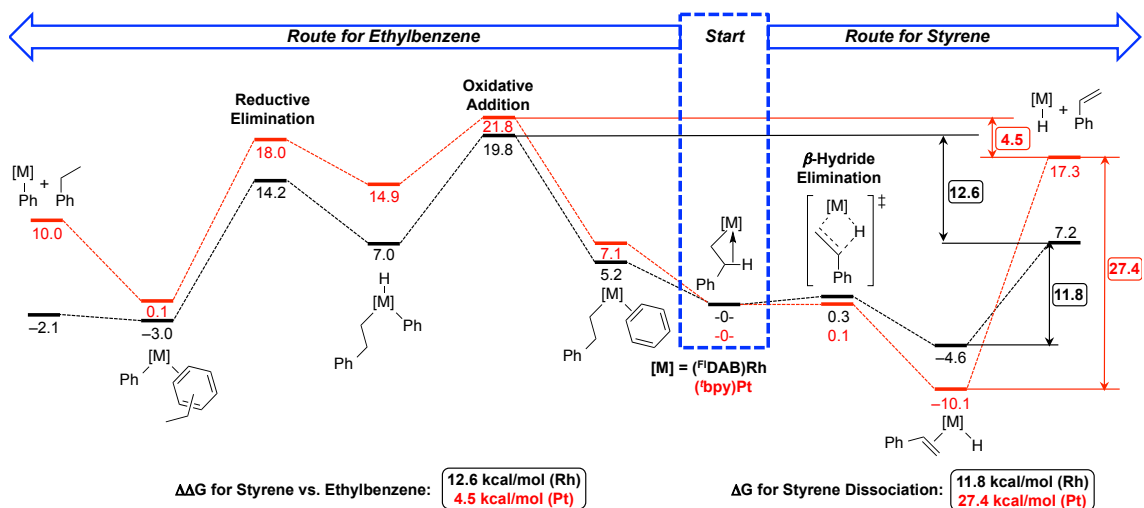
intermediate that subsequently liberates styrene. In the pathway to form ethylbenzene, a second equivalent of benzene coordinates to the coordinatively-unsaturated M-CH₂CH₂Ph complex, and subsequent benzene C-H activation affords free ethylbenzene and a new M-Ph complex.

For the [(^tbpy)Pt]⁺ catalyst, the difference in energy between these two pathways was calculated to be 4.5 kcal/mol (favoring styrene production). For the Rh complex, the energy difference between the two pathways is 12.6 kcal/mol. Thus, the calculations predict a greater predilection toward styrene formation for (^{F1}DAB)Rh vs. [(^tbpy)Pt]⁺, which is consistent with experimental results.¹⁹ Interestingly, the calculations reveal that energy differences for benzene C-H activation ($\Delta\Delta G^\ddagger = 2$ kcal/mol) and β -hydride elimination ($\Delta\Delta G^\ddagger = 0.2$ kcal/mol), the two key steps for the formation of ethylbenzene and styrene, respectively, are small and likely cannot be used to rationalize the switch in selectivity between (^{F1}DAB)Rh and [(^tbpy)Pt]⁺. Rather, it appears that the propensity toward styrene dissociation is the key parameter, with calculated ΔG s for styrene dissociation of 11.8 kcal/mol for (^{F1}DAB)Rh and a surprisingly much larger 27.4 kcal/mol for [(^tbpy)Pt]⁺.

Thus, we propose that both (^{F1}DAB)Rh and [(^tbpy)Pt]⁺ likely undergo β -hydride elimination from M-CH₂CH₂Ph intermediates, but for [(^tbpy)Pt]⁺ this process is reversible because the energetics for styrene dissociation are unfavorable. We have reported evidence for reversible β -hydride elimination for ethylbenzene formation by TpRu(CO)(NCMe)(Ph) (Tp = hydridotris(pyrazolyl)borate).⁴⁰ We note that the formation of diethylbenzenes by [(^tbpy)Pt]⁺ is explained by a similar rationale.¹⁹ That is, the dissociation of ethylbenzene from [(^tbpy)Pt(Ph)(ethylbenzene)]⁺ is slow (relatively),

which allows a second arene C–H activation (ultimately leading to diethylbenzenes) to compete with the dissociation of ethylbenzene. More difficult to explain are the calculations for $[(^t\text{bpy})\text{Pt}]^+$, which predict styrene formation should be preferred over ethylbenzene formation with a $\Delta\Delta G^\ddagger$ of 4.5 kcal/mol, which can arise from the functional and basis sets chosen. Previous calculations and experiments with dipyridyl-supported Pt(II) catalysts^{2,19,38,39} show that a subtle balance of factors discriminate ethylbenzene from styrene formation. Nonetheless, the present calculations are consistent with the experimental observation of much greater propensity for the latter for Rh(I) versus Pt(II).

Scheme 3.6. Comparison of Calculated Free Energies for β -Hydride Elimination to Form Styrene and Benzene C–H Activation to Form Ethylbenzene from $(^{\text{F}^1}\text{DAB})\text{Rh}(\text{CH}_2\text{CH}_2\text{Ph})$ [shown in black] and $(^t\text{bpy})\text{Pt}(\text{CH}_2\text{CH}_2\text{Ph})$ [shown in red] in kcal/mol with the Important Energy Differences Between the Two Pathways Highlighted.



3.3.6 Kinetic and Mechanistic Studies

We studied the kinetics of catalysis using **1-OAc** and $\text{Cu}(\text{OPiv})_2$. The oxidant $\text{Cu}(\text{OPiv})_2$ was used due to its solubility in benzene. The concentration of ethylene dissolved in benzene was determined according to the method described by Holder and

Macauley.⁴² To determine the order of the reaction in **1-OAc**, ethylene, and Cu(OPiv)₂, three sets of kinetic experiments were conducted in which the concentrations of two of the compounds were held constant while one was varied. Observed rates were extracted from linear fits of the initial rate regime (linear region where likely no catalyst deactivation was occurring) of [styrene] vs. time plots. Log-log plots were used to determine the order of the reaction in each of the compounds examined.

A first-order dependence on ethylene concentration is observed over a concentration range from 79 mM to 237 mM (Figure 3.15, Figure 3.16). While the first-order dependence on ethylene is consistent with the previously reported dependence of apparent TOF on ethylene pressure for catalysis with **1-TFA**,¹³ it is in contrast to previously reported Pt(II)- and Ru(II)-based hydroarylation catalysts. The rate of catalysis with these complexes shows an inverse dependence on the concentration of ethylene, which is due to the formation of M(CH₂CH₂Ph)(η^2 -C₂H₄) intermediates (M = TpRu(CO) or [(^tbpy)Pt]⁺), which were identified as off-cycle resting states.^{18,19,40} An Ir-based olefin hydroarylation catalyst shows a bell-curve dependence on the concentration of ethylene, exhibiting first-order kinetics at low concentrations and inverse first-order kinetics at higher concentrations.⁴³ The observed first-order dependence on [C₂H₄] for catalysis with **1-OAc** is consistent with a different resting state and/or rate-determining step than our Pt(II) and Ru(II) catalysts. In fact, for catalysis with **1-OAc**, the energy of the (^FlDAB)Rh(CH₂CH₂Ph)(η^2 -C₂H₄) complex, which is the analog of the proposed resting states for the Pt(II) and Ru(II) catalysts,^{19,40} is calculated to be higher than that of **1-OAc** by 7.6 kcal/mol.

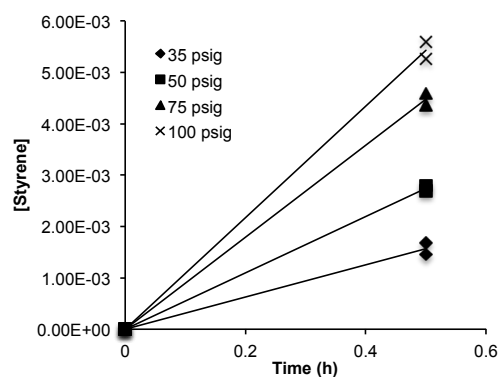


Figure 3.15. Concentration of styrene vs. time plot for the initial rate regime of catalysis with **1-OAc** at various ethylene pressures/concentrations: 35 psig (slope = 0.0031), 50 psig (slope = 0.0055), 75 psig (slope = 0.009), and 100 psig (slope = 0.011). Reaction conditions: 20 mL C_6H_6 , 0.11 mM **1-OAc**, 13.4 mM $Cu(OPiv)_2$, 150 °C. Data for two independent reactions at each concentration level are shown. Data for initial time points were used to calculate k_{obs} .

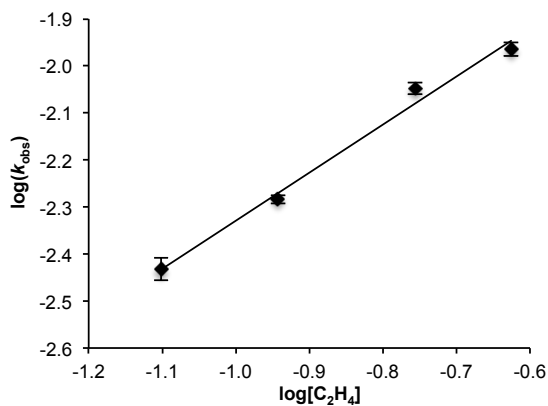


Figure 3.16. Log-log plot of observed rate constant as a function of concentration of C_2H_4 (slope = 1.02(8), $R^2 = 0.99$). Reaction conditions: 0.11 mM **1-OAc**, 20 mL C_6H_6 , 13.4 mM $Cu(OPiv)_2$, 150 °C. Each data point represents the average of two independent catalytic reactions, each analyzed in duplicate by GC/FID. Error bars represent the standard deviation of all four values.

The log-log plot for Cu(OPiv)_2 (Figure 3.17, Figure 3.18) shows a near zero-order dependence {slope = $-0.17(2)$ } on $[\text{Cu(OPiv)}_2]$ over a concentration range from 13 mM to 54 mM. Given that the involvement of Cu(II) occurs after the proposed rate-limiting step (*vide infra*), a zero-order dependence is expected. This type of mechanism has been reported for similar oxidative processes, and has been shown to exhibit a zero-order dependence on oxidant.⁴⁴ The slight negative slope indicates that Cu(II) might suppress catalytic activity. The need for Cu(II) as an oxidant, but the apparent need of access to low valent Rh(I) for C–H activation sets up a difficult balance. Thus, one possible explanation of the slight inverse dependence on Cu(II) concentration is that Cu(II) oxidizes a Rh(I) intermediate, pulling it out of the catalytic cycle, but that the equilibrium favors Rh(I); however, the slight magnitude of the apparent inhibition makes it difficult to draw a definitive conclusion.

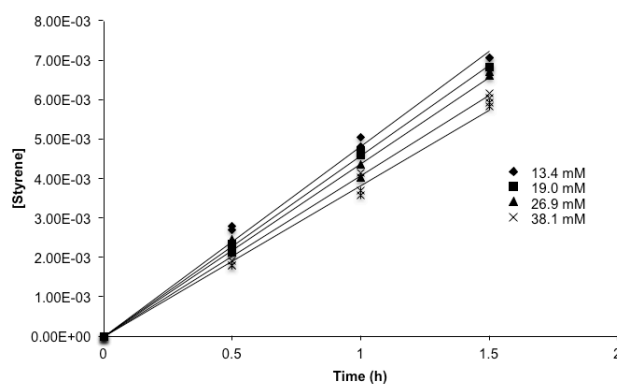


Figure 3.17. Concentration of styrene vs. time plot for the initial rate regime of catalysis with **1-OAc** at various concentrations of Cu(OPiv)_2 : 13.4 mM (slope = 0.0048, $R^2 = 0.99$), 19.0 mM (slope = 0.0046, $R^2 = 0.99$), 26.9 mM (slope = 0.0044, $R^2 = 0.99$), 38.1 mM (slope = 0.0041, $R^2 = 0.99$), and 53.8 mM (slope = 0.0038, $R^2 = 0.99$). Reaction conditions: 20 mL C_6H_6 , 0.11 mM **1-OAc**, 50 psig C_2H_4 , 150 °C. Data for two independent reactions at each concentration level are shown.

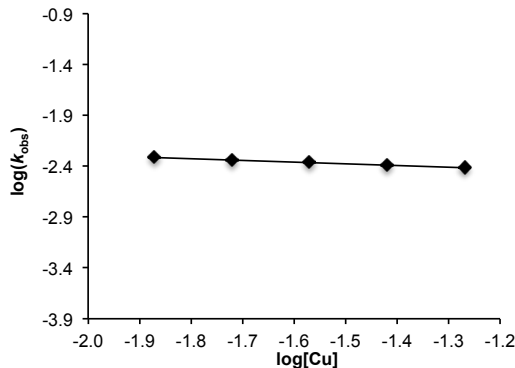


Figure 3.18. Log-log plot of observed rate constant as a function of concentration of Cu(OPiv)_2 (slope = $-0.17(2)$, $R^2 = 0.99$). Reaction conditions: 0.11 mM **1-OAc**, 20 mL C_6H_6 , 50 psig C_2H_4 , 150 °C. Each data point represents the average of two independent catalytic reactions, each analyzed in duplicate by GC/FID. Error bars represent the standard deviation of all four values.

The log-log plot for [**1-OAc**] at 50 psig C_2H_4 reveals a slope of 0.67(2), this between first-order and half-order (Figure 3.22). Further studies showed that the dependence of the reaction rate on **1-OAc** is complicated, varying between first- and half-order as a function of both $[\text{C}_2\text{H}_4]$ and temperature. For example, the order in Rh was determined over a concentration range from 0.056 mM to 0.23 mM at *three different concentrations* of C_2H_4 (Figure 3.19, Figure 3.20, Figure 3.21), and, in a separate series of experiments, the order in **1-OAc** was determined at *three different temperatures* (Figure 3.23, Figure 3.24). With $[\text{C}_2\text{H}_4]$ variation, the order in Rh varied exhibiting close to half-order kinetics at lower $[\text{C}_2\text{H}_4]$ {at 7.9 mM C_2H_4 , reaction order in **1-OAc** = 0.58(3)} and close to first order kinetics at higher $[\text{C}_2\text{H}_4]$ {at 17.5 mM C_2H_4 , reaction order in **1-OAc** = 0.96(1)} (Figure 3.22). The order in Rh was found to vary inversely with temperature, exhibiting closer to first-order kinetics at lower temperatures {at 130 °C, order in **1-OAc** = 0.83(1)} and closer to half-order kinetics at higher temperatures {at 160 °C, order in **1-OAc** =

0.64(1)} (Figure 3.25). Limitations of the catalytic process make kinetic studies outside of this temperature range challenging. These results indicate the possibility of competing catalytic pathways (*vide infra*).

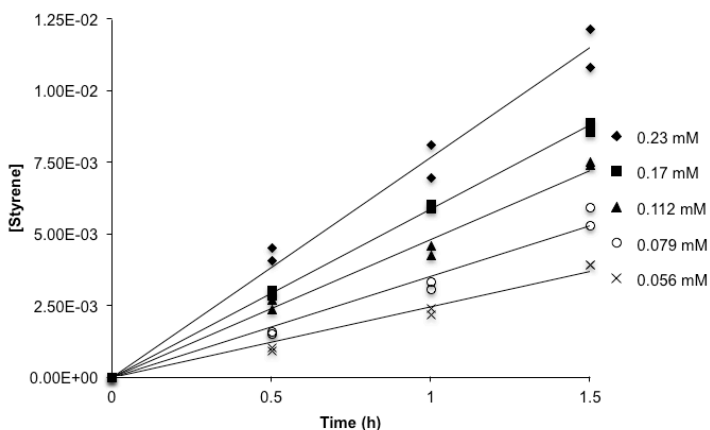


Figure 3.19. Concentration of styrene vs. time plot for the initial rate regime of catalysis with **1-OAc** at 50 psig C_2H_4 with various catalyst concentrations: 0.23 mM (slope = 0.0077, $R^2 = 0.98$), 0.17 mM (slope = 0.0059, $R^2 = 0.99$), 0.112 mM (slope = 0.0048, $R^2 = 0.99$), 0.079 mM (slope = 0.0035, $R^2 = 0.97$), and 0.056 mM (slope = 0.0025, $R^2 = 0.97$). Reaction conditions: 20 mL C_6H_6 , 26.9 mM $Cu(OPiv)_2$, 50 psig C_2H_4 , 150 °C. Data for two independent reactions at each concentration level are shown.

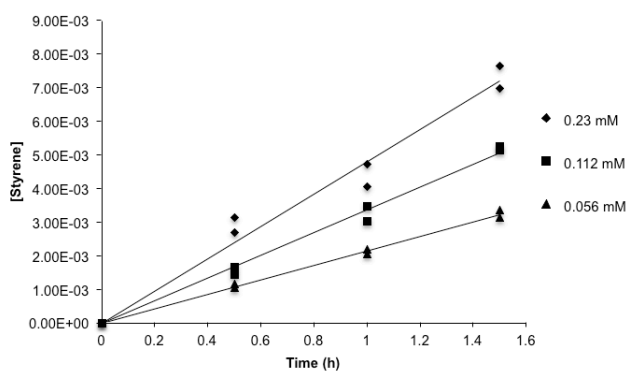


Figure 3.20. Concentration of styrene vs. time plot for the initial rate regime of catalysis with **1-OAc** at 35 psig C_2H_4 with various catalyst concentrations: 0.23 mM (slope = 0.0048, $R^2 = 0.96$), 0.112 mM (slope = 0.0034, $R^2 = 0.99$), and 0.056 mM (slope = 0.0022, $R^2 = 0.99$). Reaction conditions: 20 mL C_6H_6 , 26.9 mM $Cu(OPiv)_2$, 35 psig C_2H_4 , 150 °C. Data for two independent reactions at each concentration level are shown.

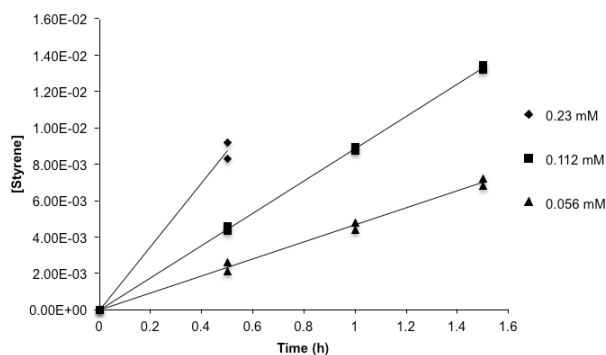


Figure 3.21. Concentration of styrene vs. time plot for the initial rate regime of catalysis with **1-OAc** at 75 psig C_2H_4 with various catalyst concentrations: 0.23 mM (slope = 0.0176, $R^2 = 0.99$), 0.112 mM (slope = 0.0089, $R^2 = 0.99$), and 0.056 mM (slope = 0.0047, $R^2 = 0.99$). Reaction conditions: 20 mL C_6H_6 , 26.9 mM $Cu(OPiv)_2$, 75 psig C_2H_4 , 150 °C. Data for two independent reactions at each concentration level are shown.

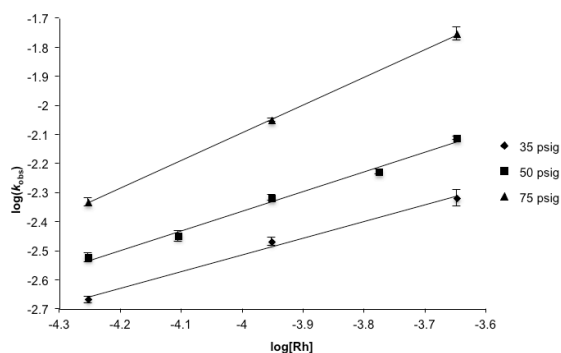


Figure 3.22. Log-log plot of observed rate constant vs. [**1-OAc**] at 35 psig of C_2H_4 (slope = 0.58, $R^2 = 0.99$), 50 psig of C_2H_4 (slope = 0.67, $R^2 = 0.99$), and 75 psig of C_2H_4 (slope = 0.96, $R^2 = 0.99$). Reaction conditions: 20 mL C_6H_6 , 26.9 mM $Cu(OPiv)_2$, 150 °C.

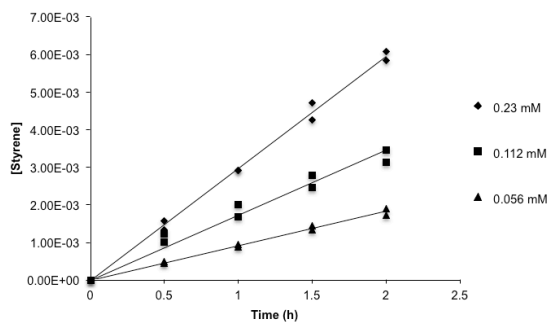


Figure 3.23. Concentration of styrene vs. time plot for the initial rate regime of catalysis with **1-OAc** at 130 °C with various catalyst concentrations: 0.23 mM (slope = 0.003, $R^2 = 0.99$), 0.112 mM (slope = 0.0017, $R^2 = 0.96$), and 0.056 mM (slope = 0.0009, $R^2 = 0.99$). Reaction conditions: 20 mL C_6H_6 , 26.9 mM $Cu(OPiv)_2$, 30 psig C_2H_4 , 130 °C. Data for two independent reactions at each concentration level are shown.

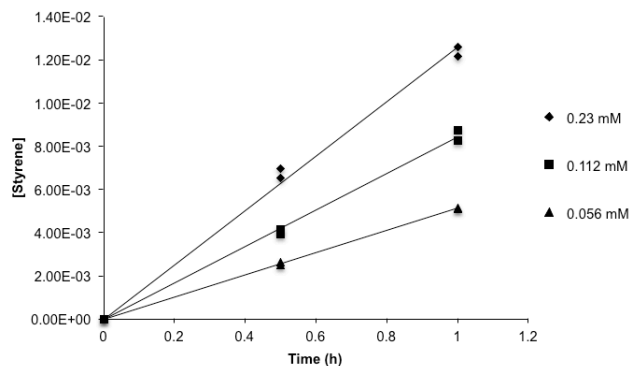


Figure 3.24. Concentration of styrene vs. time plot for the initial rate regime of catalysis with **1-OAc** at 160 °C with various catalyst concentrations: 0.23 mM (slope = 0.0126, $R^2 = 0.99$), 0.112 mM (slope = 0.0084, $R^2 = 0.99$), and 0.056 mM (slope = 0.0051, $R^2 = 0.99$). Reaction conditions: 20 mL C_6H_6 , 26.9 mM $Cu(OPiv)_2$, 60 psig C_2H_4 , 160 °C. Data for two independent reactions at each concentration level are shown.

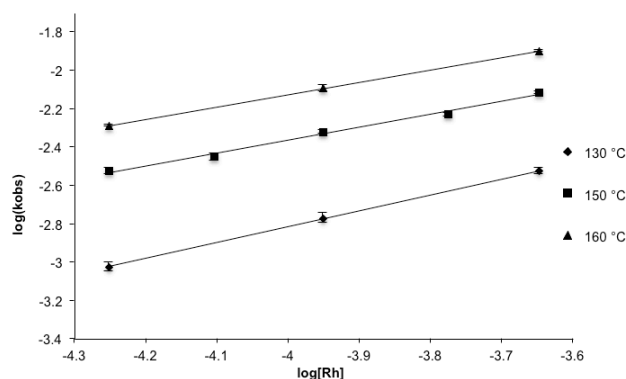
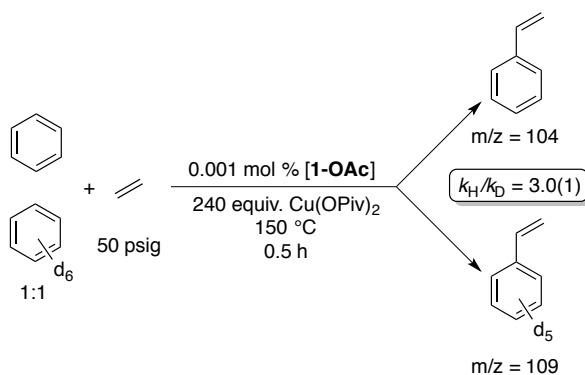


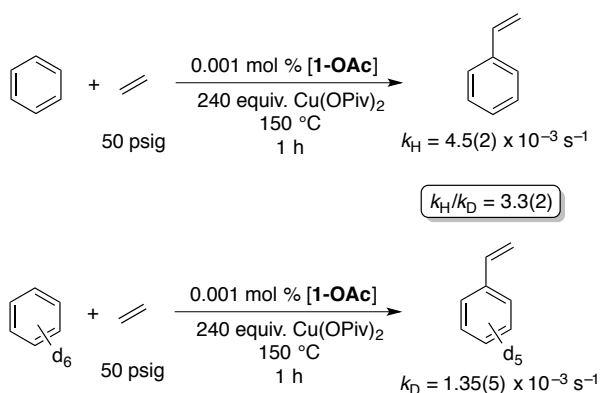
Figure 3.25. Log-log plot of observed rate constant vs. [1-OAc] at 130 °C (slope = 0.83, $R^2 = 0.99$), 150 °C (slope = 0.67, $R^2 = 0.99$), and 160 °C (slope = 0.64, $R^2 = 0.99$). Reaction conditions: 20 mL C_6H_6 , 26.9 mM $Cu(OPiv)_2$.

The kinetic isotope effect (KIE) for catalysis with **1-OAc** using C_6H_6 vs. C_6D_6 was determined using two methods. In one experiment, catalysis was performed using an equimolar mixture of per-protio and per-deutero benzene (Scheme 3.7). After 30 mins, a k_H/k_D of 3.0(1) was observed upon comparison of the peaks for per-protio styrene ($m/z = 104$) and styrene- d_5 ($m/z = 109$) by mass spectrometry. In a separate series of reactions, catalysis was performed in C_6H_6 and C_6D_6 independently (Scheme 3.8). A k_H/k_D of 3.3(2) was determined for these reactions using observed rate values calculated after 1 h of reaction. The two k_H/k_D values are statistically identical (for further discussion of the KIE for this reaction, *vide infra*). The KIEs are consistent with reported values for C–H activation by d^8 complexes, which often exhibit KIE values of ≥ 2.5 .^{45,46} It is also important to note that d_{6-8} products were not observed except those predicted by the natural abundance of deuterium in ethylene, which suggests that H/D scrambling is not occurring and that C–H activation is likely irreversible (Figure 3.26).

Scheme 3.7. Kinetic isotope experiment with **1-OAc** using a 1:1 molar mixture of $C_6H_6:C_6D_6$. k_H/k_D value represents the average of three independent catalytic reactions, each analyzed in triplicate by GC/MS. Reported error represents the standard deviation of all nine values.



Scheme 3.8. Kinetic isotope experiment with **1-OAc** using independent reactions in C_6H_6 and C_6D_6 . k_H and k_D values were determined using the method of initial rates for two independent catalytic reactions each, with all samples analyzed in duplicate by GC/FID. The reported error represents the propagated standard deviation of all values and linear regressions.



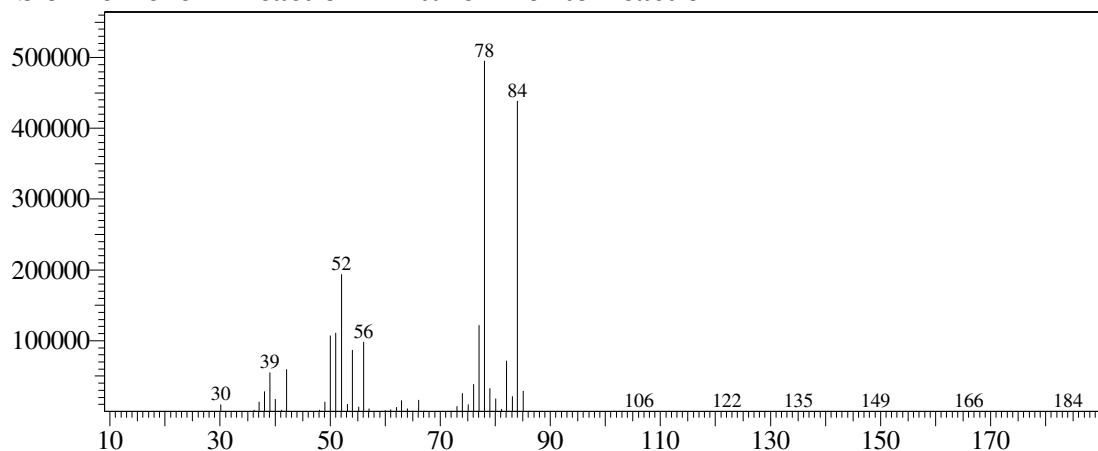
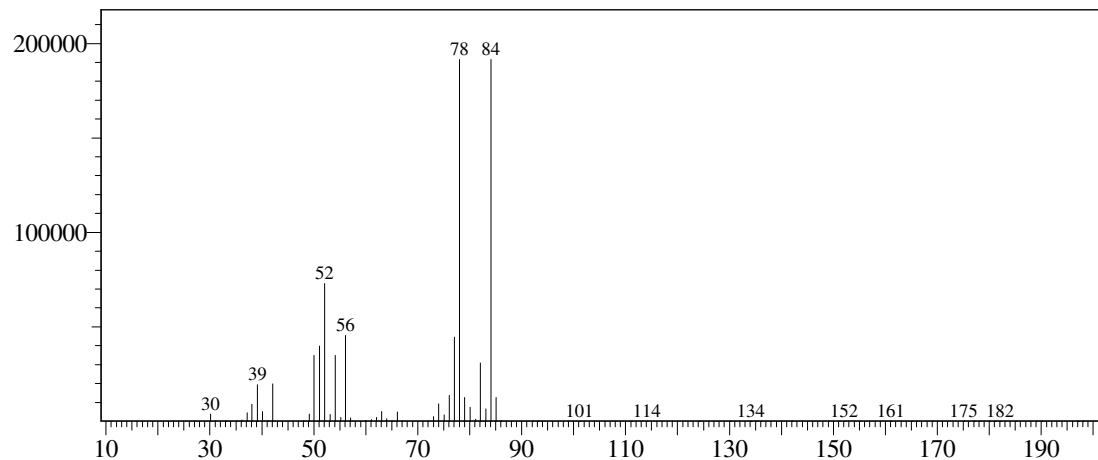
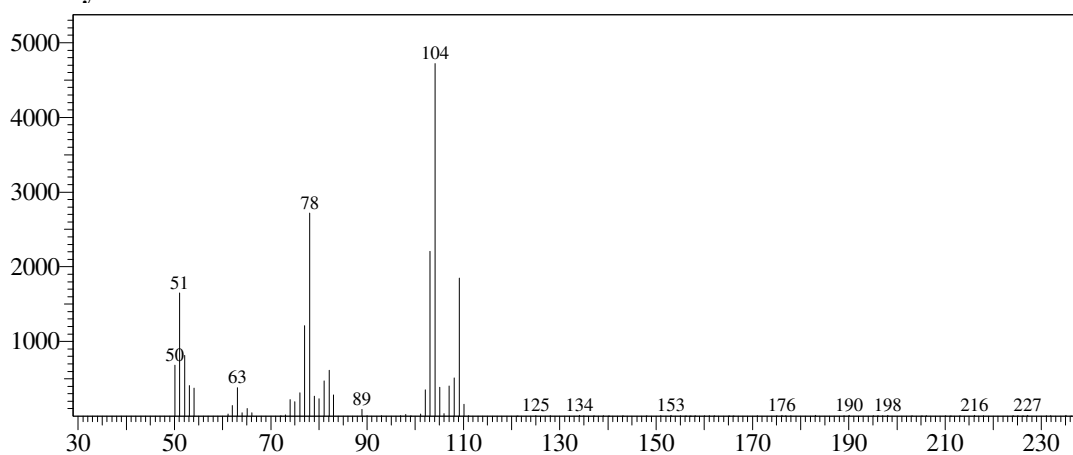
MS of Benzene in Reaction Mixture Prior to Reaction**MS of Benzene in Reaction Mixture after 0.5 h of Reaction****MS of Styrene in Reaction Mixture after 0.5 h of Reaction**

Figure 3.26. Mass spectra for kinetic isotope effect experiments using a 1:1 molar mixture of C_6H_6 and C_6D_6 . Reaction conditions: 5 mL C_6H_6 , 5 mL C_6D_6 , 0.112 mM **1-OAc**, 26.9 mM $Cu(OPiv)_2$, 50 psig C_2H_4 , 150 °C.

We also sought to probe the reversibility of the benzene C–H activation step through benzene H/D exchange experiments. A solution of **1-OAc** (0.001 mol %) and Cu(OPiv)₂ (120 equiv.) in a 1:1 molar mixture of C₆H₆ and C₆D₆ was heated to 150 °C. The isotopic distribution of benzene was determined by GC/MS for the initial solution prior to heating, after 4 h of heating, and after 24 h of heating. No change was observed in the isotopic distribution (Figure 3.27). To determine whether the acetic acid generated in the catalytic cycle could contribute to the reversibility of benzene C–H activation, a solution of **1-OAc** (0.001 mol %), Cu(OPiv)₂ (120 equiv.), and CD₃CO₂D (500 equiv.) in C₆H₆ was heated to 150 °C. The isotopic distribution of benzene was determined by GC/MS for the initial solution prior to heating, after 4 h of heating, and after 24 h of heating and no changes were observed (Figure 3.28).

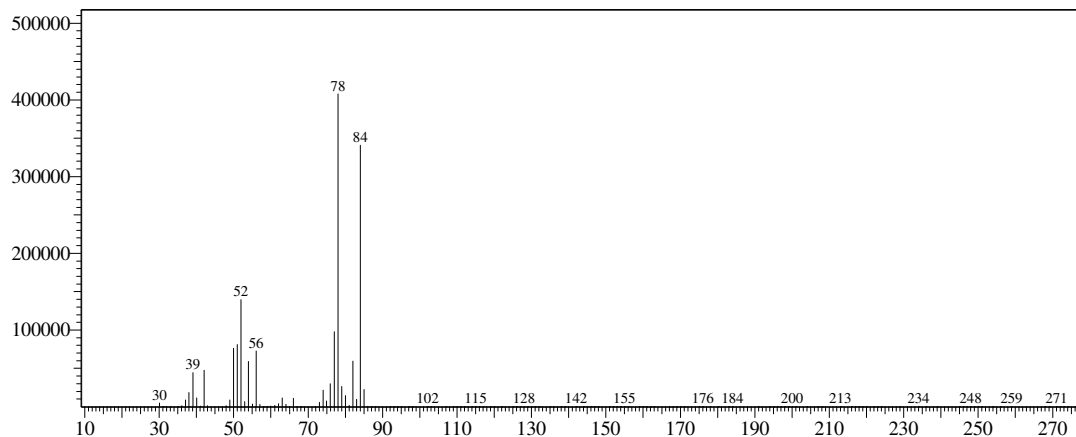
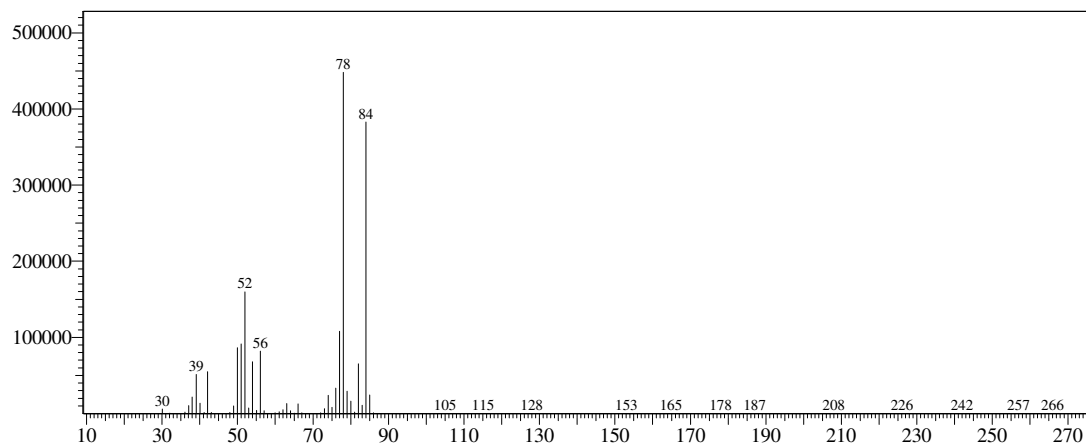
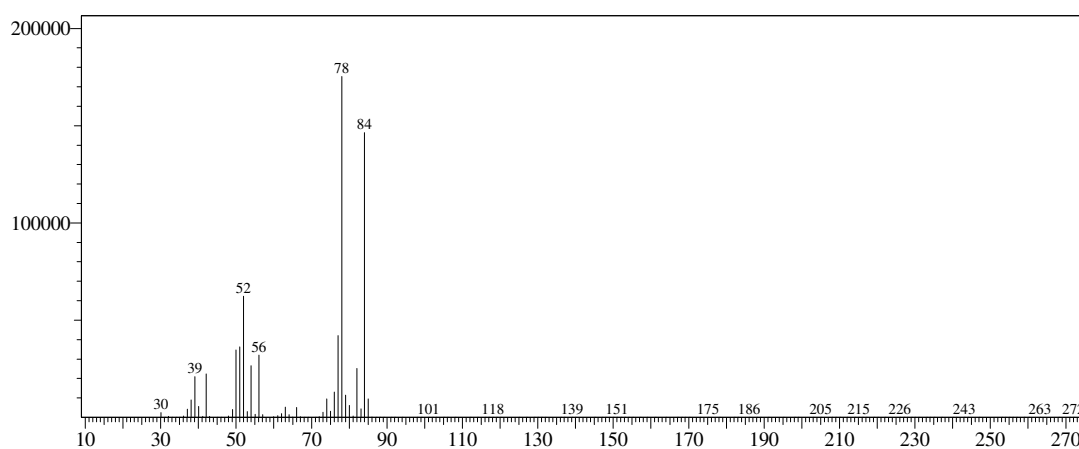
MS of Benzene in Reaction Mixture Prior to Reaction**MS of Benzene in Reaction Mixture after 4 h of Reaction****MS of Benzene in Reaction Mixture after 24 h of Reaction**

Figure 3.27. Mass spectra for H/D exchange experiments using a 1:1 molar mixture of C_6H_6 and C_6D_6 . Reaction conditions: 5 mL C_6H_6 , 5 mL C_6D_6 , 0.112 mM **1-OAc**, 13.4 mM $Cu(OPiv)_2$, 150 °C.

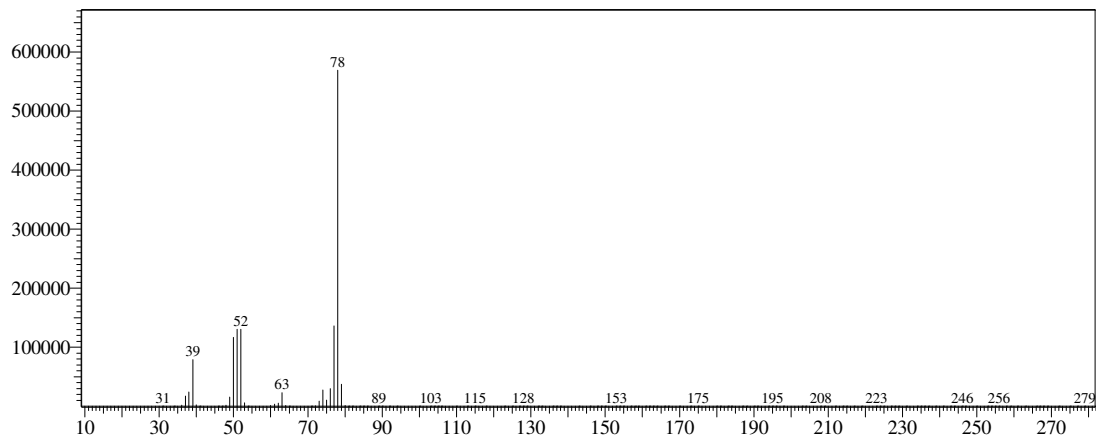
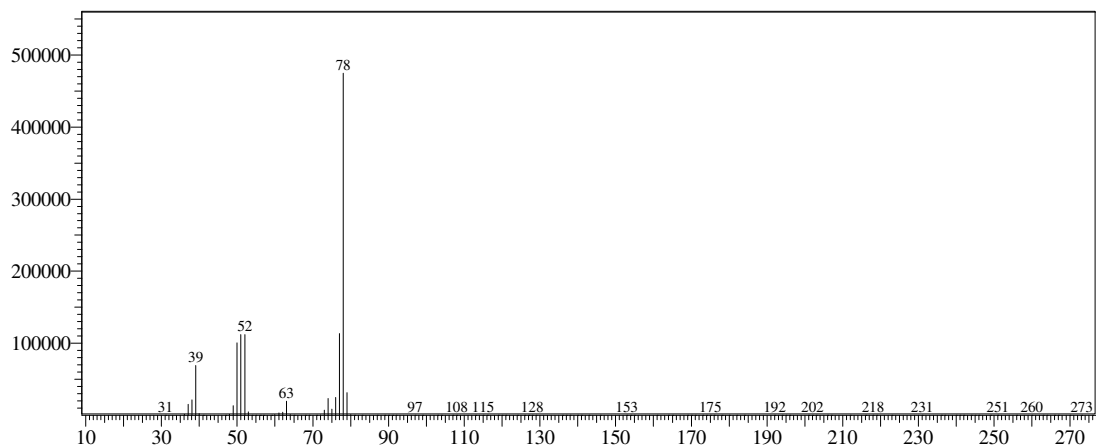
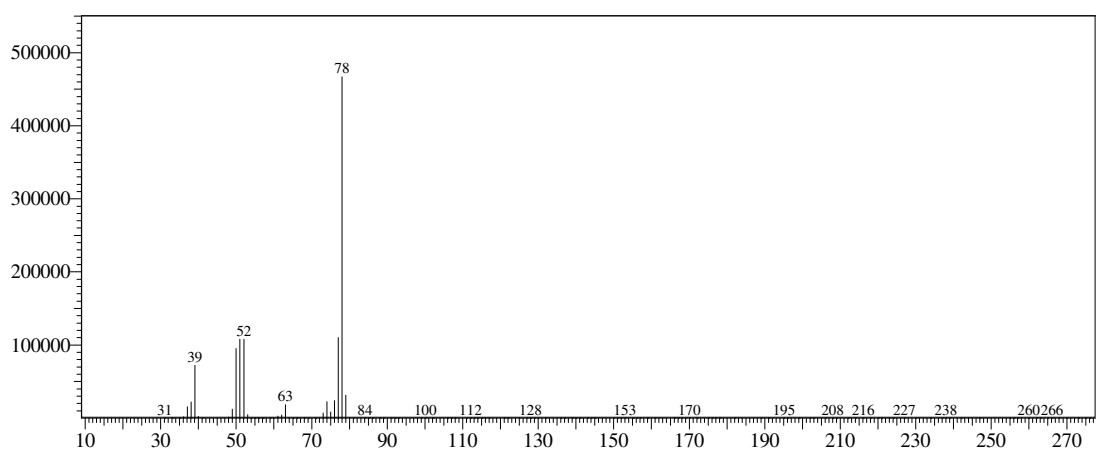
MS of Benzene in Reaction Mixture Prior to Reaction**MS of Benzene in Reaction Mixture after 4 h of Reaction****MS of Benzene in Reaction Mixture after 24 h of Reaction**

Figure 3.28. Mass spectra for H/D exchange experiments with added CD_3COOD . Reaction conditions: 10 mL C_6H_6 , 0.112 mM **1-OAc**, 13.4 mM $\text{Cu}(\text{OPiv})_2$, 56 mM CD_3COOD , 150 °C.

To determine if the equilibrium between monomer and dimer plays a role in benzene C–H activation, ethylene was added to H/D exchange reactions as experiments show that only monomer exists in the presence of ethylene. A solution of **1-OAc** (0.001 mol %), Cu(OPiv)₂ (120 equiv.), ethylene (50 psig), and CD₃CO₂D (500 equiv.) in C₆H₆ was heated to 150 °C. The isotopic distribution of benzene was determined by GC/MS for the initial solution prior to heating, after 4 h of heating, and after 24 h of heating and no change was observed over time (Figure 3.29). The isotopic distribution of the reaction product, styrene was also determined by GC/MS (Figure 3.29). Comparing the isotopic distribution in the reaction after 4 h and 24 h to the MS of an authentic standard, the amount of styrene-*d*₁ increased by ~5% over the course of the reaction. This indicates that the acid could be catalyzing H/D exchange with styrene, but the lack of deuterium incorporation into the benzene indicates *that the C–H activation step is likely irreversible.*

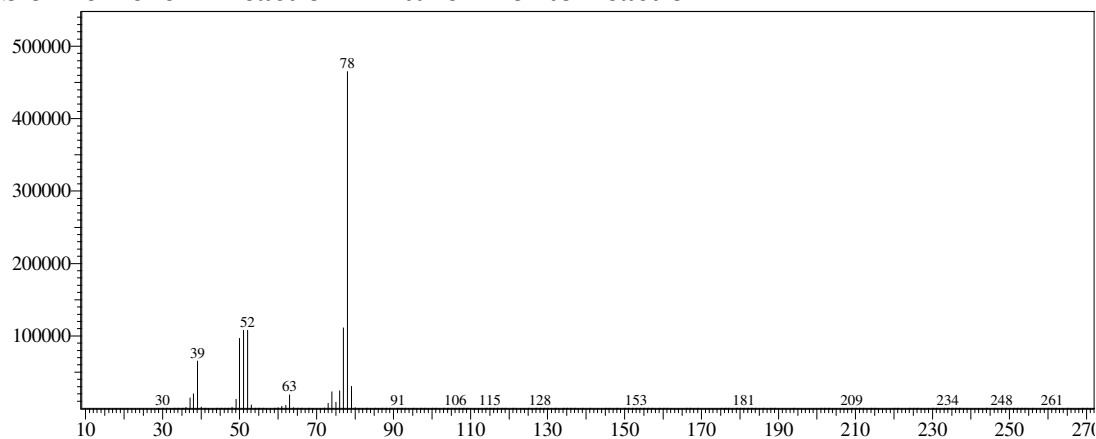
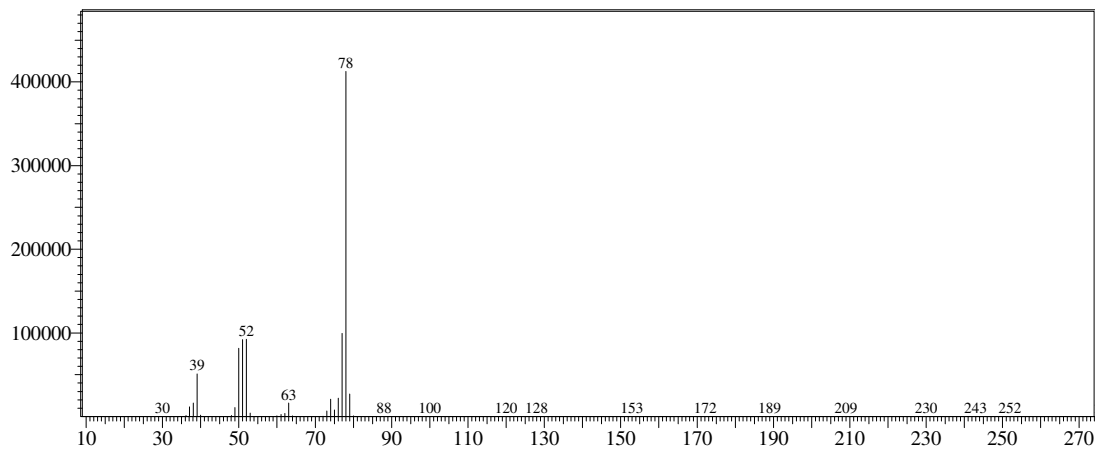
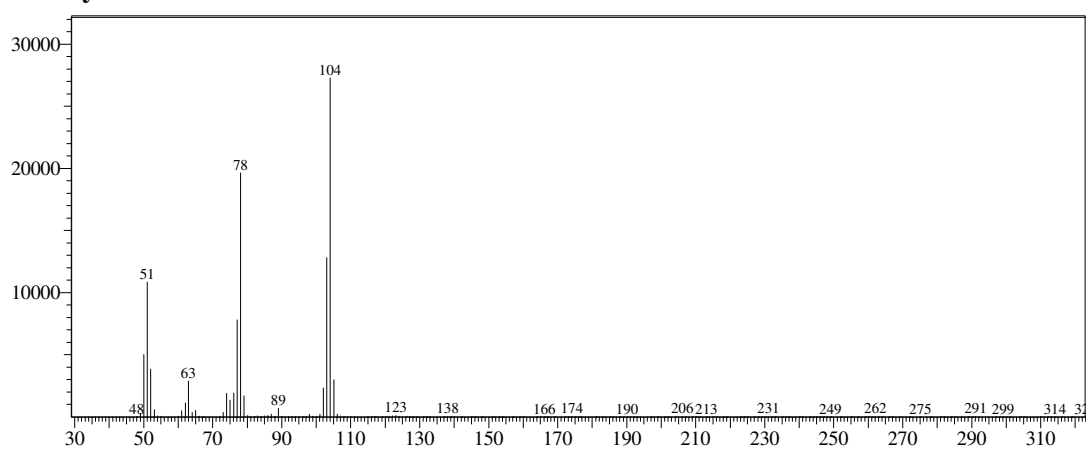
MS of Benzene in Reaction Mixture Prior to Reaction**MS of Benzene in Reaction Mixture after 4 h of Reaction****MS of Styrene in Reaction Mixture after 4 h of Reaction**

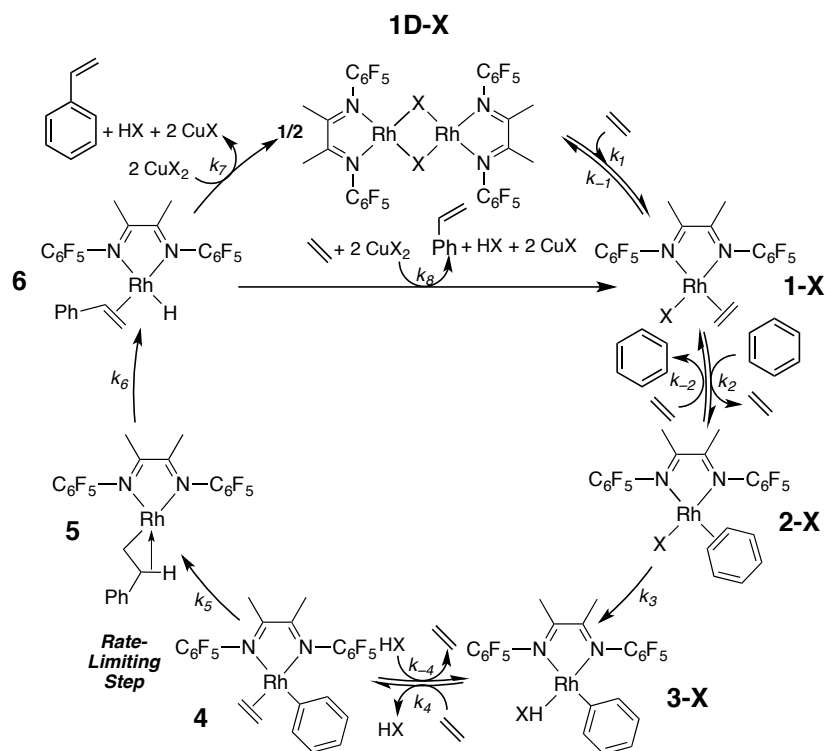
Figure 3.29. Mass spectra for H/D exchange experiments with added CD_3COOD and ethylene. Reaction conditions: 10 mL C_6H_6 , 0.112 mM **1-OAc**, 13.4 mM $\text{Cu}(\text{OPiv})_2$, 56 mM CD_3COOD , 50 psig C_2H_4 , 150 °C.

Wang and coworkers proposed that a Rh(I) catalyst precursor was rapidly converted to catalytically active Rh(III) in the presence of a Cu(II) oxidant and O₂.⁴⁷ To probe whether a similar reaction was occurring under our catalytic conditions, the Rh(III) complex (^{F1}DAB)RhCl₃(η²-C₂H₄) was synthesized *in situ* and tested for catalytic activity. Heating a solution of ^{F1}DAB (0.001 mol %), RhCl₃ (0.001 mol %), Cu(OPiv)₂ (120 equiv.), and ethylene (50 psig) in benzene at 150 °C afforded no styrene production after 24 h, suggesting that Rh(III) can not catalyze styrene production under our conditions.

3.3.7 Proposed Mechanism for the Catalytic Cycle

Based on the experimental and computational results, a cycle for styrene production using **1-OAc** is proposed in Scheme 3.9. Benzene coordinates to **1-OAc**, displacing ethylene to form **2-OAc**. The benzene C–H bond is cleaved in an irreversible reaction, consistent with lack of H/D exchange into benzene (*vide supra*), to afford (^{F1}DAB)Rh(Ph)(HOAc) (**3-OAc**). Acetic acid is displaced by ethylene to form (^{F1}DAB)Rh(Ph)(η²-C₂H₄) (**4**), which inserts ethylene to afford (^{F1}DAB)Rh(CH₂CH₂Ph) (**5**). Rapid, irreversible β-hydride elimination occurs to give (^{F1}DAB)Rh(H)(η²-styrene) (**6**). Two divergent pathways from **6** are proposed, one in which styrene dissociates and the Rh complex reacts with the Cu(II) oxidant to regenerate the dimer **1D-OAc** (favored at low [C₂H₄]), and another in which styrene is displaced by ethylene (likely via associative ligand exchange) before reaction with the oxidant (favored at high [C₂H₄]). The pathway that proceeds through **1D-OAc** would give rise to half-order kinetics with respect to Rh, and the pathway that does not would give rise to first-order kinetics with respect to Rh.

A rate law for the cycle shown in Scheme 3.9 was derived using both the King-Altman method (full derivation given in Scheme 3.10) and the steady-state approximation (full derivation given in Scheme 3.11).⁴⁸ The two rate laws differ slightly, which is a result of the methods by which they were derived (rate laws for the two cycles were derived simultaneously with steady-state vs. separately for King-Altman), though the limiting forms of the rate law are identical (*vide infra*). The two divergent pathways give rise to two terms in the rate law, one of which describes first-order behavior with respect to Rh and the other of which describes half-order behavior. Considering the limiting forms of the rate law where $[C_6H_6]$ is substantial predicts two kinetic regimes. One that is operative at low $[C_2H_4]$ in which the first-order term cancels, predicts a half-order dependence on [Rh], first-order dependence on ethylene, zero-order dependence on Cu, and an inverse dependence on HX. The other that is operative at high $[C_2H_4]$, in which the half-order term cancels, predicts a first-order dependence on [Rh] and saturation in all other components. Under catalytic conditions, the observed rate is likely a convolution of both the half- and first-order terms, as observed in the experiment where a change in the order in [Rh] is observed at different $[C_2H_4]$ (*vide supra*). Also, at low $[C_2H_4]$, the concentration of dimer $[1D-X]^{1/2}$ dominates the $[Rh]_{Tot}$ term, which gives rise to the half-order dependence on Rh and is consistent with experimental observations.



$$\frac{d[P]}{dt} = \frac{k_1 k_2 k_3 k_4 k_5 k_6 k_7 [\text{Rh}]^{1/2} [\text{C}_2\text{H}_4] [\text{C}_6\text{H}_6] [\text{Cu}]^2 + k_1 k_2 k_3 k_4 k_5 k_6 k_8 [\text{Rh}]_{\text{TO}} [\text{C}_2\text{H}_4]^2 [\text{C}_6\text{H}_6] [\text{Cu}]^2}{k_1 k_3 k_4 k_5 k_6 k_7 [\text{C}_2\text{H}_4] [\text{Cu}]^2 + k_1 k_2 k_4 k_5 k_6 k_7 [\text{C}_2\text{H}_4]^2 [\text{Cu}]^2 + k_1 k_2 k_4 k_5 k_6 k_7 [\text{C}_6\text{H}_6] [\text{Cu}]^2 + k_1 k_2 k_3 k_4 k_5 k_6 k_7 [\text{C}_6\text{H}_6] [\text{HX}] [\text{C}_6\text{H}_6] [\text{Cu}]^2 + k_1 k_2 k_3 k_4 k_6 k_7 [\text{C}_2\text{H}_4] [\text{C}_6\text{H}_6] [\text{Cu}]^2 + k_1 k_2 k_3 k_4 k_5 k_7 [\text{C}_2\text{H}_4] [\text{C}_6\text{H}_6] [\text{Cu}]^2 + k_1 k_3 k_4 k_5 k_6 k_8 [\text{C}_2\text{H}_4]^2 [\text{Cu}]^2 + k_1 k_2 k_4 k_5 k_6 k_8 [\text{C}_2\text{H}_4]^2 [\text{Cu}]^2 + k_1 k_2 k_4 k_5 k_6 k_8 [\text{C}_2\text{H}_4]^2 [\text{C}_6\text{H}_6] [\text{Cu}]^2 + k_1 k_2 k_3 k_4 k_5 k_6 k_8 [\text{C}_6\text{H}_6] [\text{Cu}]^2 [\text{C}_2\text{H}_4] + k_1 k_2 k_3 k_4 k_6 k_8 [\text{C}_2\text{H}_4]^2 [\text{C}_6\text{H}_6] [\text{Cu}]^2 + k_1 k_2 k_3 k_4 k_5 k_6 k_8 [\text{C}_2\text{H}_4]^2 [\text{C}_6\text{H}_6] [\text{Cu}]^2 + k_1 k_2 k_3 k_4 k_5 k_6 k_8 [\text{C}_2\text{H}_4]^2 [\text{C}_6\text{H}_6] [\text{HX}] [\text{C}_6\text{H}_6] [\text{Cu}]^2 [\text{C}_2\text{H}_4] + k_1 k_3 k_4 k_5 k_6 k_7 [\text{C}_6\text{H}_6] [\text{Cu}]^2 + k_1 k_2 k_3 k_4 k_5 k_6 k_8 [\text{C}_2\text{H}_4]^2 [\text{C}_6\text{H}_6] [\text{Cu}]^2 + k_1 k_2 k_4 k_5 k_6 k_7 [\text{C}_2\text{H}_4] [\text{Cu}]^2 + k_1 k_2 k_4 k_5 k_6 k_8 [\text{C}_2\text{H}_4]^2 [\text{Cu}]^2 + k_2 k_3 k_4 k_5 k_6 k_7 [\text{C}_6\text{H}_6] [\text{Cu}]^2}$$

At Low $[\text{C}_2\text{H}_4]$

$k_7 \gg k_8 [\text{C}_2\text{H}_4]$

and

$[\text{C}_2\text{H}_4]$ is small

At High $[\text{C}_2\text{H}_4]$

$k_7 \ll k_8 [\text{C}_2\text{H}_4]$

and

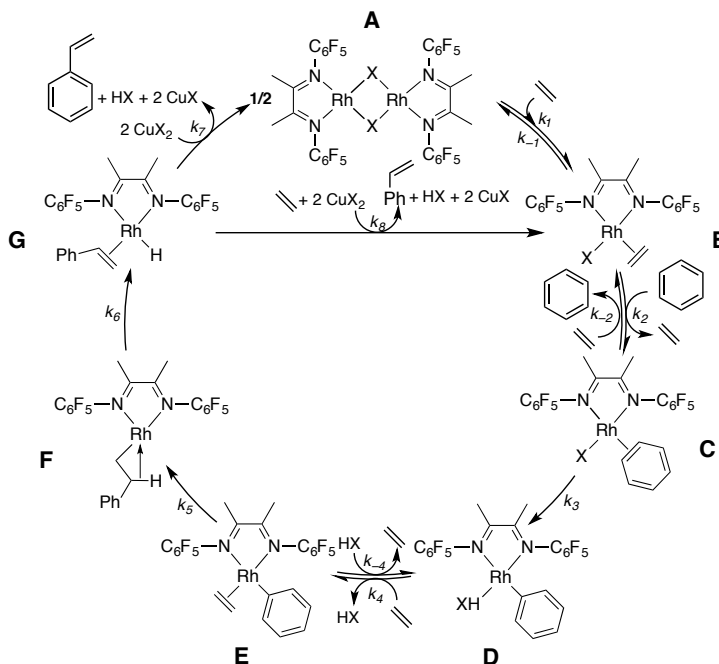
$[\text{C}_2\text{H}_4]$ is subst.

$$\frac{d[P]}{dt} = \frac{k_1 k_2 k_4 k_5 [\text{Rh}]^{1/2} [\text{C}_6\text{H}_6] [\text{C}_2\text{H}_4]}{k_2 k_4 k_5 [\text{C}_6\text{H}_6] + k_1 k_4 k_5 + k_1 k_2 k_5 [\text{C}_6\text{H}_6] + k_1 k_2 k_4 [\text{C}_6\text{H}_6] [\text{HX}]}$$

$$\frac{d[P]}{dt} = \frac{k_2 k_3 k_5 k_6 [\text{Rh}] [\text{C}_6\text{H}_6]}{k_3 k_5 k_6 + k_2 k_5 k_6 [\text{C}_6\text{H}_6] + k_2 k_3 k_6 [\text{C}_6\text{H}_6] + k_2 k_3 k_5 [\text{C}_6\text{H}_6]}$$

Scheme 3.9. Proposed Mechanism and Rate Law for Catalysis with **1-OAc**.

Scheme 3.10. Rate Law Derivation- King-Altman Method



$$[A] = k_2 k_3 k_4 k_5 k_6 k_7 [C_6H_6] [C_2H_4] [CuX_2]^2 + k_{-1} k_3 k_4 k_5 k_6 k_7 [C_2H_4] [CuX_2]^2 + k_{-1} k_{-2} k_4 k_5 k_6 k_7 [C_2H_4]^2 [CuX_2]^2$$

$$[B] = k_1 k_3 k_4 k_5 k_6 k_7 [C_2H_4]^2 [CuX_2]^2 + k_1 k_{-2} k_4 k_5 k_6 k_7 [C_2H_4]^3 [CuX_2]^2 + k_3 k_4 k_5 k_6 k_8 [C_2H_4]^2 [CuX_2]^2 + k_{-2} k_4 k_5 k_6 k_8 [C_2H_4]^3 [CuX_2]^2$$

$$[C] = k_1 k_2 k_4 k_5 k_6 k_7 [C_6H_6] [C_2H_4]^2 [CuX_2]^2 + k_2 k_4 k_5 k_6 k_8 [C_6H_6] [C_2H_4]^2 [CuX_2]^2$$

$$[D] = k_1 k_2 k_3 k_5 k_6 k_7 [C_6H_6] [C_2H_4] [CuX_2]^2 + k_1 k_2 k_3 k_{-4} k_6 k_7 [C_6H_6] [C_2H_4] [HX] [CuX_2]^2 + k_2 k_3 k_5 k_6 k_8 [C_6H_6] [C_2H_4] [CuX_2]^2 + k_2 k_3 k_{-4} k_6 k_8 [C_6H_6] [C_2H_4] [HX] [CuX_2]^2$$

$$[E] = k_1 k_2 k_3 k_4 k_6 k_7 [C_6H_6] [C_2H_4]^2 [CuX_2]^2 + k_2 k_3 k_4 k_6 k_8 [C_6H_6] [C_2H_4]^2 [CuX_2]^2$$

$$[F] = k_1 k_2 k_3 k_4 k_5 k_7 [C_6H_6] [C_2H_4]^2 [CuX_2]^2 + k_2 k_3 k_4 k_5 k_8 [C_6H_6] [C_2H_4]^2 [CuX_2]^2$$

$$[G] = k_1 k_2 k_3 k_4 k_5 k_6 [C_6H_6] [C_2H_4]^2 + k_2 k_3 k_4 k_5 k_6 [C_6H_6] [C_2H_4]$$

The total concentration of Rh is equal to the sum of each intermediate:

$$[Rh]_{tot}^{1/2} = [A]^{1/2} + [B] + [C] + [D] + [E] + [F] + [G] \quad [Rh]_{tot} = [B] + [C] + [D] + [E] + [F] + [G]$$

$$\frac{[Rh]_{tot}^{1/2}}{[A]^{1/2} + [B] + [C] + [D] + [E] + [F] + [G]} = 1 \quad \frac{[Rh]_{tot}}{[B] + [C] + [D] + [E] + [F] + [G]} = 1$$

Assuming Step 5 is Rate-Limiting:

$$\frac{d[P]}{dt} = k_5 [E] = \frac{k_5 [E] [Rh]_{tot}^{1/2}}{[A]^{1/2} + [B] + [C] + [D] + [E] + [F] + [G]} + \frac{k_5 [E] [Rh]_{tot}}{[B] + [C] + [D] + [E] + [F] + [G]}$$

$$\frac{d[P]}{dt} = \frac{k_1 k_2 k_3 k_4 k_5 k_6 k_7 [Rh]^{1/2} [C_6H_6] [C_2H_4]^2 [CuX_2]^2}{k_2 k_3 k_4 k_5 k_6 k_7 [C_6H_6] [C_2H_4] [CuX_2]^2 + k_{-1} k_3 k_4 k_5 k_6 k_7 [C_2H_4] [CuX_2]^2 + k_{-1} k_{-2} k_4 k_5 k_6 k_7 [C_2H_4]^2 [CuX_2]^2 + k_1 k_3 k_4 k_5 k_6 k_7 [C_2H_4]^2 [CuX_2]^2 + k_1 k_{-2} k_4 k_5 k_6 k_7 [C_2H_4]^3 [CuX_2]^2 + k_1 k_2 k_4 k_5 k_6 k_7 [C_6H_6] [C_2H_4]^2 [CuX_2]^2 + k_1 k_2 k_3 k_4 k_5 k_6 k_7 [C_6H_6] [C_2H_4] [CuX_2]^2 + k_1 k_2 k_3 k_4 k_5 k_6 k_7 [C_6H_6] [C_2H_4] [HX] [CuX_2]^2 + k_1 k_2 k_3 k_4 k_5 k_6 k_7 [C_6H_6] [C_2H_4]^2 [CuX_2]^2 + k_1 k_2 k_3 k_4 k_5 k_6 [C_6H_6] [C_2H_4]^2 [CuX_2]^2 + k_1 k_2 k_3 k_4 k_5 k_6 [C_6H_6] [C_2H_4]^2} \\ + \frac{k_2 k_3 k_4 k_5 k_6 k_8 [Rh]_{tot} [C_6H_6] [C_2H_4]^2 [CuX_2]^2}{k_3 k_4 k_5 k_6 k_8 [C_2H_4]^2 [CuX_2]^2 + k_{-2} k_4 k_5 k_6 k_8 [C_2H_4]^3 [CuX_2]^2 + k_2 k_4 k_5 k_6 k_8 [C_6H_6] [C_2H_4]^2 [CuX_2]^2 + k_2 k_3 k_4 k_5 k_6 k_8 [C_6H_6] [C_2H_4] [CuX_2]^2 + k_2 k_3 k_4 k_5 k_6 k_8 [C_6H_6] [C_2H_4] [HX] [CuX_2]^2 + k_2 k_3 k_4 k_5 k_6 k_8 [C_6H_6] [C_2H_4]^2 [CuX_2]^2 + k_2 k_3 k_4 k_5 k_6 [C_6H_6] [C_2H_4]^2 [CuX_2]^2 + k_2 k_3 k_4 k_5 k_6 [C_6H_6] [C_2H_4]}$$

$$\frac{d[P]}{dt} = \frac{k_1 k_2 k_3 k_4 k_5 k_6 k_7 [Rh]^{1/2} [C_6H_6] [C_2H_4] [CuX_2]^2}{k_2 k_3 k_4 k_5 k_6 k_7 [C_6H_6] [CuX_2]^2 + k_{-1} k_3 k_4 k_5 k_6 k_7 [CuX_2]^2 + k_{-1} k_{-2} k_4 k_5 k_6 k_7 [C_2H_4] [CuX_2]^2 + k_1 k_3 k_4 k_5 k_6 k_7 [C_2H_4] [CuX_2]^2 + k_1 k_{-2} k_4 k_5 k_6 k_7 [C_2H_4]^2 [CuX_2]^2 + k_1 k_2 k_4 k_5 k_6 k_7 [C_6H_6] [C_2H_4] [CuX_2]^2 + k_1 k_2 k_3 k_4 k_5 k_6 k_7 [C_6H_6] [CuX_2]^2 + k_1 k_2 k_3 k_4 k_5 k_6 k_7 [C_6H_6] [C_2H_4] [HX] [CuX_2]^2 + k_1 k_2 k_3 k_4 k_5 k_6 k_7 [C_6H_6] [C_2H_4]^2 [CuX_2]^2 + k_1 k_2 k_3 k_4 k_5 k_6 k_7 [C_6H_6] [C_2H_4] [CuX_2]^2 + k_1 k_2 k_3 k_4 k_5 k_6 [C_6H_6] [C_2H_4]} \\ + \frac{k_2 k_3 k_4 k_5 k_6 k_8 [Rh]_{tot} [C_6H_6] [C_2H_4] [CuX_2]^2}{k_3 k_4 k_5 k_6 k_8 [C_2H_4] [CuX_2]^2 + k_{-2} k_4 k_5 k_6 k_8 [C_2H_4]^2 [CuX_2]^2 + k_2 k_4 k_5 k_6 k_8 [C_6H_6] [C_2H_4] [CuX_2]^2 + k_2 k_3 k_4 k_5 k_6 k_8 [C_6H_6] [CuX_2]^2 + k_2 k_3 k_4 k_5 k_6 k_8 [C_6H_6] [HX] [CuX_2]^2 + k_2 k_3 k_4 k_5 k_6 k_8 [C_6H_6] [C_2H_4] [CuX_2]^2 + k_2 k_3 k_4 k_5 k_6 [C_6H_6] [C_2H_4]^2 [CuX_2]^2 + k_2 k_3 k_4 k_5 k_6 [C_6H_6]}$$

When $[C_6H_6]$ is substantial:

$$\frac{d[P]}{dt} = \frac{k_1 k_3 k_4 k_5 k_6 k_7 [Rh]^{1/2} [C_2H_4] [CuX_2]^2}{k_3 k_4 k_5 k_6 k_7 [CuX_2]^2 + k_1 k_4 k_5 k_6 k_7 [C_2H_4] [CuX_2]^2 + k_1 k_3 k_5 k_6 k_7 [CuX_2]^2 + k_1 k_3 k_4 k_6 k_7 [HX] [CuX_2]^2 + k_1 k_3 k_4 k_6 k_7 [C_2H_4] [CuX_2]^2 + k_1 k_3 k_4 k_5 k_7 [C_2H_4] [CuX_2]^2 + k_1 k_3 k_4 k_5 k_6 [C_2H_4]} \\ + \frac{k_3 k_4 k_5 k_6 k_8 [Rh]_{tot} [C_2H_4] [CuX_2]^2}{k_4 k_5 k_6 k_8 [C_2H_4] [CuX_2]^2 + k_3 k_5 k_6 k_8 [CuX_2]^2 + k_3 k_4 k_6 k_8 [HX] [CuX_2]^2 + k_3 k_4 k_6 k_8 [C_2H_4] [CuX_2]^2 + k_3 k_4 k_5 k_6 [C_2H_4] [CuX_2]^2 + k_3 k_4 k_5 k_6}$$

At Low $[C_2H_4]$:

$$k_7 \gg k_8 [C_2H_4]: \\ \frac{d[P]}{dt} = \frac{k_1 k_3 k_4 k_5 k_6 k_7 [Rh]^{1/2} [C_2H_4] [CuX_2]^2}{k_3 k_4 k_5 k_6 k_7 [CuX_2]^2 + k_1 k_4 k_5 k_6 k_7 [C_2H_4] [CuX_2]^2 + k_1 k_3 k_5 k_6 k_7 [CuX_2]^2 + k_1 k_3 k_4 k_6 k_7 [HX] [CuX_2]^2 + k_1 k_3 k_4 k_6 k_7 [C_2H_4] [CuX_2]^2 + k_1 k_3 k_4 k_5 k_7 [C_2H_4] [CuX_2]^2 + k_1 k_3 k_4 k_5 k_6 [C_2H_4]} \\ + \frac{k_3 k_4 k_5 k_6 k_8 [Rh]_{tot} [C_2H_4] [CuX_2]^2}{k_4 k_5 k_6 k_8 [C_2H_4] [CuX_2]^2 + k_3 k_5 k_6 k_8 [CuX_2]^2 + k_3 k_4 k_6 k_8 [HX] [CuX_2]^2 + k_3 k_4 k_6 k_8 [C_2H_4] [CuX_2]^2 + k_3 k_4 k_5 k_6 [C_2H_4] [CuX_2]^2 + k_3 k_4 k_5 k_6}$$

$[C_2H_4]$ is small:

$$\frac{d[P]}{dt} = \frac{k_1 k_4 k_5 [Rh]^{1/2} [C_2H_4]}{k_4 k_5 + k_1 k_5 + k_1 k_{-4} [HX]}$$

At High $[C_2H_4]$:

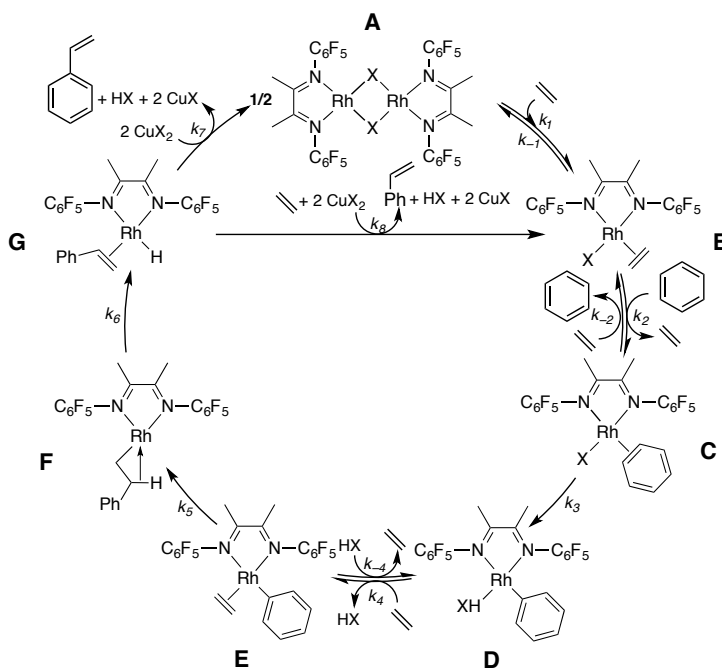
$k_7 \ll k_8 [C_2H_4]$:

$$\frac{d[P]}{dt} = \frac{k_3 k_4 k_5 k_6 k_8 [Rh]_{tot} [C_2H_4] [CuX_2]^2}{k_4 k_5 k_6 k_8 [C_2H_4] [CuX_2]^2 + k_3 k_5 k_6 k_8 [CuX_2]^2 + k_3 k_4 k_6 k_8 [HX] [CuX_2]^2 + k_3 k_4 k_6 k_8 [C_2H_4] [CuX_2]^2 + k_3 k_4 k_5 k_6 [C_2H_4] [CuX_2]^2 + k_3 k_4 k_5 k_6}$$

$[C_2H_4]$ is substantial:

$$\frac{d[P]}{dt} = \frac{k_3 k_5 k_6 [Rh]_{tot}}{k_5 k_6 + k_3 k_6 + k_3 k_5}$$

Scheme 3.11. Rate Law Derivation- Steady-State Method



$$[A]^{1/2} = \frac{k_{-1}[B] + k_7[G][Cu]^2}{k_1[C_2H_4]}$$

$$[B] = \frac{k_{-2}[C][C_2H_4] + k_1[A]^{1/2}[C_2H_4] + k_6[G][Cu]^2[C_2H_4]}{k_2[C_6H_6] + k_{-1}}$$

$$[C] = \frac{k_2[B][C_6H_6]}{k_3 + k_{-2}[C_2H_4]}$$

$$[D] = \frac{k_3[C] + k_4[E][HX]}{k_4[C_2H_4]}$$

$$[E] = \frac{k_4[D][C_2H_4]}{k_5 + k_{-4}[HX]}$$

$$[F] = \frac{k_5[E]}{k_6}$$

$$[G] = \frac{k_6[F]}{k_7[Cu]^2 + k_8[Cu]^2[C_2H_4]}$$

$$[Rh]_{Tot} = [A]^{1/2} + [B] + [C] + [D] + [E] + [F] + [G]$$

$$[Rh]_{Tot} = \frac{k_{-1}k_3k_5k_7[E] + k_{-1}k_3k_5k_8[E][C_2H_4] + k_{-1}k_2k_5k_7[C_2H_4][E] + k_{-1}k_2k_5k_8[C_2H_4]^2[E] + k_2k_3k_5k_7[C_6H_6][E]}{k_1k_2k_3k_7[C_6H_6][C_2H_4] + k_1k_2k_3k_8[C_2H_4]^2[C_6H_6]} + \frac{k_3k_5[E] + k_2k_5[C_2H_4][E]}{k_2k_3[C_6H_6]} + \frac{k_5[E]}{k_3} + \frac{k_5[E] + k_4[E][HX]}{k_4[C_2H_4]} + [E] + \frac{k_5[E]}{k_6} + \frac{k_5[E]}{k_7[Cu]^2 + k_8[Cu]^2[C_2H_4]}$$

Based on these derivations, the rate constant for C–H activation (k_3) is not included in the low $[\text{C}_2\text{H}_4]$ limiting form of the rate law, which indicates that catalysis in this regime should not exhibit a KIE. Thus, the KIE for the overall reaction would be expected to decrease as the order in $[\text{Rh}]$ approaches half-order. In contrast, at higher concentrations of C_2H_4 a KIE is expected as the limiting form of the rate law contains k_3 . To probe this, catalysis was performed in an equimolar mixture of per-protio and per-deutero benzene at 35 and 150 psig ethylene, and the resulting $k_{\text{H}}/k_{\text{D}}$ values were compared to the data from the initial KIE experiments at 50 psig ethylene (*vide supra*). A plot of observed KIE vs. order in $[\text{Rh}]$ (Figure 3.30, *vide supra* for discussion of variable order of the reaction in $[\text{Rh}]$) shows a linear correlation that predicts a KIE of 1.2(6) in the half-order regime (extrapolated from the linear fit) and a KIE of 6.7(6) in the first-order regime. Within deviation of the data, these results are consistent with the proposed reaction pathways. While a KIE of 6.7 is relatively high, it is not unprecedented.⁴⁹ Similarly high KIEs have been reported for complexes that perform carboxylate-assisted C–H activation, with some complexes exhibiting KIEs in excess of 8.⁵⁰

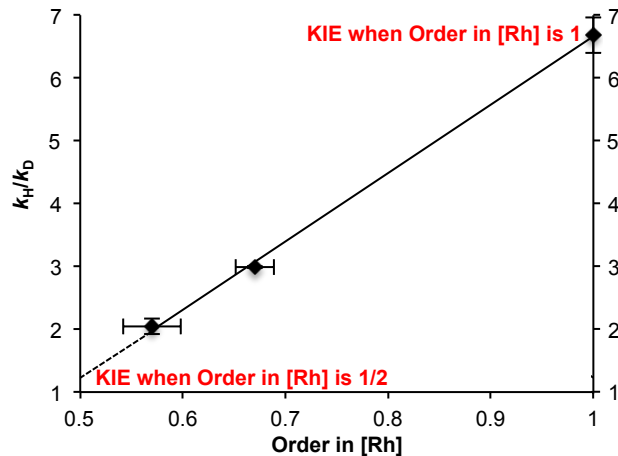


Figure 3.30. Plot of k_H/k_D vs. order in [Rh] ($R^2 = 0.99$). Reaction conditions: 0.11 mM **1-OAc**, 10 mL 1:1 C_6H_6 and C_6D_6 , 26.8 mM $Cu(OPiv)_2$, 35-150 psig C_2H_4 , 150 °C. Order in [Rh] (and the corresponding horizontal error bars) was determined using the data shown in **Figure 3.25**. Each data point represents the average of three independent catalytic reactions, each analyzed in triplicate by GC/MS. Vertical error bars represent the standard deviation of all nine values.

To further probe our proposed mechanism, experiments were run at high $[C_2H_4]$ in an attempt to observe saturation kinetics, which would be consistent with our proposed rate law (Figure 3.31). At $[C_2H_4]$ less than 237 mM, a first-order dependence on ethylene is observed, but above 237 mM, saturation is observed. In an attempt to observe the inverse dependence on acid (HX) predicted by the proposed rate law, catalysis with **1-OAc** was performed in the presence of added AcOH (500 and 1000 equiv. relative to **1-OAc**). Using initial rates, we found that the rate of catalysis is suppressed by AcOH (Figure 3.32). This is consistent with the limiting form for the low $[C_2H_4]$ regime. It is important to note that while the inverse dependence on acid would predict inhibition as the reaction proceeds, this is not observed under the catalytic conditions we tested. This is likely due to the low concentration of acid in solution under those conditions. The

limiting form for the high $[\text{C}_2\text{H}_4]$ regime predicts a zero-order dependence on acid (HX), so catalysis was performed at 400 psig C_2H_4 with 0, 500, and 1000 equiv. AcOH added (relative to Rh). At this high concentration of ethylene, the observed rate of reaction without added AcOH is statistically identical to catalytic experiments with added acid, which is consistent with the proposed reaction pathway (Figure 3.33). Rationalization of the change in the dependence on Rh as temperature is varied is more difficult since the route that is first-order in Rh involves a series of ill-defined reactions with Cu(II). But, it is not surprising that the contribution of the two competing pathways varies with temperature.

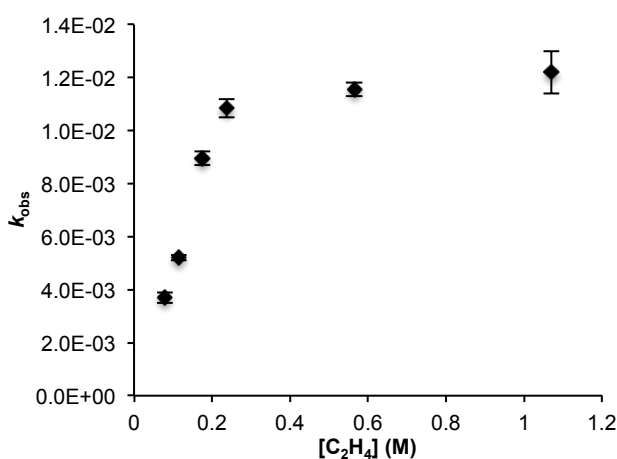


Figure 3.31. Plot of k_{obs} vs. $[\text{C}_2\text{H}_4]$. Reaction conditions: 0.11 mM **1-OAc**, 20 mL C_6H_6 , 13.4 mM $\text{Cu}(\text{OPiv})_2$, 150 °C. Each data point represents the average of two independent catalytic reactions, each analyzed in duplicate by GC/FID. Error bars represent the standard deviation of all four values.

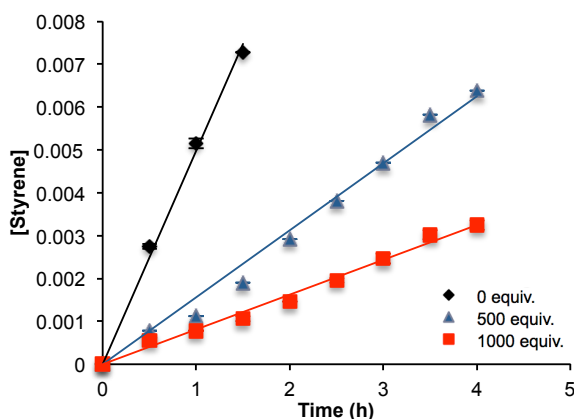


Figure 3.32. [Styrene] vs. time plot for the initial rate regime of catalysis with **1-OAc** upon the addition of 0 equiv. (slope = 0.005, $R^2 = 0.99$), 500 equiv. (slope = 0.0016, $R^2 = 0.99$), and 1000 equiv. (slope = 0.0008, $R^2 = 0.99$) AcOH relative to the concentration of **1-OAc**. Reaction conditions: 20 mL C_6H_6 , 13.4 mM $Cu(OPiv)_2$, 50 psig C_2H_4 , AcOH (0, 500, or 1000 equiv. relative to **1-OAc**), 150 °C. Each data point represents the average of two independent catalytic reactions, each analyzed in duplicate by GC/FID. Error bars represent the standard deviation of all four values.

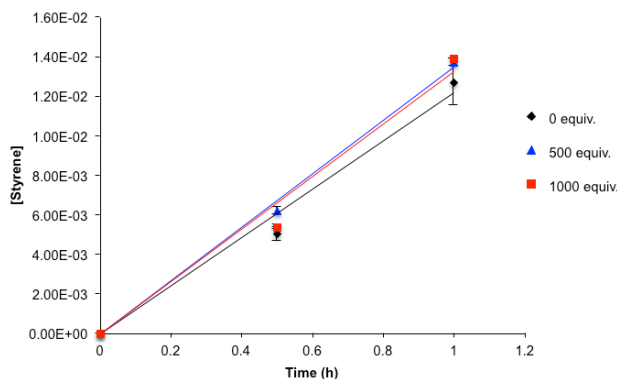


Figure 3.33. [Styrene] vs. time plot for the initial rate regime of catalysis with **1-OAc** upon the addition of 0 equiv. (slope = 0.012, $R^2 = 0.98$), 500 equiv. (slope = 0.0014, $R^2 = 0.99$), and 1000 equiv. (slope = 0.013, $R^2 = 0.98$) AcOH relative to the concentration of **1-OAc**. Reaction conditions: 20 mL C_6H_6 , 13.4 mM $Cu(OPiv)_2$, 400 psig C_2H_4 , AcOH (0, 500, or 1000 equiv. relative to **1-OAc**), 150 °C. Each data point represents the average of two independent catalytic reactions, each analyzed in duplicate by GC/FID. Error bars represent the standard deviation of all four values.

3.4 Summary and Conclusions

The complexes (^{F1}DAB)Rh(X)(η^2 -C₂H₄) [X = TFA, OAc] are effective catalysts for the direct conversion of benzene, ethylene, and Cu(II) oxidant to styrene. These Rh catalyst precursors are unique for their selectivity for styrene formation as well as catalyst longevity. The mechanism of this reaction has been studied and compared to both electron-rich Ru(II) and related electrophilic cationic Pt(II) catalysts. Based on these results, the following conclusions can be drawn:

- (1) Combined experimental and computational studies are consistent with catalysis that proceeds through benzene C–H activation, displacement of coordinated acetic acid by ethylene, insertion of ethylene into the Rh–Ph bond, and β -hydride elimination followed by liberation of styrene and reaction with Cu(II).
- (2) The apparent induction period observed for catalysis with **1-TFA** when using Cu(OAc)₂ as the oxidant is not likely the result of *in situ* formation of insoluble Rh nanoparticles as the active catalyst. Rather, **1-TFA** converts to **1-OAc** *in situ*, which catalyzes styrene production at a faster rate than the TFA analog. The difference in rate of catalysis for **1-OAc** and **1-TFA** is likely a result of the difference in ground state energies rather than OAc/TFA influence on transition states, since the proposed rate-determining step occurs once the carboxylate ligands are completely dissociated.
- (3) A mechanism for catalysis with (^{F1}DAB)Rh(X)(η^2 -C₂H₄) (X = OAc or TFA) has been proposed that involves two pathways whose contributions vary with [C₂H₄] and temperature. Accordingly, the derived rate law predicts different behavior at low and high [C₂H₄]. At low [C₂H₄], the limiting form predicts half-

order in Rh, first-order in ethylene, zero-order in Cu, and an inverse dependence on acid concentration. At high $[C_2H_4]$, the limiting form predicts first-order in Rh, and zero-order dependence on all others. Saturation behavior has been observed for ethylene, and the rate of reaction is suppressed in the presence of added acid at low $[C_2H_4]$ but not at high $[C_2H_4]$, which is consistent with the proposed mechanism and rate law. The kinetics are also consistent with computational modeling, which predicts rate-limiting ethylene insertion into the Rh–Ph bond. However, alternative explanations of the kinetic data are possible, such as inhibition of catalysis upon reaction of the catalyst with acid (to remove Rh from the catalytic cycle) that is influenced by concentration of ethylene. Despite other possible explanations for this complex catalytic process, our mechanistic proposal is consistent with both experimental and computational data and, we believe, is the mechanistic model that is most consistent with the data.

- (4) The selectivity for styrene production (versus ethylbenzene) using $(^F\text{DAB})\text{Rh}(\text{X})(\eta^2\text{-C}_2\text{H}_4)$ appears to result from more favorable styrene dissociation compared to related cationic Pt(II) catalysts.

3.5 Experimental

General Considerations. All manipulations were performed under an atmosphere of dry nitrogen using standard Schlenk or high vacuum techniques and/or in a Vac Atmospheres Dri-Lab glovebox equipped with a Dri-Train MO-41 purifier. Dry, oxygen-free solvents were employed throughout. THF was dried by passage through columns of

activated alumina, followed by distillation from sodium benzophenone ketyl. Pentane was dried over sodium benzophenone ketyl. Deuterated solvents were purchased from Cambridge Isotope Labs, degassed, and dried over molecular sieves. NMR spectra were recorded on a Varian Inova 300 MHz NMR spectrometer (^{19}F , 282.21 MHz operating frequency), Bruker Avance III 600 MHz NMR spectrometer (^1H , 600.13 MHz operating frequency), or a Bruker Avance III 800 MHz NMR spectrometer (^{13}C , 201.27 MHz operating frequency), and are reported with reference to residual solvent resonances. GC/MS was performed using a Shimadzu GCMS-QP2010 Plus system with a 30 m x 0.25 mm SHRXI-5MS column with 0.25 μm film thickness using electron impact (EI) ionization. GC/FID was performed using a Shimadzu GC-2014 system with a 30 m x 90.25 mm HP5 column with 0.25 μm film thickness.

Styrene production was quantified using linear regression analysis of gas chromatograms of standard samples of authentic product. A plot of peak area ratios versus molar ratios gave a regression line. For the GC/FID system, the slope and correlation coefficient of the regression line were 1.34 and 0.99, respectively. FID response factors for other products were determined in a similar fashion, using authentic standards of products. Ethylene was purchased in gas cylinders from GTS-Welco and used as received. All other reagents were purchased from commercial sources and used as received. $[\text{Rh}(\eta^2\text{-C}_2\text{H}_4)_2(\mu\text{-Cl})_2]$ was prepared according to literature procedures.⁵¹ $[\text{Rh}(\eta^2\text{-C}_2\text{H}_4)_2(\mu\text{-TFA})_2]$ was prepared using an adaptation of literature procedures, substituting AgTFA for TITFA.⁵² ^{19}F DAB was synthesized according to literature procedures.⁵³ While the synthesis of $[\text{Rh}(\eta^2\text{-C}_2\text{H}_4)_2(\mu\text{-OAc})_2]$ has been reported previously,⁵⁴ higher yields were obtained by using the same method as for the synthesis

of $[\text{Rh}(\eta^2\text{-C}_2\text{H}_4)_2(\mu\text{-TFA})]_2$,⁵² substituting TIOAc for TITFA. Copper(II) pivalate $[\text{Cu}(\text{OPiv})_2]$ was synthesized according to literature procedures.⁵⁵ The Maitlis filtration test was performed according to the previously reported procedure.²⁷

Procedure for TEM/EDS Experiments. Transmission electron microscopy images were obtained using a JEOL 2000FX-II electron microscope equipped with a Gresham high-angle x-ray detector. An accelerating voltage of 200 kV was used with a resolution of 1.4 Å. Energy dispersive x-ray spectroscopy (EDS) data were used to detect the presence of Rh and Cu, and were collected using an incident beam diameter of approximately 25 nm. Samples for electron microscopy were prepared by ultrasonic dispersion in 1,4-dioxane followed by deposition onto a holey carbon film supported on a 400 mesh Cu grid. Samples were allowed to dry in air for 24 hours before insertion into the microscope vacuum chamber.

Computational Methods. Density functional theory (DFT) was applied to the study of styrene formation using both **1-TFA** and **1-OAc**. The Gaussian 09 package was used to perform all simulations.⁵⁶ All stationary points were obtained using the B3LYP^{57,58} functional along with the LANL2DZ pseudopotential basis set for Rh and the 6-31G(d) basis set for main group elements; the 6-311++G(d,p) pseudopotential basis set was used on main group elements for single point calculations at the B3LYP/LANL2DZ+6-31G(d) stationary points. Free energies are reported in kcal/mol at 423.15 K assuming a pressure of 1 atm. Unscaled B3LYP/LANL2DZ+6-31G(d) vibrational frequencies were used for the enthalpic and entropic corrections. The GD3BJ dispersion correction⁵⁹ and the SMD solvation model⁶⁰ were utilized in the presence of benzene as the continuum solvent on the single point calculations. Stationary points were differentiated as minima or transition

states based on the number of imaginary frequencies (zero or one, respectively) calculated based on the energy Hessian.

The monomer/dimer equilibrium of both **1-TFA** and **1-OAc** was also examined using DFT. All stationary points were obtained using the M06⁶¹ functional along with the LANL2DZ pseudopotential basis set for Rh and the 6-31G(d) basis set for main group elements; the 6-311++G(d,p) pseudopotential basis set was used on main group elements for single point calculations at the M06/LANL2DZ+6-31G(d) stationary points. Free energies are reported in kcal/mol at 423.15 K assuming a pressure of 1 atm. Unscaled M06/LANL2DZ+6-31G(d) vibrational frequencies were used for the enthalpic and entropic corrections. The SMD solvation model⁶⁰ was utilized in the presence of benzene as the continuum solvent on the single point calculations.

Synthesis of (^{F1}DAB)Rh(TFA)(η^2 -C₂H₄) [1-TFA]. To a stirring solution of [Rh(η^2 -C₂H₄)₂(μ -TFA)]₂ (200 mg, 0.368 mmol) in THF (25 mL), ^{F1}DAB (310 mg, 0.735 mmol) was added, and the mixture was stirred for 10 minutes. The solvent was removed *in vacuo*, and the purple solid was washed with pentane (c.a. 80 mL) and dried to afford **1-TFA** as a purple powder (330 mg, 0.501 mmol, 68%). Upon prolonged drying *in vacuo*, the ethylene is removed to form [(^{F1}DAB)Rh(μ -TFA)]₂ (eq. 1), characterization data for which is as follows. ¹H NMR (800 MHz, DMF-*d*₇): δ -0.6 (s, 6H, DAB-CH₃). ¹³C{¹H} NMR (800 MHz, DMF-*d*₇): δ 163.8 (s, DAB-C=N), 142.0 (d, ³J_{CF} = 8 Hz, C₆F₅-*ortho* C), 140.8 (d, ³J_{CF} = 12 Hz, C₆F₅-*ortho* C), 139.6 (t, ³J_{CF} = 13 Hz, C₆F₅-*meta* C), 139.0 (t, ³J_{CF} = 15 Hz, C₆F₅-*meta* C), 137.8 (t, ³J_{CF} = 13 Hz, C₆F₅-*para* C), 129.9 (s, C₆F₅-*ipso* C), 115.8 (q, ¹J_{CF} = 293 Hz, CO₂CF₃), 20.9 (s, DAB-CH₃), 13.7 (q, ³J_{CF} = 23 Hz, CO₂CF₃). ¹⁹F{¹H} NMR (300 MHz, DMSO-*d*₆): δ -74.0 (s, TFA), -151.9 (dd, *J* = 24 Hz, 6 Hz,

C_6F_5 *para* F), -162.3 (t, $J = 23$ Hz, C_6F_5 *meta* F), -163.4 (td, $J = 23$ Hz, 6 Hz, C_6F_5 *ortho* F). Anal. Calcd for $\text{C}_{36}\text{H}_{12}\text{F}_{26}\text{N}_4\text{O}_4\text{Rh}_2$: C, 34.20; H, 0.96; N, 4.43. Found: C, 33.61; H, 1.05; N, 4.14. Upon pressurizing with ethylene, complex **1-TFA** can be regenerated, and its *in situ* characterization data is as follows: ^1H NMR (800 MHz, DMF-d_7): δ 5.9 (s, 4H, C_2H_4), 3.5 (s, 6H, DAB- CH_3).

Synthesis of $(^{\text{F1}}\text{DAB})\text{Rh}(\text{OAc})(\eta^2\text{-C}_2\text{H}_4)$ [1-OAc**].** To a stirring solution of $[\text{Rh}(\eta^2\text{-C}_2\text{H}_4)_2(\mu\text{-OAc})_2]$ (200 mg, 0.459 mmol) in THF (20 mL), $^{\text{F1}}\text{DAB}$ (382 mg, 0.918 mmol) was added, and the mixture was stirred for 30 minutes. The solvent was removed *in vacuo*, and the purple solid was washed with pentane (c.a. 80 mL) and dried to afford **1-OAc** as a purple powder (218 mg, 0.360 mmol, 40%). Upon prolonged drying *in vacuo*, the ethylene is removed to form $[(^{\text{F1}}\text{DAB})\text{Rh}(\mu\text{-OAc})_2]$ (**1D-OAc**), the characterization data for which is as follows. ^1H NMR (600.13 MHz, C_6D_6): δ 1.75 (s, 6H, COOCH_3), -0.95 (s, 12H, DAB- CH_3). $^{13}\text{C}\{^1\text{H}\}$ NMR (201.27 MHz, C_6D_6): δ 186.0 (s, COOCH_3), 163.9 (s, $\text{C}=\text{N}$), 141.2 (m, C_6F_5 -*meta* C), 140.0 (m, C_6F_5 -*meta* C), 138.9 (m, C_6F_5 -*ortho* C), 137.7 (m, C_6F_5 -*ortho* C), 131.0 (m, C_6F_5 -*para* C), 130.1 (s, C_6F_5 -*ipso* C), 22.8 (s, COOCH_3), 19.7 (s, DAB- CH_3). $^{19}\text{F}\{^1\text{H}\}$ NMR (564.33 MHz, C_6D_6): δ -144.0 (d, $^3J_{\text{FF}} = 23$ Hz, C_6F_5 -*ortho* F), -151.3 (d, $^3J_{\text{FF}} = 23$ Hz, C_6F_5 -*ortho* F), -156.6 (t, $^3J_{\text{FF}} = 23$ Hz, C_6F_5 -*meta* F), -163.1 (t, $^3J_{\text{FF}} = 23$ Hz, C_6F_5 -*meta* F), -165.9 (t, $^3J_{\text{FF}} = 23$ Hz, C_6F_5 -*para* F). IR (KBr): ν 1530, 1497 cm^{-1} (O_2CMe sym and asym). Upon pressurizing with ethylene, **1-OAc** can be regenerated, and its *in situ* characterization data is as follows: ^1H NMR (600.13 MHz, C_6D_6): δ 2.5 (broad s, 4H, C_2H_4), 1.68 (s, 3H, COOCH_3), -1.79 (s, 6H, DAB- CH_3).

Catalytic Oxidative Hydrophenylation of Ethylene with 1-TFA. A representative catalytic reaction is described. A stock solution containing **1-TFA** (0.015 g, 0.023 mmol), decane (44 μ L, 0.23 mmol), and benzene (200 mL) was prepared in a volumetric flask. Fisher-Porter reactors were charged with stock solution (20 mL) and copper 2-ethylhexanoate (0.095 g, 0.27 mmol). The vessels were sealed, pressurized with ethylene (25 psig), and subsequently stirred and heated to 150 °C. The reaction was sampled every 4 h for the first 12 h, then every subsequent 12 h. At each time point, the reactors were cooled to room temperature, sampled, recharged with ethylene, and reheated. Aliquots of the reaction mixture were analyzed by GC/FID using relative peak areas versus an internal standard (decane).

Catalyst Loading Experiments with 1-TFA. Three separate stock solutions were prepared in 50 mL volumetric flasks, each containing **1-TFA** (0.05 mol %, 0.025 mol %, or 0.001 mol % relative to benzene), decane (10 equiv. relative to **1-TFA**), and benzene (50 mL). Fisher-Porter reactors (2 reactors per loading) were charged with stock solution (20 mL) and Cu(OAc)₂ (60 equiv. relative to **1-TFA**). The vessels were sealed, charged with ethylene (25 psig), and subsequently stirred and heated to 120 °C. The reaction was sampled every 4 h for the first 12 h, then every subsequent 12 h. At each time point, the reactors were cooled to room temperature, sampled, recharged with ethylene, and reheated. Aliquots of the reaction mixture were analyzed by GC/FID using relative peak areas versus an internal standard (decane).

Experiments with 0.0001 mol % of 1-TFA (relative to benzene). A 0.001 mol % stock solution containing **1-TFA** (0.002 g, 0.003 mmol), decane (6 μ L, 0.03 mmol), and benzene (25 mL) was prepared in a volumetric flask. A 0.0001 mol % stock solution was

prepared by transferring 5 mL of 0.001 mol % stock solution to a 50 mL volumetric flask and diluting with benzene. Fisher-Porter reactors were charged with 0.0001 mol % stock solution (20 mL) and $\text{Cu}(\text{OAc})_2$ (0.100 g, 0.55 mmol). The vessels were sealed, pressurized with ethylene (75 psig), and subsequently stirred and heated to 150 °C. The reaction was sampled every 24 h. At each time point, the reactors were cooled to room temperature, sampled, recharged with ethylene, and reheated. Aliquots of the reaction mixture were analyzed by GC/FID using relative peak areas versus an internal standard (decane).

Oxidant Screening Experiments with 1-TFA. A stock solution containing **1-TFA** (0.001 mol % relative to benzene), decane (10 equiv. relative to **1-TFA**), and benzene (200 mL) was prepared in a volumetric flask. Fisher-Porter reactors (2 per oxidant) were charged with stock solution (20 mL) and oxidant (120 equiv. relative to **1-TFA**). Oxidants screened included copper(II) pivalate, copper(II) 2-ethylhexanoate, copper(II) trifluoroacetate, and copper(II) acetate. The vessels were sealed, charged with ethylene (25 psig), and subsequently stirred and heated to 150 °C. The reaction was sampled at 3, 8, 12, 24, and 28 h. At each time point, the reactors were cooled to room temperature, sampled, recharged with ethylene, and reheated. Aliquots of the reaction mixture were analyzed by GC/FID using relative peak areas versus an internal standard (decane).

Oxidant Amount Experiments with 1-TFA. A stock solution containing **1-TFA** (0.001 mol % relative to benzene), decane (10 equiv. relative to **1-TFA**), and benzene (200 mL) was prepared in a volumetric flask. Fisher-Porter reactors (2 per oxidant amount) were charged with stock solution (20 mL) and $\text{Cu}(\text{OAc})_2$ (60, 120, or 240 equiv. relative to **1-TFA**). The vessels were sealed, charged with ethylene (25 psig), and

subsequently stirred and heated to 120 °C. The reaction was sampled every 4 h for the first 12 h, then every subsequent 12 h. At each time point, the reactors were cooled to room temperature, sampled, recharged with ethylene, and reheated. Aliquots of the reaction mixture were analyzed by GC/FID using relative peak areas versus an internal standard (decane).

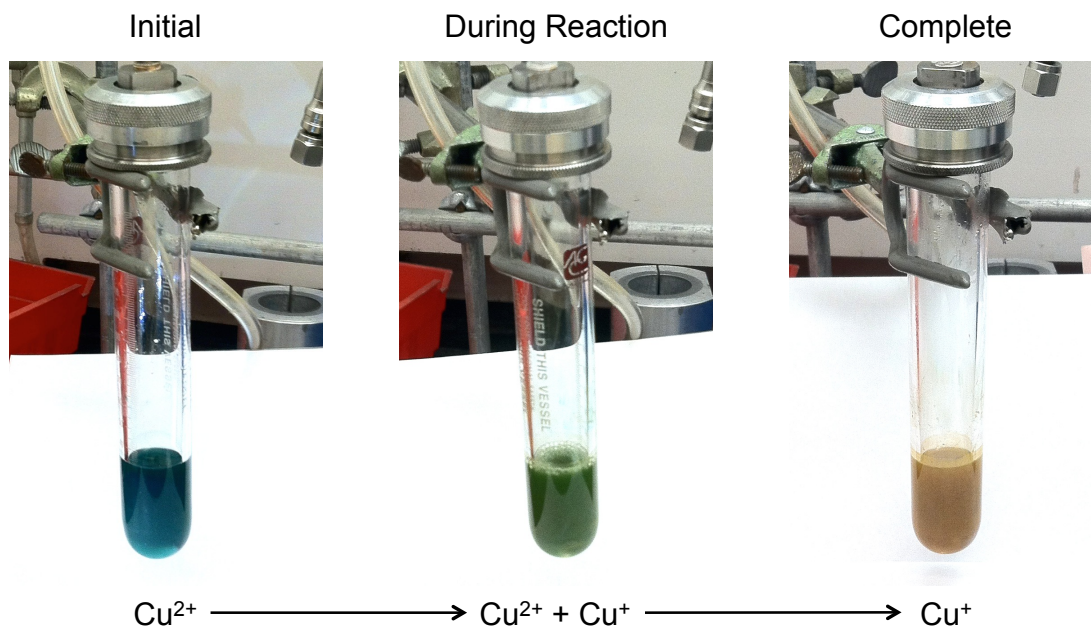
Temperature Variation Experiments with 1-TFA. A stock solution containing **1-TFA** (0.001 mol % relative to benzene), decane (10 equiv. relative to **1-TFA**), and benzene (200 mL) was prepared in a volumetric flask. Fisher-Porter reactors were charged with stock solution (20 mL) and $\text{Cu}(\text{OAc})_2$ (120 equiv. relative to **1-TFA**). The vessels were sealed, charged with ethylene (25 psig), and subsequently stirred and heated to 90, 120, 150, or 180 °C (2 reactors per temperature). The reaction was sampled every 4 h for the first 12 h, then every subsequent 12 h. At each time point, the reactors were cooled to room temperature, sampled, recharged with ethylene, and reheated. Aliquots of the reaction mixture were analyzed by GC/FID using relative peak areas versus an internal standard (decane).

Ethylene Pressure Experiments with 1-TFA. A stock solution containing **1-TFA** (0.001 mol % relative to benzene), decane (10 equiv. relative to **1-TFA**), and benzene (200 mL) was prepared in a volumetric flask. Fisher-Porter reactors were charged with stock solution (20 mL) and $\text{Cu}(\text{OAc})_2$ (120 equiv. relative to **1-TFA**). The vessels were sealed, charged with ethylene (15, 25, 50, or 100 psig, 2 reactors at each pressure), and subsequently stirred and heated to 150 °C. The reaction was sampled every 4 h for the first 12 h, then every subsequent 12 h. At each time point, the reactors were cooled to room temperature, sampled, recharged with ethylene, and reheated. Aliquots of the

reaction mixture were analyzed by GC/FID using relative peak areas versus an internal standard (decane).

Kinetic Isotope Effect Experiments Using 1-TFA. A stock solution containing **1-TFA** (0.001 mol % relative to benzene) and a 1:1 molar mixture of C_6H_6 and C_6D_6 (50 mL) was prepared in a volumetric flask. Fisher-Porter reactors were charged with stock solution (10 mL) and $Cu(OAc)_2$ (200 equiv. relative to **1-TFA**). The vessels were sealed, charged with ethylene (50 psig), and subsequently stirred and heated to 150 °C. The reaction was sampled at 1, 2, and 4 h. At each time point, the reactors were cooled to room temperature, sampled, recharged with ethylene, and reheated. Aliquots of the reaction mixture were analyzed by GC/MS. KIE was determined by examining the ratio of styrene ($m/z = 104$) to styrene- d_5 ($m/z = 109$) in the mass spectrum, accounting for the initial isotopic distribution and natural abundance. No change in the isotopic distribution for benzene was observed over the course of the reaction, and the observed isotopic distribution of product was consistent with the initial distribution. No d_{6-8} products were observed, except those predicted by the natural abundance of deuterium in ethylene.

Photographs of Reactors Over the Course of the Reaction:



Reaction of 1-TFA with Ethylbenzene. A stock solution containing **1-TFA** (0.112 mM), decane (10 equiv. relative to **1-TFA**), and ethylbenzene (50 mL) was prepared in a volumetric flask. Fisher-Porter reactors were charged with stock solution (20 mL) and copper acetate (13.4 mM). The vessels were sealed, pressurized with ethylene (50 psig), and stirred while heated to 150 °C. The reactions were sampled at 4, 8, 12, and 24 h. At each time point the reactors were cooled to room temperature, sampled, recharged with ethylene, and reheated. Aliquots of the reaction mixture were analyzed by GC/MS, and products were identified using through a search of the NIST mass spectral database.

Attempted Oxidative Hydrophenylation of Ethylene using Washed Materials Recovered from Catalysis with 1-TFA and Cu(OAc)₂. Two duplicate catalytic reactions with **1-TFA** were run to completion. The resulting mixtures were combined and dried *in vacuo*. The solid was sonicated in 1,4-dioxane for 30 minutes, after which the

solution was decanted leaving only insoluble materials, which were dried *in vacuo*. Two Fisher-Porter reactors were each charged with half of the recovered material, decane (4 uL, 0.022 mmol), benzene (20 mL), and Cu(OAc)₂ (49 mg, 0.27 mmol). The vessels were sealed, pressurized with ethylene (50 psig), and stirred while heated to 150 °C. The reactions were sampled at 4 h and 24 h. At each time point the reactors were cooled to room temperature, sampled, recharged with ethylene, and reheated. Aliquots of the reaction mixture were analyzed by GC/FID using relative peak area vs. an internal standard (decane). No styrene was observed after 24 h of heating.

Oxidative Hydrophenylation of Ethylene using 1-OAc. A representative catalytic reaction is described. A stock solution containing **1-OAc** (3.4 mg, 0.0056 mmol), decane (11 uL, 0.056 mmol), and benzene (50 mL) was prepared in a volumetric flask. Fisher-Porter reactors were charged with stock solution (20 mL) and Cu(OAc)₂ (49 mg, 0.27 mmol). The vessels were sealed, pressurized with ethylene (25 psig), and stirred while heated to 150 °C. The reactions were sampled every hour until complete. At each time point the reactors were cooled to room temperature, sampled, recharged with ethylene, and reheated. Aliquots of the reaction mixture were analyzed by GC/FID using relative peak area vs. an internal standard (decane).

Oxidative Hydrophenylation of Ethylene as a Function of [C₂H₄]. A stock solution containing **1-OAc** (0.112 mM), decane (10 equiv. relative to **1-OAc**), and benzene (250 mL) was prepared in a volumetric flask. Fisher-Porter reactors (2 reactors per concentration level) were charged with stock solution (20 mL) and copper pivalate (13.4 mM). The vessels were sealed, pressurized with ethylene (35 psig, 50 psig, 75 psig, or 100 psig), and stirred while heated to 150 °C. The reactions were sampled every 30

minutes until complete. At each time point the reactors were cooled to room temperature, sampled, recharged with ethylene, and reheated. Aliquots of the reaction mixture were analyzed by GC/FID using relative peak area vs. an internal standard (decane).

Oxidative Hydrophenylation of Ethylene as a Function of [Cu(OPiv)₂]. A stock solution containing **1-OAc** (0.112 mM), decane (10 equiv. relative to **1-OAc**), and benzene (250 mL) was prepared in a volumetric flask. Fisher-Porter reactors (2 reactors per concentration level) were charged with stock solution (20 mL) and copper pivalate (13.4 mM, 19.0 mM, 26.9 mM, 38.1 mM, or 53.8 mM). The vessels were sealed, pressurized with ethylene (50 psig), and stirred while heated to 150 °C. The reactions were sampled every 30 minutes until complete. At each time point the reactors were cooled to room temperature, sampled, recharged with ethylene, and reheated. Aliquots of the reaction mixture were analyzed by GC/FID using relative peak area vs. an internal standard (decane).

Oxidative Hydrophenylation of Ethylene as a Function of [1-OAc]. Five separate stock solutions were prepared in 50 mL volumetric flasks, each containing **1-OAc** (0.225 mM, 0.168 mM, 0.112 mM, 0.079 mM, or 0.056 mM), decane (10 equiv. relative to **1-OAc**), and benzene (50 mL). Fisher-Porter reactors (2 reactors per concentration level) were charged with stock solution (20 mL) and copper pivalate (26.9 mM). The vessels were sealed, pressurized with ethylene (50 psig), and stirred while heated to 150 °C. The reactions were sampled every 30 minutes until complete. At each time point the reactors were cooled to room temperature, sampled, recharged with ethylene, and reheated. Aliquots of the reaction mixture were analyzed by GC/FID using relative peak area vs. an internal standard (decane).

Dependence of order in [1-OAc] on [C₂H₄]. Three separate stock solutions were prepared in 50 mL volumetric flasks, each containing **1-OAc** (0.225 mM, 0.112 mM, or 0.056 mM), decane (10 equiv. relative to **1-OAc**), and benzene (50 mL). Fisher-Porter reactors (6 reactors per concentration of Rh) were charged with stock solution (20 mL) and copper pivalate (26.9 mM). The vessels were sealed, pressurized with ethylene (35 psig, 50 psig, or 75 psig; 2 reactors per pressure at each Rh concentration), and stirred while heated to 150 °C. The reactions were sampled every 30 minutes until complete. At each time point the reactors were cooled to room temperature, sampled, recharged with ethylene, and reheated. Aliquots of the reaction mixture were analyzed by GC/FID using relative peak area vs. an internal standard (decane).

Dependence of order in [1-OAc] on Temperature. Three separate stock solutions were prepared in 50 mL volumetric flasks, each containing **1-OAc** (0.225 mM, 0.112 mM, or 0.056 mM), decane (10 equiv. relative to **1-OAc**), and benzene (50 mL). Fisher-Porter reactors (6 reactors per concentration of Rh) were charged with stock solution (20 mL) and copper pivalate (26.9 mM). The vessels were sealed, pressurized with ethylene (to keep the concentration of ethylene dissolved in solution constant across all temperatures, different pressures were used, all of which correspond to 114 mM C₂H₄: 30 psig for 130 °C reactions, 50 psig for 150 °C reactions, or 60 psig for 160 °C reactions; 2 reactors per pressure at each Rh concentration), and stirred while heated to 130 °C, 150 °C, or 160 °C. The reactions were sampled every 30 minutes until complete. At each time point the reactors were cooled to room temperature, sampled, recharged with ethylene, and reheated. Aliquots of the reaction mixture were analyzed by GC/FID using relative peak area vs. an internal standard (decane).

H/D Exchange Experiments- 1:1 ratio of C₆H₆ to C₆H₆. A stock solution containing **1-OAc** (0.112 mM), Cu(OPiv)₂ (13.4 mM), and a 1:1 molar mixture of C₆H₆ and C₆D₆ (25 mL) was prepared in a volumetric flask. PTFE-valved reaction tubes were charged with stock solution (10 mL), sealed, and heated to 150 °C. The reactions were sampled at 4 h and 24 h. At each time point the reactors were cooled to room temperature, sampled, and reheated. Aliquots of the reaction mixture were analyzed by GC/MS. The isotopic distribution of benzene-*d_n* (n = 0 – 6) was measured for the initial stock solution and at each time point.

H/D Exchange Experiments- 500 equiv. CD₃COOD. A stock solution containing **1-OAc** (0.112 mM), Cu(OPiv)₂ (13.4 mM), CD₃COOD (56 mM), and C₆H₆ (25 mL) was prepared in a volumetric flask. PTFE-valved reaction tubes were charged with stock solution (10 mL), sealed, and heated to 150 °C. The reactions were sampled at 4 h and 24 h. At each time point the reactors were cooled to room temperature, sampled, and reheated. Aliquots of the reaction mixture were analyzed by GC/MS. The isotopic distribution of benzene-*d_n* (n = 0 – 6) was measured for the initial stock solution and at each time point.

H/D Exchange Experiments- 500 equiv. CD₃COOD with Added Ethylene. A stock solution containing **1-OAc** (0.112 mM) and C₆H₆ (25 mL) was prepared in a volumetric flask. Fisher-Porter reactors were charged with stock solution (10 mL), copper pivalate (13.4 mM), and CD₃COOD (56 mM). The vessels were sealed, pressurized with ethylene (50 psig), and stirred while heated to 150 °C. The reactions were sampled at 4 h and 24 h. At each time point the reactors were cooled to room temperature, sampled, and reheated. Aliquots of the reaction mixture were analyzed by GC/MS. The isotopic

distribution of benzene- d_n ($n = 0 - 6$) was measured for the initial stock solution and at each time point. The isotopic distribution of styrene- d_n ($n = 0 - 8$) was also measured at each time point.

Kinetic Isotope Effect Experiments Using a 1:1 Molar Mixture of C_6H_6 and C_6D_6 . A stock solution containing **1-OAc** (0.112 mM) and a 1:1 molar mixture of C_6H_6 and C_6D_6 (50 mL) was prepared in a volumetric flask. Fisher-Porter reactors were charged with stock solution (10 mL) and copper pivalate (240 equiv. relative to **1-OAc**). The vessels were sealed, pressurized with ethylene (50 psig), and stirred while heated to 150 °C. The reactions were sampled at 30 min, 1 h, 2 h, and 3 h. At each time point the reactors were cooled to room temperature, sampled, recharged with ethylene, and reheated. Aliquots of the reaction mixture were analyzed by GC/MS. KIE was determined by examining the ratio of styrene ($m/z = 104$) to styrene- d_5 ($m/z = 109$) in the mass spectrum, accounting for the initial isotopic distribution and natural abundance. No change in the isotopic distribution for benzene was observed over the course of the reaction, and the observed isotopic distribution of product was consistent with the initial distribution. No d_{6-8} products were observed, except those predicted by the natural abundance of deuterium in ethylene.

Oxidative Hydrophenylation of Ethylene Using 1-OAc in C_6D_6 . A stock solution containing **1-OAc** (0.112 mM), decane (10 equiv. relative to **1-OAc**), and C_6D_6 (50 mL) was prepared in a volumetric flask. Fisher-Porter reactors were charged with stock solution (20 mL) and copper pivalate (26.9 mM). The vessels were sealed, pressurized with ethylene (50 psig), and stirred while heated to 150 °C. The reactions were sampled every 30 mins for 3 h. At each time point the reactors were cooled to room temperature,

sampled, recharged with ethylene, and reheated. Aliquots of the reaction mixture were analyzed by GC/FID using relative peak area vs. an internal standard (decane).

Oxidative Hydrophenylation of Ethylene Using *in situ* Generated (^{F1}DAB)RhCl₃(η^2 -C₂H₄). A stock solution containing RhCl₃ (0.112 mM), ^{F1}DAB (0.112 mM), decane (1.12 mM), and benzene (50 mL) was prepared in a volumetric flask. Fisher-Porter reactors were charged with stock solution (20 mL) and Cu(OPiv)₂ (27 mM). The vessels were sealed, pressurized with ethylene (50 psig), and stirred while heated to 150 °C. The reactions were sampled at 4 h and 24 h. At each time point the reactors were cooled to room temperature, sampled, recharged with ethylene, and reheated. Aliquots of the reaction mixture were analyzed by GC/FID using relative peak area vs. an internal standard (decane).

Oxidative Hydrophenylation of Ethylene Using 1-OAc at Pressures > 100 psig. A representative catalytic reaction is described. A stock solution containing 1-OAc (0.112 mM), decane (1.12 mM), and benzene (50 mL) was prepared in a volumetric flask. Stainless steel high pressure reactors equipped with glass liners were charged with stock solution (10 mL) and Cu(OPiv)₂ (27 mM). The vessels were sealed, pressurized with ethylene (400 psig), and stirred while heated to 150 °C. The reactions were sampled every hour until complete. At each time point the reactors were sampled at temperature using a narrow bore dip tube. Aliquots of the reaction mixture were analyzed by GC/FID using relative peak area vs. an internal standard (decane).

Oxidative Hydrophenylation of Ethylene Using 1-OAc with Added AcOH at Low Pressures < 100 psig. A representative catalytic reaction is described. A stock solution containing 1-OAc (0.112 mM), decane (1.12 mM), and benzene (50 mL) was

prepared in a volumetric flask. Fisher-Porter reactors were charged with stock solution (20 mL), AcOH (56 mM), and Cu(OPiv)₂ (27 mM). The vessels were sealed, pressurized with ethylene (50 psig), and stirred while heated to 150 °C. The reactions were sampled every 30 minutes until complete. At each time point the reactors were cooled to room temperature, sampled, recharged with ethylene, and reheated. Aliquots of the reaction mixture were analyzed by GC/FID using relative peak area vs. an internal standard (decane).

Oxidative Hydrophenylation of Ethylene Using 1-OAc with Added AcOH at High Pressures > 100 psig. A representative catalytic reaction is described. A stock solution containing 1-OAc (0.112 mM), decane (1.12 mM), and benzene (50 mL) was prepared in a volumetric flask. Stainless steel high pressure reactors equipped with glass liners were charged with stock solution (10 mL), AcOH (56 mM), and Cu(OPiv)₂ (27 mM). The vessels were sealed, pressurized with ethylene (400 psig), and stirred while heated to 150 °C. The reactions were sampled every 30 minutes until complete. At each time point the reactors were sampled at temperature using a narrow bore dip tube. Aliquots of the reaction mixture were analyzed by GC/FID using relative peak area vs. an internal standard (decane).

3.6 References

- (1) In *CRC Handbook of Chemistry and Physics* Weast, R. C., Ed.; CRC Press/Taylor & Francis: Boca Raton, FL, 1977.
- (2) McKeown, B. A.; Gonzalez, H. E.; Friedfeld, M. R.; Brosnahan, A. M.; Gunnoe, T. B.; Cundari, T. R.; Sabat, M. *Organometallics* **2013**, *32*, 2857.
- (3) Hong, P.; Yamazaki, H. *J. Mol. Catal.* **1984**, *26*, 297.

- (4) Taube, D.; Periana, R.; Matsumoto, T. 6127590A, 2000. (US Patent 6127590A)
- (5) Fujiwara, Y.; Noritani, I.; Danno, S.; Asano, R.; Teranishi, S. *J. Am. Chem. Soc.* **1969**, *91*, 7166.
- (6) Yamada, T.; Sakakura, A.; Sakaguchi, S.; Obora, Y.; Ishii, Y. *New J. Chem.* **2008**, *32*, 738.
- (7) Kubota, A.; Emmert, M. H.; Sanford, M. S. *Org. Lett.* **2012**, *14*, 1760.
- (8) Sasaki, K.; Sakakura, T.; Tokunaga, Y.; Wada, K.; Tanaka, M. *Chem. Lett.* **1988**, *17*, 685.
- (9) Milstein, D.; Weissmann, H.; Song, X.-P. 2004/0073075 A1, 2004. (US Patent 2004/0073075 A1)
- (10) *Chemical & Engineering News Archive* **1961**, *39*, 52.
- (11) W. In *Catalysis from A to Z*; Cornils, B., Herrmann, W. A., Muhler, M., Wong, C.-H., Eds.; Wiley: 2007, pp 1511.
- (12) Eckert, M.; Fleischmann, G.; Jira, R.; Bolt, H. M.; Golka, K. Acetaldehyde. In *Ullmann's Encyclopedia of Industrial Chemistry*; Wiley-VCH Verlag GmbH & Co. KGaA: 2000.
- (13) Vaughan, B. A.; Webster-Gardiner, M. S.; Cundari, T. R.; Gunnoe, T. B. *Science* **2015**, *348*, 421.
- (14) Vaughan, B. A.; Khani, S. K.; Gary, J. B.; Kammert, J. D.; Webster-Gardiner, M. S.; McKeown, B. A.; Davis, R. J.; Cundari, T. R.; Gunnoe, T. B. *J. Am. Chem. Soc.* **2017**, *139*, 1485.
- (15) Reprinted (adapted) with permission from (Vaughan, B. A.; Webster-Gardiner, M. S.; Cundari, T. R.; Gunnoe, T. B. *Science*, **2015**, *348*, 421.) Copyright 2015 AAAS.
- (16) Webster-Gardiner, M. S.; Fu, R.; Fortman, G. C.; Nielsen, R. J.; Gunnoe, T. B.; Goddard III, W. A. *Cat. Sci. Tech.* **2015**, *5*, 96.
- (17) Webster-Gardiner, M. S.; Chen, J., Unpublished Work.
- (18) Foley, N. A.; Lee, J. P.; Ke, Z.; Gunnoe, T. B.; Cundari, T. R. *Acc. Chem. Res.* **2009**, *42*, 585.
- (19) McKeown, B. A.; Gonzalez, H. E.; Friedfeld, M. R.; Gunnoe, T. B.; Cundari, T. R.; Sabat, M. *J. Am. Chem. Soc.* **2011**, *133*, 19131.

- (20) Gómez-Gallego, M.; Sierra, M. A. *Chem. Rev.* **2011**, *111*, 4857.
- (21) Jones, W. D. *Acc. Chem. Res.* **2003**, *36*, 140.
- (22) Reprinted (adapted) with permission from (Vaughan, B. A.; Khani, S. K.; Gary, J. B.; Kammert, J. D.; Webster-Gardiner, M. S.; McKeown, B. A.; Davis, R. J.; Cundari, T. R.; Gunnoe, T. B. *J. Am. Chem. Soc.*, **2017**, *139*, 1485.) Copyright 2017 American Chemical Society.
- (23) Webb, J. R.; Pierpont, A. W.; Munro-Leighton, C.; Gunnoe, T. B.; Cundari, T. R.; Boyle, P. D. *J. Am. Chem. Soc.* **2010**, *132*, 4520.
- (24) Widegren, J. A.; Bennett, M. A.; Finke, R. G. *J. Am. Chem. Soc.* **2003**, *125*, 10301.
- (25) Finney, E. E.; Finke, R. G. *Inorg. Chim. Acta* **2006**, *359*, 2879.
- (26) Widegren, J. A.; Finke, R. G. *J. Mol. Catal. A* **2003**, *198*, 317.
- (27) Hamlin, J. E.; Hirai, K.; Gibson, V. C.; Maitlis, P. M. *J. Mol. Catal.* **1982**, *15*, 337.
- (28) Gorelsky, S. I.; Lapointe, D.; Fagnou, K. *J. Am. Chem. Soc.* **2008**, *130*, 10848.
- (29) Sperger, T.; Sanhueza, I. A.; Kalvet, I.; Schoenebeck, F. *Chem. Rev.* **2015**, *115*, 9532.
- (30) Balcells, D.; Clot, E.; Eisenstein, O. *Chem. Rev.* **2010**, *110*, 749.
- (31) Ackermann, L. *Acc. Chem. Res.* **2014**, *47*, 281.
- (32) Boutadla, Y.; Davies, D. L.; Macgregor, S. A.; Poblador-Bahamonde, A. I. *Dalton Trans.* **2009**, 5820.
- (33) Webb, J. R.; Burgess, S. A.; Cundari, T. R.; Gunnoe, T. B. *Dalton Trans.* **2013**, *42*, 16646.
- (34) Gunnoe, T. B. *Eur. J. Inorg. Chem.* **2007**, *2007*, 1185.
- (35) McKeown, B. A.; Prince, B. M.; Ramiro, Z.; Gunnoe, T. B.; Cundari, T. R. *ACS Catal.* **2014**, *4*, 1607.
- (36) Shiotsuki, M.; White, P. S.; Brookhart, M.; Templeton, J. L. *J. Am. Chem. Soc.* **2007**, *129*, 4058.
- (37) McKeown, B. A.; Foley, N. A.; Lee, J. P.; Gunnoe, T. B. *Organometallics* **2008**, *27*, 4031.

- (38) McKeown, B. A.; Gonzalez, H. E.; Michaelos, T.; Gunnoe, T. B.; Cundari, T. R.; Crabtree, R. H.; Sabat, M. *Organometallics* **2013**, *32*, 3903.
- (39) McKeown, B. A.; Gonzalez, H. E.; Gunnoe, T. B.; Cundari, T. R.; Sabat, M. *ACS Catal.* **2013**, *3*, 1165.
- (40) Lail, M.; Bell, C. M.; Conner, D.; Cundari, T. R.; Gunnoe, T. B.; Petersen, J. L. *Organometallics* **2004**, *23*, 5007.
- (41) Oxgaard, J.; Periana, R. A.; Goddard, W. A. *J. Am. Chem. Soc.* **2004**, *126*, 11658.
- (42) Holder, G. A.; Macauley, D. *J. Chem. Eng. Data* **1992**, *37*, 100.
- (43) Bhalla, G.; Bischof, S. M.; Ganesh, S. K.; Liu, X. Y.; Jones, C. J.; Borzenko, A.; Tenn, I. I. I. W. J.; Ess, D. H.; Hashiguchi, B. G.; Lokare, K. S.; Leung, C. H.; Oxgaard, J.; Goddard, I. I. I. W. A.; Periana, R. A. *Green Chem.* **2011**, *13*, 69.
- (44) Baxter, R. D.; Sale, D.; Engle, K. M.; Yu, J.-Q.; Blackmond, D. G. *J. Am. Chem. Soc.* **2012**, *134*, 4600.
- (45) Northcutt, T. O.; Wick, D. D.; Vetter, A. J.; Jones, W. D. *J. Am. Chem. Soc.* **2001**, *123*, 7257.
- (46) Vetter, A. J.; Flaschenriem, C.; Jones, W. D. *J. Am. Chem. Soc.* **2005**, *127*, 12315.
- (47) Zheng, L.; Wang, J. *Chem. Eur. J.* **2012**, *18*, 9699.
- (48) King, E. L.; Altman, C. *J. Phys. Chem.* **1956**, *60*, 1375.
- (49) Ackermann, L. *Chem. Rev.* **2011**, *111*, 1315.
- (50) Cannon, J. S.; Zou, L.; Liu, P.; Lan, Y.; O'Leary, D. J.; Houk, K. N.; Grubbs, R. H. *J. Am. Chem. Soc.* **2014**, *136*, 6733.
- (51) Cramer, R. *Inorg. Synth.* **1990**, *28*, 86.
- (52) Bianchi, F.; Gallazzi, M. C.; Porri, L.; Diversi, P. *J. Organomet. Chem.* **1980**, *202*, 99.
- (53) Khusniyarov, M. M.; Harms, K.; Burghaus, O.; Sundermeyer, J. *Eur. J. Inorg. Chem.* **2006**, *2006*, 2985.
- (54) Werner, H.; Poelsma, S.; Schneider, M. E.; Windmüller, B.; Barth, D. *Chem. Ber.* **1996**, *129*, 647.
- (55) Xie, L.-H.; Suh, M. P. *Chem. Eur. J.* **2011**, *17*, 13653.

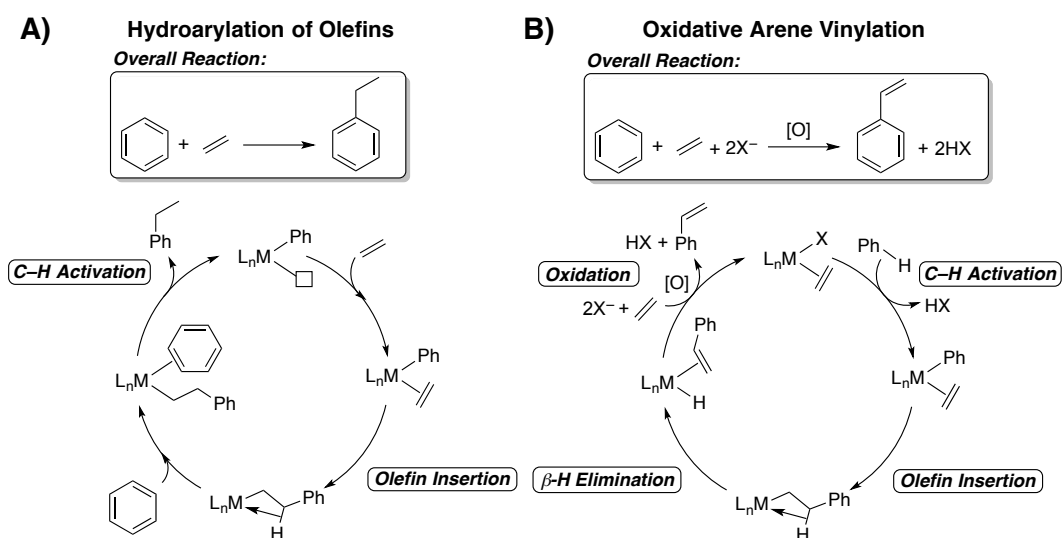
- (56) Frisch, M. J.; Trucks, G. W.; Schlegel, H. B.; Scuseria, G. E.; Robb, M. A.; Cheeseman, J. R.; Scalmani, G.; Barone, V.; Mennucci, B.; Petersson, G. A.; Nakatsuji, H.; Caricato, M.; Li, X.; Hratchian, H. P.; Izmaylov, A. F.; Bloino, J.; Zheng, G.; Sonnenberg, J. L.; Hada, M.; Ehara, M.; Toyota, K.; Fukuda, R.; Hasegawa, J.; Ishida, M.; Nakajima, T.; Honda, Y.; Kitao, O.; Nakai, H.; Vreven, T.; Montgomery Jr., J. A.; Peralta, J. E.; Ogliaro, F.; Bearpark, M. J.; Heyd, J.; Brothers, E. N.; Kudin, K. N.; Staroverov, V. N.; Kobayashi, R.; Normand, J.; Raghavachari, K.; Rendell, A. P.; Burant, J. C.; Iyengar, S. S.; Tomasi, J.; Cossi, M.; Rega, N.; Millam, N. J.; Klene, M.; Knox, J. E.; Cross, J. B.; Bakken, V.; Adamo, C.; Jaramillo, J.; Gomperts, R.; Stratmann, R. E.; Yazyev, O.; Austin, A. J.; Cammi, R.; Pomelli, C.; Ochterski, J. W.; Martin, R. L.; Morokuma, K.; Zakrzewski, V. G.; Voth, G. A.; Salvador, P.; Dannenberg, J. J.; Dapprich, S.; Daniels, A. D.; Farkas, Ö.; Foresman, J. B.; Ortiz, J. V.; Cioslowski, J.; Fox, D. J. *Gaussian 09*; Gaussian, Inc.: Wallingford, CT, USA, **2009**.
- (57) Becke, A. D. *Phys. Rev. A* **1988**, *38*, 3098.
- (58) Lee, C.; Yang, W.; Parr, R. G. *Phys. Rev. B* **1988**, *37*, 785.
- (59) Grimme, S.; Ehrlich, S.; Goerigk, L. *J. Comput. Chem.* **2011**, *32*, 1456.
- (60) Marenich, A. V.; Cramer, C. J.; Truhlar, D. G. *J. Phys. Chem. B* **2009**, *113*, 6378.
- (61) Zhao, Y.; Truhlar, D. G. *Theor. Chem. Acc.* **2008**, *120*, 215.

4. Advances in Catalyst Development for the Direct Synthesis of Alkyl and Alkenyl Arenes: Mechanistic Insights and Future Outlook

4.1 Overview

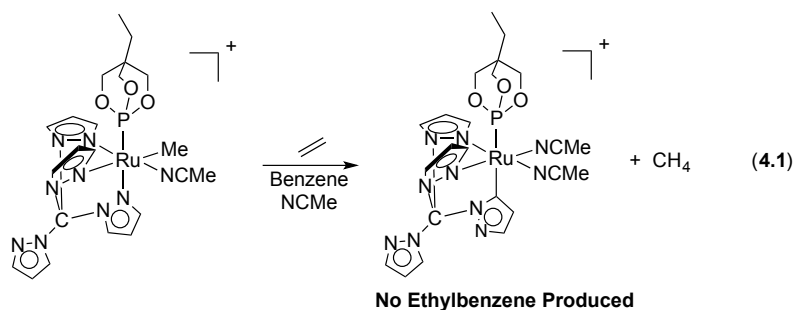
An alternative to traditional acid-based arene alkylation is a transition metal-mediated process that operates through aromatic C–H activation and olefin insertion into a metal–aryl bond (Scheme 4.1A). If this step is followed by β -hydride elimination, vinyl arenes can be produced through oxidative arene vinylation (Scheme 4.1B). Our group has studied these types of transition metal catalysts for the production of both alkyl and vinyl arenes for the past 18 years.¹⁻¹⁹ Over the course of our work, we have developed an understanding of the steric and electronic requirements to tune the activity and selectivity of these catalysts. An overview of the work in this area is presented below, followed by mechanistic comparisons and insights into future catalyst design.

Scheme 4.1. General Catalytic Cycles for A) Hydroarylation of Olefins, and B) Oxidative Arene Vinylation.



4.2 Ruthenium(II) Catalysts

Given our previous work with TpRu complexes, which showed that less electron-rich metal centers afforded higher TON and longevity (see Chapter 1), we sought to design more electron-poor Ru(II) complexes through substitution of the formally anionic Tp ligand with charge-neutral poly(pyrazolyl)alkane ligands, which would ultimately result in an overall cationic complex and therefore a less electron-rich metal center. The reaction of benzene and ethylene in the presence of $[(C(Pz)_4)Ru(P(OCH_2)_3CEt)(NCMe)(Me)][BAR^F_4]$ ($C(Pz)_4$ = tetra(pyrazolyl)methane; BAR^F_4 = tetrakis[3,5-bis(trifluoromethyl)phenyl]borate) afforded no ethylbenzene production, but instead resulted in the intramolecular C–H activation of the 5-position of one of the pyrazolyl rings and liberation of methane (Eq. 4.1).⁸



To combat this intramolecular reactivity, the complex $[(HC(Pz^5)_3)Ru(P(OCH_2)_3CEt)(NCMe)(Ph)][BAR^F_4]$ [$HC(Pz^5)_3$ = tris(5-methylpyrazolyl)methane; $(Pz^5)_3Ru$] was synthesized in which the 5-positions of the pyrazolyl rings were protected by methyl groups. Heating a solution of $(Pz^5)_3Ru$ in benzene to 90 °C with 15 psi C_2H_4 affords 565 TO of ethylbenzene after 131 h. This

represents approximately a 28-fold increase in TON compared to the Tp derivative, **TpRuBP**, which affords 20 TO of ethylbenzene before catalyst deactivation occurs at 24 h.² **(Pz⁵)₃Ru** is also more stable than its Tp congener, exhibiting catalytic activity at temperatures up to 150 °C. The Tp variant **TpRuBP** rapidly decomposes above 90 °C (Scheme 4.2).^{2,6,7}

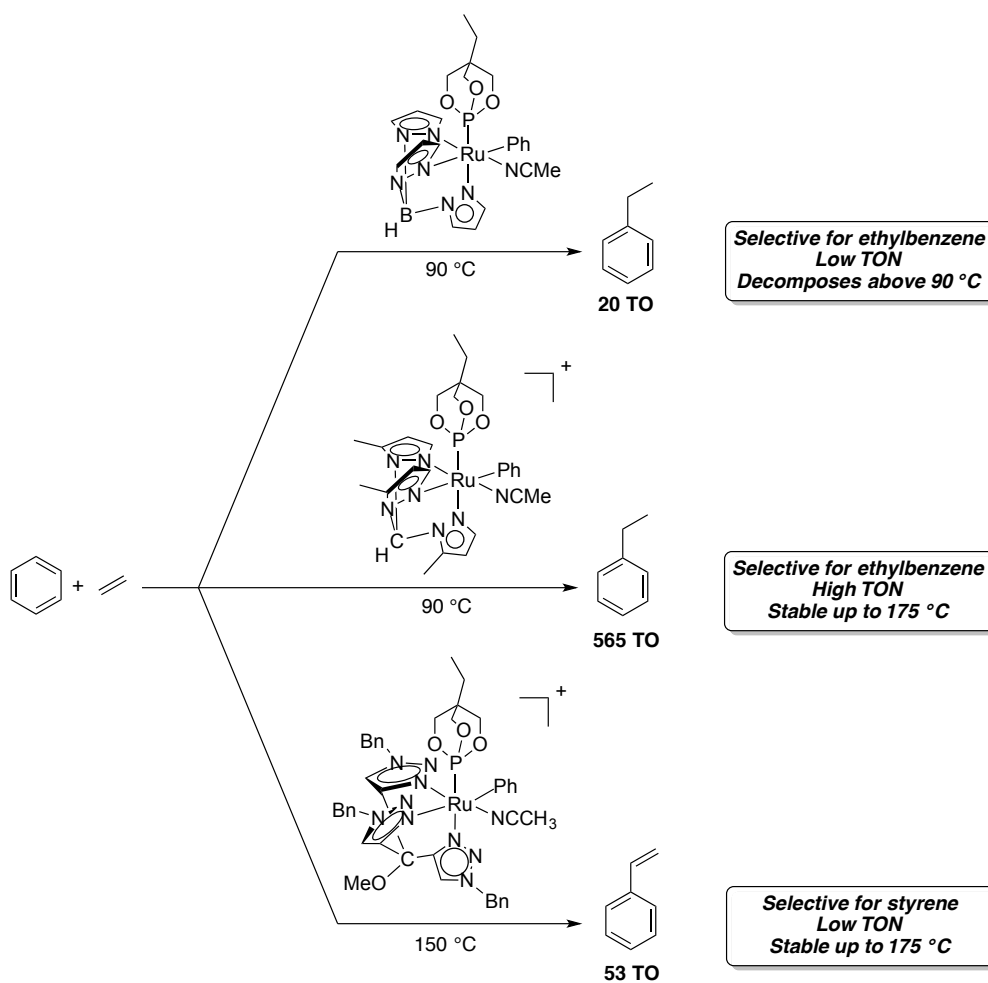
Given the promising results of catalytic olefin hydroarylation reactions using **(Pz⁵)₃Ru**, we sought to explore Ru complexes based on other tris(heterocyclic)alkane ligands. Tris(1,2,3-triazolyl)methanol ligands have been demonstrated to coordinate in a similar scorpionate κ^3 fashion to both Tp and tris(pyrazolyl)alkanes.²⁰⁻²² A benzene solution of [(BzTTM)Ru(BP)(NCMe)(Ph)]⁺ (BzTTM = tris(1-benzyl-1*H*-1,2,3-triazol-4-yl)methoxymethane, **BzTTMRu**) was heated to 150 °C with C₂H₄ to afford a mixture of ethylbenzene and styrene.²³

Surprisingly, catalysis with **BzTTMRu** is selective for styrene production over EtPh (*n.b.*, ethylene acts as the oxidant for this transformation and is reduced to ethane during the course of reaction, and addition of Cu(II) oxidants and O₂ did not increase yield). The highest yields are obtained at 40 psig of ethylene (53 TO of styrene), although the highest selectivity for styrene is afforded at 75 psig C₂H₄ (100% selectivity for styrene). Given the electronic similarity between **BzTTMRu** and **(Pz⁵)₃Ru** [Ru(III/II) potentials are within 0.04 V of one another], it is surprising that the selectivities for styrene vs. ethylbenzene are opposite (Scheme 4.2).²³

It was hypothesized that this difference in selectivity could be a result of the increased steric bulk of the benzyl substituents on the BzTTM ligand. As such, we synthesized the complex [(PhTTM)Ru(BP)(NCMe)(Ph)]⁺ (PhTTM = tris(1-phenyl-1*H*-

1,2,3-triazol-4-yl)methanol, **PhTTMRu**) and tested its activity as a catalyst for the hydrophenylation of ethylene. Catalytic reactions conducted over a range of temperatures (90 – 150 °C) and ethylene pressures (15 – 75 psig) showed that **PhTTMRu** was less selective for styrene formation than **BzTTMRu** under all conditions examined.²³

Scheme 4.2. Comparison of catalysis with **TpRuBP**, **(Pz⁵)₃Ru**, and **BzTTMRu**.



4.3 Platinum(II) Catalysts

Our group has reported that the cationic complex $[(^t\text{bpy})\text{Pt}(\text{Ph})(\text{THF})][\text{BAr}^{\text{F}}_4]$ (^tbpy = 4,4'-di-tert-butyl-2,2'-bipyridyl, BAr^{F}_4 = tetra(3,5-bis(trifluoromethyl)phenyl)borate, $^t\text{bpyPt}$) catalyzes the hydrophenylation of ethylene (see Chapter 1).¹¹ To study the effect of electronic modulation of the metal center on the selectivity of ethylene hydrophenylation reactions with $^t\text{bpyPt}$, we varied the 4,4' substituents on the bpy ligand. The complexes of the general form $[(^{\text{X}}\text{bpy})\text{Pt}(\text{Ph})(\text{THF})][\text{BAr}^{\text{F}}_4]$ ($^{\text{X}}\text{bpy}$ = 4,4'-(X)-2,2'-bipyridyl; X = OMe, $^{\text{MeO}}\text{bpyPt}$; H, bpyPt ; Br, $^{\text{Br}}\text{bpyPt}$; CO₂Et, $^{\text{CO}_2\text{Et}}\text{bpyPt}$; NO₂, $^{\text{NO}_2}\text{bpyPt}$) were synthesized and tested for catalytic activity in the hydrophenylation of ethylene.¹² As the donor ability of the bpy ligand decreased, the selectivity shifted dramatically to favor the production of styrene over ethylbenzene. Figure 4.1 shows a plot of Hammett σ_p vs. ethylbenzene to styrene ratio which shows the switch in selectivity to favor styrene with more electron-withdrawing ligands. Unfortunately, for these Pt(II) complexes, the pathway to form styrene results in catalyst deactivation which is likely a result of the formation of unstable Pt–H species, so while catalysis with $^{\text{NO}_2}\text{bpyPt}$ is selective for styrene formation, catalyst deactivation is observed after ~1 TO of styrene is produced.¹²

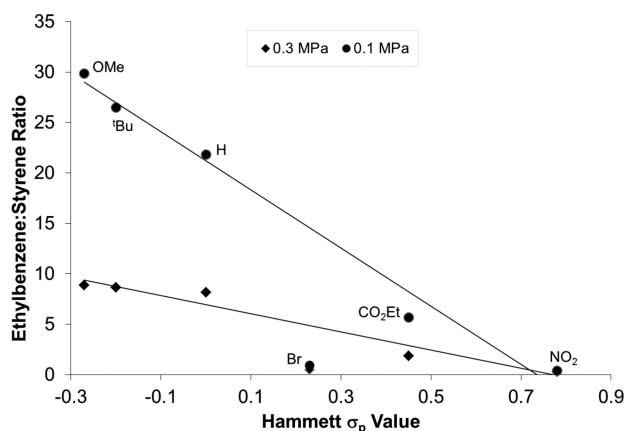


Figure 4.1. Plot of Hammett σ_p vs. Ethylbenzene:Styrene ratio for ethylene hydrophenylation using $[(^X\text{bpy})\text{Pt}(\text{Ph})(\text{THF})][\text{BAr}^{\text{F}}_4]$. Reprinted (adapted) with permission from reference¹². Copyright 2013 American Chemical Society.

The $[(^X\text{bpy})\text{Pt}(\text{Ph})]^+$ series of catalysts were also tested for the hydrophenylation of propylene.¹⁶ All complexes in this series catalyze the formation of alkyl arene products, and all favor the branched (Markovnikov) product, in this case cumene. A trend based on ligand donor ability was also observed with this chemistry, with ratios of linear to branched products increasing with ligand donor ability (Figure 4.2). For the complex with the most donating ligand in the series, $^{\text{MeO}}\text{bpyPt}$, a 1:3 ratio of *n*-propyl benzene to cumene was observed after 4 h. In contrast, the complex with the least donating ligand in the series, $^{\text{NO}_2}\text{bpyPt}$, afforded even higher selectivity for branched product (1:4.6).¹⁶

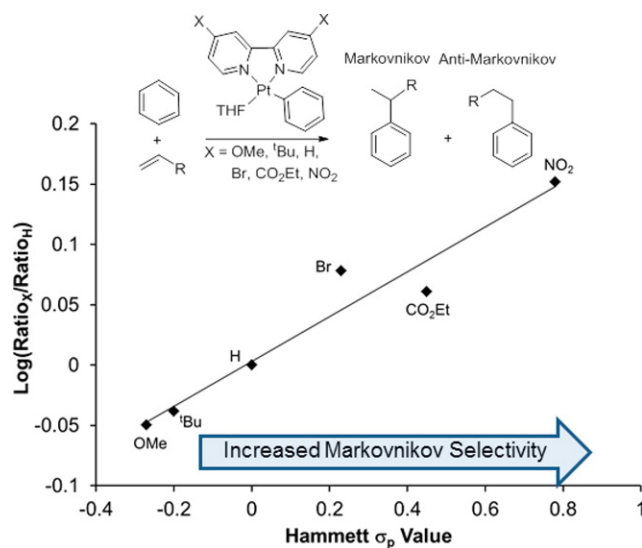


Figure 4.2. Hammett plot for propylene hydrophenylation using $[(^X\text{bpy})\text{Pt}(\text{Ph})(\text{THF})][\text{BAr}^{\text{F}}_4]$. Reprinted (adapted) with permission from reference¹⁶. Copyright 2014 American Chemical Society.

To examine the effect of chelate ring size on catalysis with Pt(II), the complex $[(\text{dpm})\text{Pt}(\text{Ph})]^+$ (dpm = 2,2'-dipyridylmethane, **dpmPt**) was prepared.¹⁴ Given that Puddephat and coworkers had previously shown that the electron donor abilities of ^tbpy and dpm ligands on Pt(II) complexes are nearly identical,²⁴ it was anticipated that this substitution would provide a direct way to measure the effect of chelate ring size (ring size of the ligated metallacycle) without changing the electronics of the metal center. **dpmPt** was found to be an effective catalyst for the hydrophenylation of ethylene, affording a TON of 469 after 110 h at 100 °C (Figure 4.3). The expansion of chelate ring size also afforded higher catalyst activity (TOF = $4.6 \times 10^{-3} \text{ s}^{-1}$ for **dpmPt** compared to TOF = $1.3 \times 10^{-3} \text{ s}^{-1}$ for ^t**bpyPt**) and longevity (**dpmPt** is active up to 110 h, where complete deactivation is observed for ^t**bpyPt** after 24 h) compared to ^t**bpyPt** under certain conditions.¹⁴

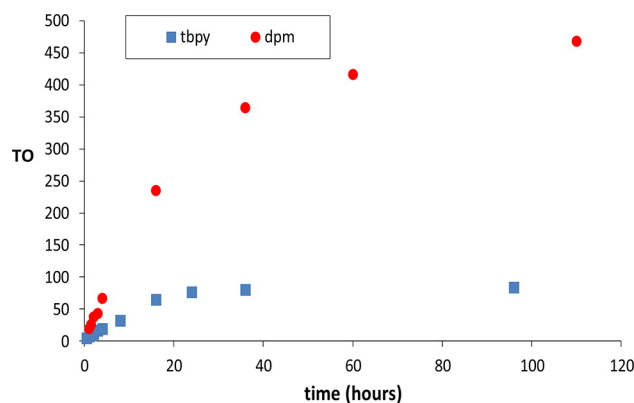


Figure 4.3. Plot of ethylbenzene TO vs. time for catalysis with **tbpyPt** and **dpmPt**. Reprinted (adapted) with permission from reference¹⁴. Copyright 2013 American Chemical Society.

4.4 Rhodium(I) Catalysts

The direct and single-step conversion of benzene, ethylene, and a Cu(II) oxidant to styrene using the Rh(I) catalyst $(^{\text{Fl}}\text{DAB})\text{Rh}(\text{TFA})(\eta^2\text{-C}_2\text{H}_4)$ [$^{\text{Fl}}\text{DAB}$ = N,N'-bis(pentafluorophenyl)-2,3-dimethyl-1,4-diaza-1,3-butadiene; TFA = trifluoroacetate; $^{\text{Fl}}\text{DABRhTFA}$] has been reported to give quantitative yields (with Cu(II) as the limiting reagent) and selectivity combined with turnover numbers > 800 (see Chapter 3).¹⁸ Examining catalysis with the complex $(^{\text{Fl}}\text{DAB})\text{Rh}(\text{OAc})(\eta^2\text{-C}_2\text{H}_4)$ [$^{\text{Fl}}\text{DABRhOAc}$] shows that the reaction rate has a dependence on catalyst concentration between first- and half-order that varies with both temperature and ethylene concentration, a first-order dependence on ethylene concentration with saturation at higher concentrations of ethylene, and a zero-order dependence on the concentration of Cu(II) oxidant. The kinetic isotope effect was found to vary linearly with the order in $^{\text{Fl}}\text{DABRhOAc}$, exhibiting

minimal KIE when [Rh] was in the half-order regime, and a k_H/k_D value of 6.7(6) when [Rh] was in the first-order regime.¹⁷

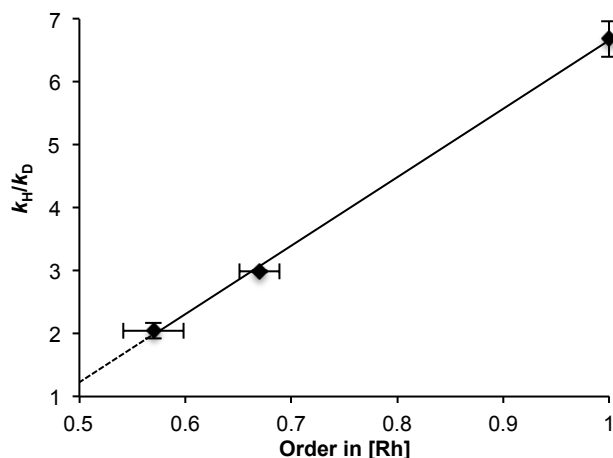
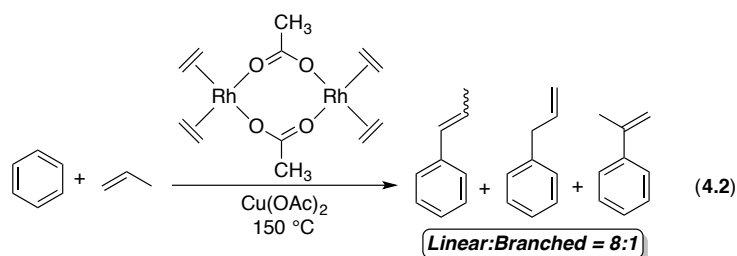


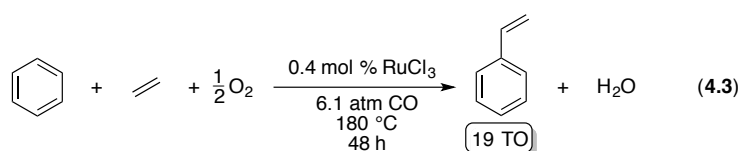
Figure 4.4. Plot of KIE vs. order in Rh for oxidative arene vinylation using $\text{F}^1\text{DABRhOAc}$. Reprinted (adapted) with permission from reference¹⁷. Copyright 2017 American Chemical Society.

We have also demonstrated that the simple Rh salt, $[\text{Rh}(\mu\text{-OAc})(\eta^2\text{-C}_2\text{H}_4)_2]_2$ ($[\text{RhOAc}]_2$) can catalyze oxidative arene vinylation with α -olefins (eq. 4.2).²⁵ This complex represents the most selective catalyst reported to date for the production of “super” linear alkenyl arenes (1-aryl alkenes), with linear to branched ratios up to 10:1. $[\text{RhOAc}]_2$ is also long-lived and high yielding, as TONs in excess of 1470 and stability up to 72 h have been demonstrated for arene alkenylation reactions with propylene.²⁵ Catalysis with $[\text{RhOAc}]_2$ is also tolerant of both electron-donating and electron-withdrawing substituents on the arene, unlike traditional Friedel-Crafts catalysis.²⁵



4.5 Aerobic Arene Vinylation

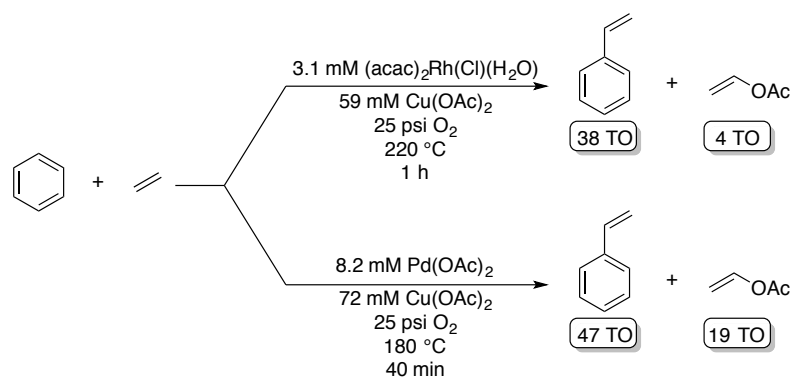
Given that O₂ from air is the cheapest form of oxidant available, the development of catalysts for oxidative arene vinylation that could tolerate the use of O₂ as an oxidant or in tandem with another oxidant would be beneficial. A few examples of aerobic arene vinylation catalysts have been reported by Milstein, Periana, and our group. In 2001, Milstein and coworkers reported the conversion of benzene and ethylene to styrene catalyzed by RuCl₃ · 3H₂O using O₂ as an oxidant (eq. 4.3).²⁶ While this chemistry uses O₂ directly as the oxidant, the TONs and yields are low, though they increase with the use of Michael acceptors and functionalized arenes.²⁶



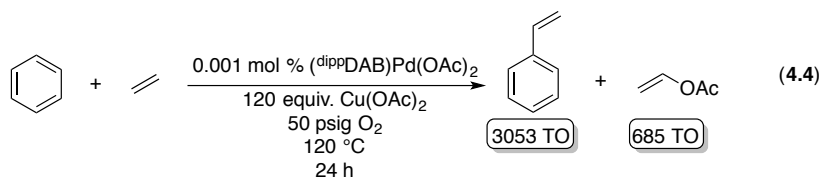
Periana and coworkers have reported both Rh(III)- and Pd(II)-catalyzed styrene production using Cu(II) oxidants that can, in theory, be regenerated *in situ* by O₂.²⁷ While these catalysts are highly active (TOFs on the order of 10⁻² s⁻¹), the overall TONs are low (Scheme 4.3). Indeed, none of the reactions reported represents more than 100%

yield relative to Cu(II), indicating either that the Cu is decomposing or that it is not being aerobically recycled by the O₂ in the reaction. Additionally, vinyl acetate is produced as a byproduct in all reported reactions, with some conditions even producing it as the major product.²⁷

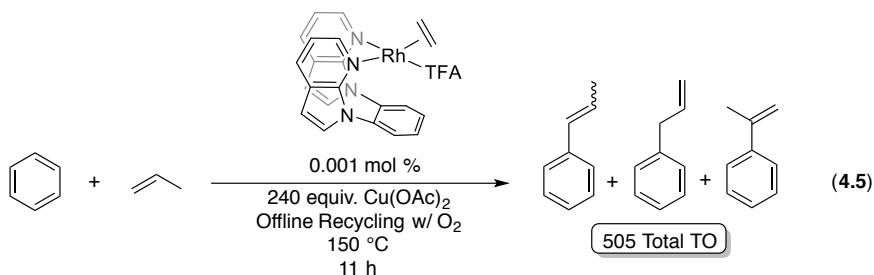
Scheme 4.3. Comparison of oxidative benzene vinylation using (acac)₂Rh(Cl)(H₂O) and Pd(OAc)₂.



Our group has studied the development of Pd(II) catalysts for aerobic arene vinylation (see chapter 2). Oxidative benzene vinylation reactions under aerobic conditions afforded > 3000 TO of styrene after 24 h (eq. 4.4). The TONs for these reactions are ~50 times the maximum theoretical yield based on Cu, which indicates that the Cu is being successfully recycled. Unfortunately, similarly to Periana's chemistry, catalysis with our Pd(II) complexes also results in significant production of vinyl acetate (~20% of the total product mixture).



Our group has also studied aerobic benzene vinylation using Rh(I) complexes bearing bis(quinoliny)benzene ligands, which introduce steric bulk in the axial position of the metal center. These complexes do not catalyze styrene production in the presence of O₂, but do not decompose under aerobic conditions, which allows for the use of Cu(II) oxidants that can be recycled offline without decomposing the Rh catalysts (eq. 4.5).²⁸



4.6 Comparison of Mechanisms

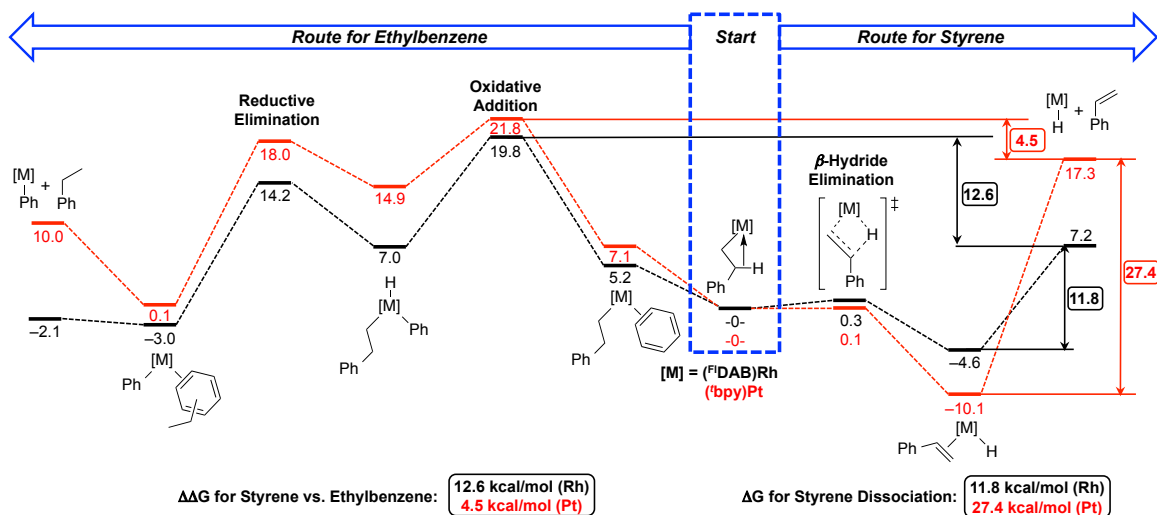
4.6.1 Selectivity for Styrene or Ethylbenzene

The fundamental mechanisms for both olefin hydroarylation and oxidative arene vinylation begin with the same two fundamental steps, arene C–H activation and olefin insertion. For oxidative arene vinylation these steps are followed by β -hydride elimination and reaction with oxidant to liberate the vinyl arene product. However, the common steps in both mechanisms allow for a comparative study of the two divergent

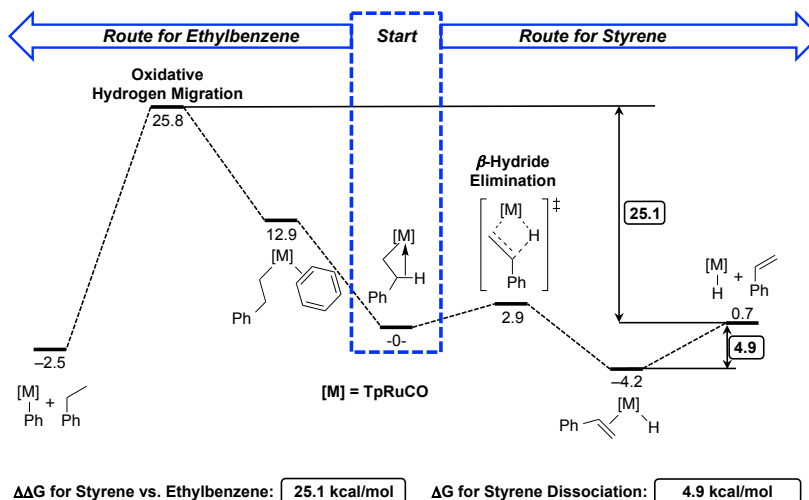
pathways that can provide insight into why catalysis with Rh is selective for styrene formation, whereas Ru and Pt both favor the production of ethylbenzene.

To better understand this change in selectivity, the two divergent pathways for ethylbenzene and styrene formation catalyzed by **TpRuCO**, **'bpyPt**, and **^{F1}DABRhOAc** were computationally modeled by the Cundari group (Scheme 4.4 and Scheme 4.5). To provide an accurate comparison, the energy values for **'bpyPt** have been recalculated using the same basis set, functionals, temperature, and dispersion corrections as were used for the Rh complexes presented herein. The energy values for **TpRuCO** have not been recalculated, and are therefore presented in a separate scheme to avoid confusion. Starting from a M-CH₂CH₂Ph intermediate, benzene coordination and subsequent C-H activation results in ethylbenzene formation, whereas β -hydride elimination results in styrene formation. For **'bpyPt** and **^{F1}DABRhOAc**, the C-H activation proceeds through oxidative addition and reductive elimination to give M(Ph)(η^2 -EtPh) which subsequently dissociates, while for **TpRuCO** it occurs through oxidative hydrogen migration to lead directly to the Ru-Ph complex and free ethylbenzene.

Scheme 4.4. Calculated Gibbs Free Energies for β -Hydride Elimination to Form Styrene and Benzene C–H Activation to Form Ethylbenzene from $(^{\text{Fl}}\text{DAB})\text{Rh}(\text{CH}_2\text{CH}_2\text{Ph})$ [shown in black] and $(^{\text{bpy}}\text{Pt})(\text{CH}_2\text{CH}_2\text{Ph})$ [shown in red] in kcal/mol with the Important Energy Differences Between the Two Pathways Highlighted.



Scheme 4.5. Calculated Gibbs Free Energies for β -Hydride Elimination to Form Styrene and Benzene C–H Activation to Form Ethylbenzene from $\text{TpRu}(\text{CO})(\text{CH}_2\text{CH}_2\text{Ph})$ in kcal/mol with the Important Energy Differences Between the Two Pathways Highlighted.



For **'bpyPt**, the difference between the two pathways is relatively small (4.5 kcal/mol), indicating that they could be competitive under certain conditions. For **^{F1}DABRh**, the energy difference is 12.6 kcal/mol, which predicts a greater predilection for styrene formation using **^{F1}DABRh** compared to **'bpyPt**. For **TpRuCO**, the energy difference between the two pathways is large (25.1 kcal/mol), which appears to indicate that styrene formation should be much more favorable than ethylbenzene formation, contrary to experimental observations.⁶

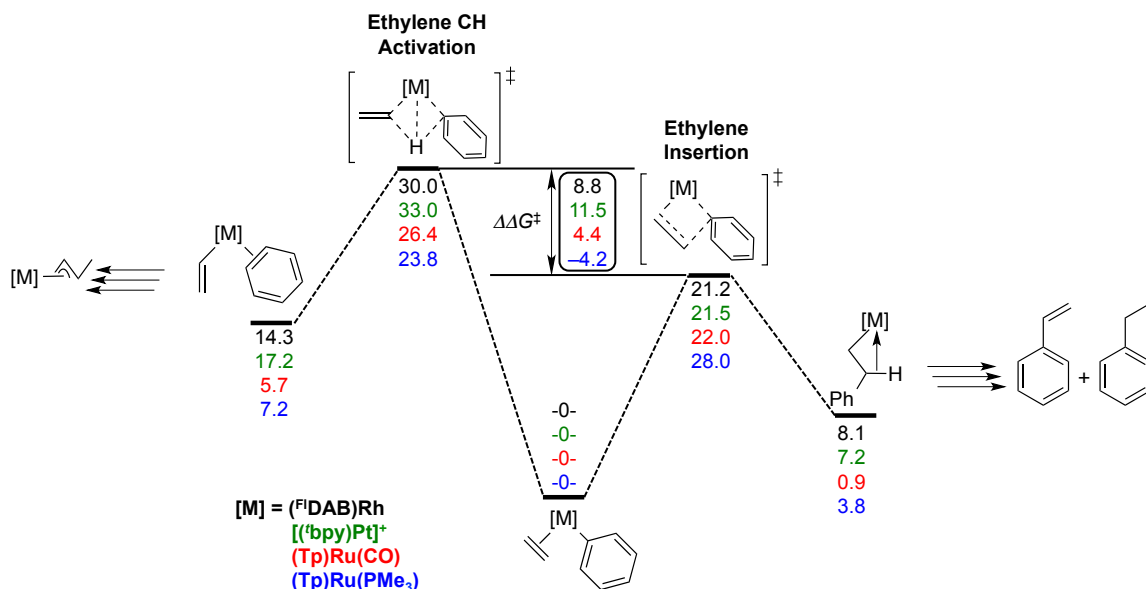
Interestingly, the calculations reveal that the $\Delta\Delta G^\ddagger$ values for C–H activation are relatively small for Rh and Pt (2 kcal/mol), and only slightly larger for Rh and Ru (6 kcal/mol). Again, for β -hydride elimination, the difference in energy barriers for Rh and Pt are negligible ($\Delta\Delta G^\ddagger = 0.2$ kcal/mol), and the difference between Rh and Ru is only slightly larger ($\Delta\Delta G^\ddagger = 2.6$ kcal/mol). Given the energy differences for the two key steps for ethylbenzene and styrene production are small, these can likely not be used to rationalize the change in selectivity for **^{F1}DABRh** compared to **'bpyPt** and **TpRuCO**.^{1,17}

Comparison of ΔG s for styrene dissociation from **^{F1}DABRh** and **'bpyPt** indicates that this may be the key parameter dictating selectivity for ethylbenzene or styrene production. For **^{F1}DABRh**, the ΔG for styrene dissociation is 11.8 kcal/mol, where for **'bpyPt** it is much larger (27.4 kcal/mol). This explanation does not hold for **TpRuCO**, which has a ΔG of 4.9 kcal/mol, which could indicate that there is an additional electronic component dictating selectivity that has not yet been identified. However, comparing **^{F1}DABRh** and **'bpyPt**, it is likely that both complexes undergo β -hydride elimination from M–CH₂CH₂Ph intermediates, but for **'bpyPt** this reaction is reversible due to the unfavorable energetics of styrene dissociation.^{1,17}

4.6.2 Potential Formation of η^3 -allyl Complexes

For previously reported olefin hydroarylation catalysts, the C–H activation of ethylene has been shown to result in the irreversible formation of an η^3 -allyl complex that is catalytically inactive.²⁻⁷ This pathway can be competitive with the pathway for ethylene insertion into the M–Ph bond and has been shown to be the major deactivation pathway for Ru-based hydroarylation catalysts.^{2,5,6} Scheme 4.6 shows a comparison of calculated energetics for ethylene insertion and ethylene C–H activation pathways for $(^{\text{Fl}}\text{DAB})\text{Rh}(\text{Ph})(\eta^2\text{-C}_2\text{H}_4)$, $(^{\text{t}}\text{bpy})\text{Pt}(\text{Ph})(\eta^2\text{-C}_2\text{H}_4)$,¹³ and $\text{TpRu}(\text{L})(\text{Ph})(\eta^2\text{-C}_2\text{H}_4)$ [L = CO, PMe_3].⁵

Scheme 4.6. Comparison of energetics of ethylene C–H activation and ethylene insertion for several reported catalysts with $\Delta\Delta G^\ddagger$ highlighted.



The $\Delta\Delta G^\ddagger$ s shown in Scheme 4.6 are the differences in the calculated ΔG^\ddagger for ethylene C–H activation and the calculated ΔG^\ddagger for ethylene insertion. A positive $\Delta\Delta G^\ddagger$ is favorable for catalytic ethylene hydrophenylation. Of the four complexes examined, **TpRuPMe₃** is the only one with a negative $\Delta\Delta G^\ddagger$ (–4.2 kcal/mol). This is consistent with the experimental observation that the formation of inactive TpRu(PMe₃)(η^3 -C₃H₄Me) is more rapid than ethylene hydrophenylation by TpRu(PMe₃)(Ph)(η^2 -C₂H₄).⁵ **TpRuCO** has a calculated $\Delta\Delta G^\ddagger$ of 4.4 kcal/mol, which indicates that ethylene insertion is more rapid than ethylene C–H activation, but since the $\Delta\Delta G^\ddagger$ is small, the formation of an η^3 -allyl could be competitive under some conditions, which is consistent with experimental data.⁵

In contrast, (**bpy**)Pt¹³ and ^{Fl}**DABRh** have $\Delta\Delta G^\ddagger$ values of 11.5 kcal/mol and 8.8 kcal/mol, respectively, which suggests that the pathway for ethylene C–H activation is likely to be kinetically inaccessible. Experimental evidence supports this hypothesis, as the formation of an η^3 -allyl complex is not observed for either catalyst under the conditions studied. These data highlight an important design feature for catalysts that convert arenes and olefins to alkyl or vinyl arenes: the rate of olefin insertion into metal–aryl bonds must be much faster than the rate of olefin C–H activation.

4.7 Looking Forward: Future Outlook and Insights into Catalyst Design

4.7.1 Future Outlook

The research presented herein represents a fundamental advancement in the field of oxidative arene vinylation, and in particular, styrene production. This work and the research it has spawned have the potential to result in a revolutionary new industrial process for styrene production, better synthetic methods for the production of surfactants

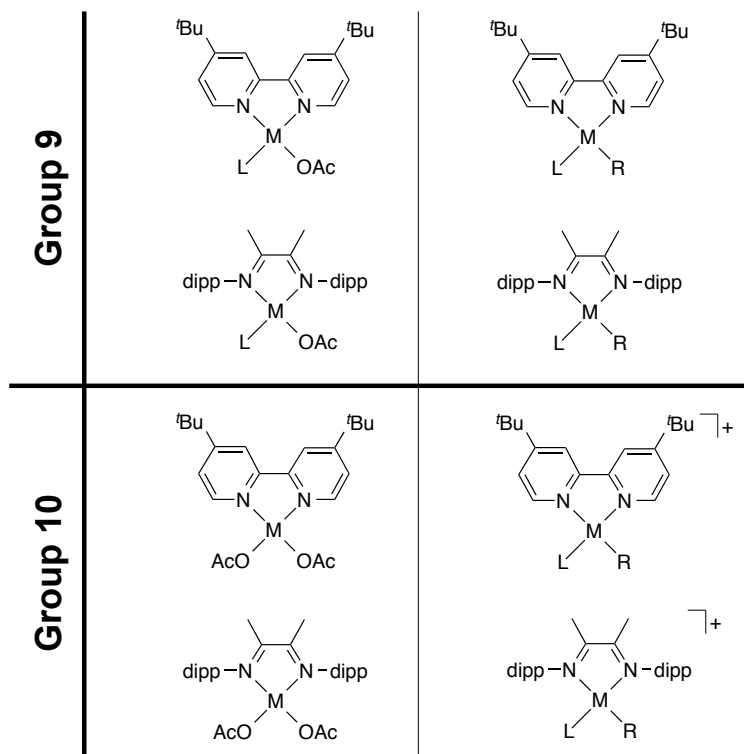
and detergents, and a novel process for naphthalene-based plastics. In the following section, a few promising projects are discussed as an example of potential future directions.

4.7.2 Impact of Metal–Carboxylate Functionality

Following the mechanistic studies of Rh-catalyzed styrene production presented in Chapter 3, one important area of further research is to examine the impact of the metal–carboxylate functionality on oxidative arene vinylation. For Rh, we now know that the accessibility of the CMD mechanism for C–H activation lowers the barrier such that olefin insertion becomes rate-limiting. Given that this change in the rate-limiting step (compared to Pt and Ru catalysts) allows for the selective formation of linear alkyl and alkenyl arenes,^{28,29} the examination of this trend across other metals would be of great interest.

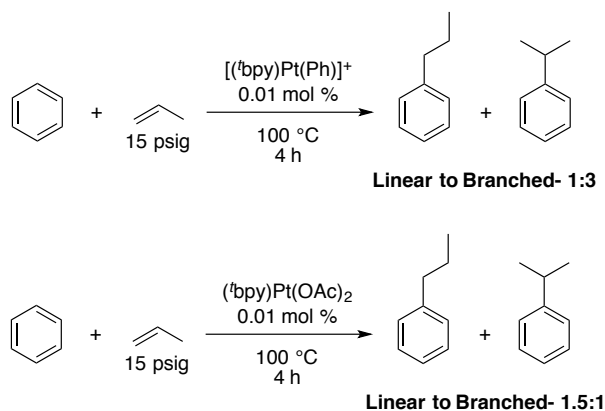
To test this hypothesis, a variety of metal complexes with either carboxylates or alkyl/aryl groups bearing identical ancillary ligand sets could be compared. Propylene would be an ideal substrate to study, as there are only two potential unsaturated products (α -methyl styrene and β -methyl styrene) and two potential saturated products (cumene and n-propyl benzene). A variety of d^8 metals should be examined, as the inherent electronics of the metal centers could offset any potential advantage provided by the carboxylate (Table 4.1). The barriers for both C–H activation and olefin insertion should be computationally modeled as well to help rationalize trends.

Table 4.1. Proposed complexes to examine the linear to branched selectivity for the hydrophenylation of propylene. Group 9 M = Co, Rh, Ir; Group 10 M = Ni, Pd, Pt.



Preliminary results comparing propylene hydrophenylation using $(^t\text{bpy})\text{Pt}(\text{OAc})_2$ and $[(^t\text{bpy})\text{Pt}(\text{Ph})(\text{NCMe})]^+$ show that the carboxylate shifts the linear to branched ratio from 1:3 for the PtPh complex to 1.5:1 for the PtOAc complex, although the acetate complex produces only a stoichiometric amount of alkyl products (Scheme 4.7). While these results are preliminary, and should be further investigated, they serve as a proof-of-concept that for the same metal, the presence of a carboxylate can dramatically shift the linear to branched selectivity, likely as a result of a lower C–H activation barrier.

Scheme 4.7. Comparison of hydrophenylation of propylene using $[(^t\text{bpy})\text{Pt}(\text{Ph})]^+$ and $(^t\text{bpy})\text{Pt}(\text{OAc})_2$.



4.7.3 Development of Air-Stable Rh(I) Catalysts for Styrene Production

One of the largest barriers to commercial implementation of the Rh(I)-catalyzed styrene production process described in chapter 3 is the aerobic instability of the catalyst. While many industrial processes are operated under inert atmosphere due to safety concerns,³⁰ the logistics of using an extremely air-sensitive catalyst requires anaerobic handling at all stages of the industrial process, which is impractical. Catalysis that can operate under aerobic conditions also offers advantages in the practicality of aerobically regenerating the Cu(II) oxidant. Reviews of our 2015 paper disclosing styrene production by leaders in the field highlighted the fact that the ability to aerobically recycle the Cu(II) oxidant would make the commercial viability for this process high.³¹

While Rh(I) complexes are not traditionally air-stable, there are a number of viable strategies for making Rh(I) complexes that can be stable under some aerobic conditions. Reports of a $(\text{NHC})_2\text{Rh}(\text{I})$ [NHC = *N*-heterocyclic carbene] complex that can reversibly

bind O₂ without being oxidized to Rh(III) (which is catalytically inactive for arene vinylation) show that it is possible to use sterics to increase aerobic stability.³²

John Gordon, an undergraduate under my supervision in our lab, has been focusing on synthesizing analogous (NHC)₂Rh complexes bearing carboxylate substituents. If these complexes exhibit the same aerobic stability as the published chloride variants, it is very likely that they will be effective catalysts for oxidative arene vinylation under aerobic conditions. He has successfully synthesized the complexes (IPr)₂Rh(Cl)(η²-C₂H₄) [IPr = 1,3-bis(2,6-diisopropylphenyl)imidazol-2-ylidene], (IPr)₂Rh(OAc)(η²-C₂H₄), (SIMes)₂Rh(Cl)(η²-C₂H₄) [SIMes = 1,3-bis(2,4,6-trimethylphenyl)-4,5-dihydroimidazol-2-ylidene], and (SIMes)₂Rh(OAc)(η²-C₂H₄).

4.8 References

- (1) Andreatta, J. R.; McKeown, B. A.; Gunnoe, T. B. *J. Organomet. Chem.* **2011**, *696*, 305.
- (2) Burgess, S. A.; Joslin, E. E.; Gunnoe, T. B.; Cundari, T. R.; Sabat, M.; Myers, W. H. *Chem. Sci.* **2014**, *5*, 4355.
- (3) Foley, N. A.; Ke, Z.; Gunnoe, T. B.; Cundari, T. R.; Petersen, J. L. *Organometallics* **2008**, *27*, 3007.
- (4) Foley, N. A.; Lail, M.; Gunnoe, T. B.; Cundari, T. R.; Boyle, P. D.; Petersen, J. L. *Organometallics* **2007**, *26*, 5507.
- (5) Foley, N. A.; Lail, M.; Lee, J. P.; Gunnoe, T. B.; Cundari, T. R.; Petersen, J. L. *J. Am. Chem. Soc.* **2007**, *129*, 6765.
- (6) Foley, N. A.; Lee, J. P.; Ke, Z.; Gunnoe, T. B.; Cundari, T. R. *Acc. Chem. Res.* **2009**, *42*, 585.
- (7) Joslin, E. E.; McMullin, C. L.; Gunnoe, T. B.; Cundari, T. R.; Sabat, M.; Myers, W. H. *Organometallics* **2012**, *31*, 6851.

- (8) Joslin, E. E.; Quillian, B.; Gunnoe, T. B.; Cundari, T. R.; Sabat, M.; Myers, W. H. *Inorg. Chem.* **2014**, *53*, 6270.
- (9) Lail, M.; Arrowood, B. N.; Gunnoe, T. B. *J. Am. Chem. Soc.* **2003**, *125*, 7506.
- (10) Lail, M.; Bell, C. M.; Conner, D.; Cundari, T. R.; Gunnoe, T. B.; Petersen, J. L. *Organometallics* **2004**, *23*, 5007.
- (11) McKeown, B. A.; Foley, N. A.; Lee, J. P.; Gunnoe, T. B. *Organometallics* **2008**, *27*, 4031.
- (12) McKeown, B. A.; Gonzalez, H. E.; Friedfeld, M. R.; Brosnahan, A. M.; Gunnoe, T. B.; Cundari, T. R.; Sabat, M. *Organometallics* **2013**, *32*, 2857.
- (13) McKeown, B. A.; Gonzalez, H. E.; Friedfeld, M. R.; Gunnoe, T. B.; Cundari, T. R.; Sabat, M. *J. Am. Chem. Soc.* **2011**, *133*, 19131.
- (14) McKeown, B. A.; Gonzalez, H. E.; Gunnoe, T. B.; Cundari, T. R.; Sabat, M. *ACS Catal.* **2013**, *3*, 1165.
- (15) McKeown, B. A.; Gonzalez, H. E.; Michaelos, T.; Gunnoe, T. B.; Cundari, T. R.; Crabtree, R. H.; Sabat, M. *Organometallics* **2013**, *32*, 3903.
- (16) McKeown, B. A.; Prince, B. M.; Ramiro, Z.; Gunnoe, T. B.; Cundari, T. R. *ACS Catal.* **2014**, *4*, 1607.
- (17) Vaughan, B. A.; Khani, S. K.; Gary, J. B.; Kammert, J. D.; Webster-Gardiner, M. S.; McKeown, B. A.; Davis, R. J.; Cundari, T. R.; Gunnoe, T. B. *J. Am. Chem. Soc.* **2017**, *139*, 1485.
- (18) Vaughan, B. A.; Webster-Gardiner, M. S.; Cundari, T. R.; Gunnoe, T. B. *Science* **2015**, *348*, 421.
- (19) Webster-Gardiner, M. S.; Chen, J.; Vaughan, B. A.; McKeown, B. A.; Schinski, W.; Gunnoe, T. B. *J. Am. Chem. Soc.* **2017**, *139*, 5474.
- (20) Ozkal, E.; Llanes, P.; Bravo, F.; Ferrali, A.; Pericàs, M. A. *Adv. Synth. Catal.* **2014**, *356*, 857.
- (21) Wang, D.; Etienne, L.; Echeverria, M.; Moya, S.; Astruc, D. *Chem. Eur. J.* **2014**, *20*, 4047.
- (22) Chen, H.; Hou, S.; Tan, Y. *Supramol. Chem.* **2016**, *28*, 801.
- (23) Jia, X., Unpublished Work.

- (24) Zhang, F.; Kirby, C. W.; Hairsine, D. W.; Jennings, M. C.; Puddephatt, R. J. *J. Am. Chem. Soc.* **2005**, *127*, 14196.
- (25) Webster-Gardiner, M. S.; Chen, J.; Vaughan, B. A.; McKeown, B. A.; Shinski, W.; Gunnoe, T. B. *J. Am. Chem. Soc.* **2017**, In Press.
- (26) Weissman, H.; Song, X.; Milstein, D. *J. Am. Chem. Soc.* **2001**, *123*, 337.
- (27) Taube, D.; Periana, R.; Matsumoto, T. 6127590A, 2000. (US Patent 6127590A)
- (28) Chen, J., Unpublished Work.
- (29) Webster-Gardiner, M. S., Unpublished Work.
- (30) Gladysz, J. A. *Pure Appl. Chem.* **2001**, *73*, 1319.
- (31) Bornman, S. *Chem. Eng. News* **2015**, *93*, 26.
- (32) Praetorius, J. M.; Allen, D. P.; Wang, R.; Webb, J. D.; Grein, F.; Kennepohl, P.; Crudden, C. M. *J. Am. Chem. Soc.* **2008**, *130*, 3724.